IRE Transactions

on Microwave Theory and Techniques

Volume MTT-9 **MAY, 1961** Number 3

Published Bimonthly

In This Issue

PUBLISHED BY THE

essional Group on Microwave Theory and Techniques

IRE PROFESSIONAL GROUP ON MICROWAVE THEORY AND TECHNIQUES

The Professional Group on Microwave Theory and Techniques is an association of IRE members with professional interest in the field of Microwave Theory and Techniques. All IRE members are eligible for membership and will receive all Group publications upon payment of the prescribed annual fee of $3.00. Members of the American Physical Society and the Institution of Electrical Engineers of Great Britain may become affiliated with PGMTT and receive all Group publications upon payment of the Affiliate fee of $7.50 per year.

PGMTT Chapters

Albuquerque-Los Alamos	R. L. O'Nan	Omaha-Lincoln	C. O. Jett
Baltimore	J. C. Wiltse	Orange Belt	D. Sabih
Boston	C. E. Faflick	Orlando	E. O. Houseman, Jr.
Buffalo-Niagara	E. S. Schlichter	Philadelphia	T. J. Vaughan
Chicago	Robert Janowiak	San Diego	H. O. Dickstein
Columbus	B. C. Potts	San Francisco	E. M. T. Jones
Denver-Boulder	G. E. Schafer	Schenectady	C. C. Allen
Long Island	B. Aaron	Syracuse	J. C. Williamson
Los Angeles	R. C. Hansen	Tokyo, Japan	Kiyoshi Morita
New York	Eugene Torgow	Washington, D.C.	Benjamin Bernstein
Northern N.J.	R. M. Foley		

IRE TRANSACTIONS®
on Microwave Theory and Techniques

Published by The Institute of Radio Engineers, Inc., for the Professional Group on Microwave Theory and Techniques, at 1 East 79 Street, New York 21, N.Y. Responsibility for the contents rests upon the authors, and not upon the IRE, the Group, or its members. Individual copies of this issue and all available back issues may be purchased at the following prices: IRE members (one copy) $2.25, libraries and colleges $3.25, all others $4.50. Annual subscription price: non-members, $17.00; colleges and public libraries, $12.75.

Address all manuscripts to Donald D. King, PGMTT Editor, Electronic Communications, Inc., 1830 York Road, Timonium, Md. Submission of three copies of manuscripts, including figures, will expedite the review.

IRE Transactions on Microwave Theory and Techniques

Volume MTT-9 MAY, 1961 Number 3
Published Bimonthly

TABLE OF CONTENTS

CORRESPONDENCE

Octave-Bandwidth UHF/*L*-Band Circulator*

F. ARAMS†, SENIOR MEMBER, IRE, B. KAPLAN‡, AND B. PEYTON†, MEMBER, IRE

Summary—Test data are presented on two aluminum-substituted yttrium-iron-garnet (YIG) materials that have low-saturation magnetizations that permit the extension of ferrite devices well into the UHF/VHF region. In particular, one composition has a saturation magnetization of 300 gauss and a line width of 50 oersteds. Measurements are presented that compare the new materials with previously available higher-saturation magnetization materials.

A broad-band UHF/*L*-band four-port circulator that operates over a 2-to-1 frequency band has been developed, using this 300 gauss material. Insertion loss is 1 db or less from 665 to 1320 Mc (with constant magnetic field) and 0.5 db or less from 800 to 1150 Mc. A compact and favorable circulator package design was obtained by using coaxial hybrids and dielectric-loaded strip transmission line. Data on the broad-band magic-tee used in the circulator are included. Isolator measurements down to 200 Mc are reported. Reverse-to-forward magnetic-loss ratios of 36 at 600 Mc and 12 at 300 Mc were obtained.

I. Introduction

NONRECIPROCAL ferrite devices—in particular' low-loss circulators—are increasingly difficult to realize at the lower microwave and UHF frequencies [1], [2]. This can be seen by considering the two magnetic-loss mechanisms in microwave ferrites (Fig. 1):

1) The low-field loss that exists at low microwave and UHF frequencies in unsaturated ferrite.
2) The ferrimagnetic resonance loss.

Because the magnetic field required for ferrimagnetic resonance is proportional to the frequency, the low-loss region below ferrimagnetic resonance gradually disappears as the frequency is decreased, thereby increasing the loss in circulators operating in this region. Similarly, the low-field loss will broaden the ferrimagnetic resonance line and deteriorate the ratio of reverse-to-forward loss of low-frequency resonance isolators.

To minimize these effects, it is necessary:

1) to use transversely magnetized thin ferrite slabs, since the demagnetizing factors for this ferrite geometry maximize the applied magnetic field required for resonance,
2) to decrease the saturation magnetization ($4\pi M_s$) of the ferrite material while keeping the resonance line width (ΔH) as narrow as possible.

Previous low-loss *S*-band and *L*-band circulators [3] used a high-density magnesium-manganese ferrite with aluminum substitution (General Ceramics R-6). Measurements show that the loss of R-6 in broad-band circulators increases rapidly when the operating frequency is decreased below 1100 Mc. Therefore, a new material is required for UHF application.

Unfortunately, the addition of aluminum to the magnesium-manganese ferrite, though it lowers the saturation magnetization, will also lower the Curie temperature (about 100°C for R-6). This increases the ferrite sensitivity to temperature variations and limits its use in high-power applications, unless external cooling is provided. The further addition of aluminum to a magnesium-manganese material is therefore undesirable.

II. Development of Materials

A more rewarding approach is to use substituted yttrium-iron garnet (YIG), since reasonable Curie temperatures can be obtained for aluminum-substituted and gallium-substituted YIG without undue line-width deterioration [4]–[6]. Accordingly, we arranged with Microwave Chemicals Laboratory to supply a number of specially prepared YIG compositions with the object of obtaining a satisfactory UHF ferrite material. Two aluminum-substituted YIG compositions were obtained

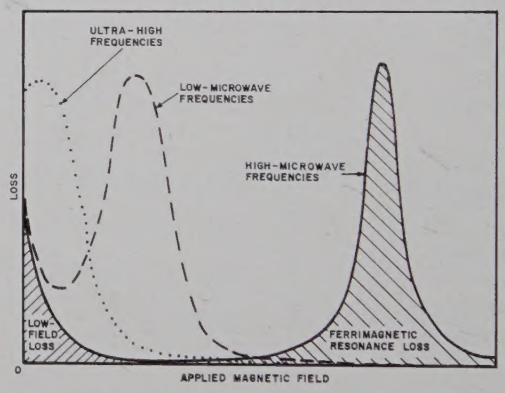

Fig. 1—Ferrite loss vs applied magnetic field.

TABLE I
Properties of Materials

Material	Saturation Magnetization (Gauss)	Line Width (Oersteds at S-Band)	Dielectric Loss Tangent (at 20 Mc)	Dielectric Constant	Curie Temperature (°C)
Al-YIG*	400	60	0.0037	13.5	140
Al-YIG*	300	50	0.0016	11.7	125
Pure YIG	1750	40 to 50	0.002	16	275
R-6 (Mg-Mn-Al)	730	90	0.0015	—	100

* Measurements by L. M. Silber, Polytechnic Inst. of Brooklyn, N. Y.

* Received by the IRE, December 5, 1960. This work was supported by the Dept. of Defense.

† Airborne Instruments Lab., Div. of Cutler-Hammer, Inc., Melville, L. I., N. Y.

‡ Airtron, Inc., Morris Plains, N. J. Formerly with Airborne Instruments Lab., Div. of Cutler-Hammer, Inc., Melville, L. I., N. Y.

that combined low-saturation magnetization (400 and 300 gauss), narrow line width, reasonable Curie temperature, and low dielectric-loss tangent. Table I shows the measured magnetic and dielectric properties of these materials, and compares them to the properties of pure (unsubstituted) YIG and R-6. It was possible to obtain a material having a saturation magnetization of only 300 gauss, a line width of 50 oersteds, a dielectric-loss tangent of 0.0016, and a Curie temperature of 125°C. This proved to be the best material for UHF circulators and had extremely good performance (reverse-to-forward loss ratio) when measured as an isolator at frequencies down to 200 Mc.

III. Microwave and UHF Measurements

The magnetic loss at 1200 Mc as a function of applied magnetic field for R-6, pure YIG, and the 400-gauss substituted YIG material are compared in Fig. 2. The

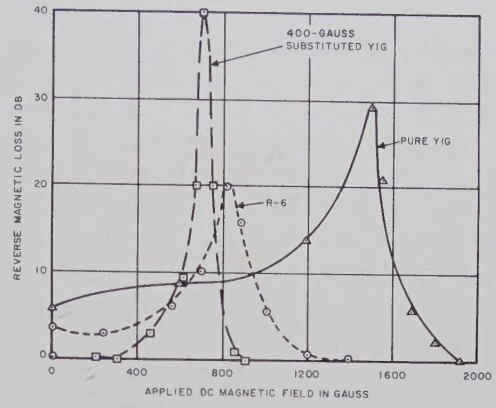

Fig. 2—Comparison of magnetic loss (1200 Mc).

TABLE II

Microwave Measurements on Substituted-YIG Materials

Test Frequency (mc)	Material (Gauss)	Test Section*	Resonant Loss per 6-Inch Length (db)	Zero Field Loss per 6-Inch Length (db)	Differential Phase Shift per 12-Inch Length (Degrees)	Figure of Merit (Degrees per db)
900	400	A	9.0	0.8	33.4	420
900	400	B	23.2	2.4	88.0	440
900	300	B	15.6	0.4	112	410
1200	400	C	10.8	0.2	50.4	505
1200	400	B	24	0.4	97.6	490
1200	300†	B	16	0.1	111	520

* Test sections are designated as: A) 9.2 by 1 inch (inside dimension) waveguide; B) dielectric-loaded strip transmission line (Fig. 4) C) 6.5 by 1 inch (inside dimension) waveguide.

† Phase-shift measurements were made with the magnetic field above ferrimagnetic resonance, except for the measurements with the 300-gauss material.

400-gauss material shows a narrow line width, a very low zero-field loss, and a high-resonance loss. The dimensions of the various samples were not identical, but the conclusions are qualitatively correct.

Microwave measurements at 900 and 1200 Mc for the 300- and 400-gauss materials are given in Table II. The substituted-YIG compositions show high figures of merit for both circulator and isolator application in the UHF region. Note that only in the case of the 300-gauss material was it possible to obtain low-loss phase-shift data below resonance. Reverse magnetic-loss measurements of the 300- and 400-gauss materials at 900 Mc are compared in Fig. 3. The 300-gauss material, with lowest saturation magnetization and good line width, shows a broader low-loss region than the 400-gauss material, and hence can be used to lower frequencies. Therefore, the 300-gauss material is the most suitable for broad-band UHF circulators and isolators.

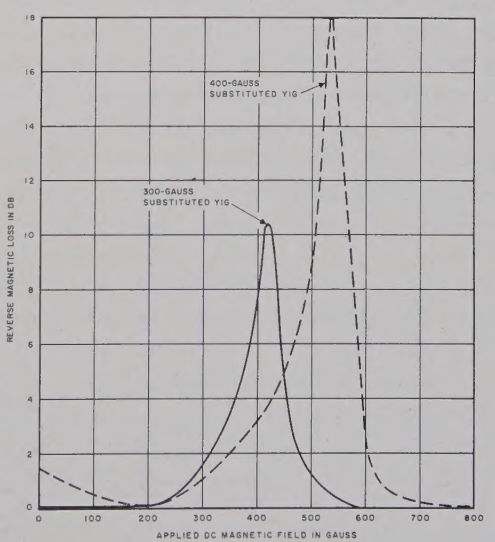

Fig. 3—Comparison of magnetic loss (900 Mc).

IV. Broad-Band Circulator Design

To obtain as large a bandwidth as possible, and in view of its superiority for use with broad-band maser and parametric amplifiers, a four-port differential phase-shift type circulator was developed. The feasibility of a very broad-band coaxial *S*-band circulator has previously been demonstrated [7]. To achieve large bandwidth as well as a compact unit, TEM-mode transmission lines were used. Strip transmission lines using partial dielectric loading (Fig. 4) were used for the nonreciprocal phase-shift sections, thereby distorting the TEM mode [8], [9] sufficiently to produce a longitudinal component of the RF magnetic field. The strip transmission line was chosen instead of coaxial line because it is easier to fabricate the structure and shape the ferrite and dielectric pieces, and the dielectric pieces can be readily adjusted and interchanged for optimum circulator performance during testing.

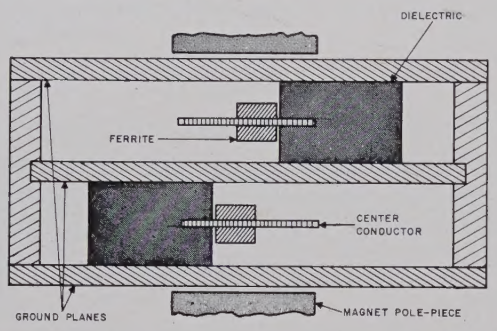

Fig. 4—Cross section of strip-transmission-line circulator structure.

The mode resulting from the dielectric loading does not have a complete circularly-polarized RF magnetic field [10]. However, the field produced is almost circularly polarized—sufficiently so to produce efficient nonreciprocal action when the structure is loaded with ferrite. The ellipticity (deviation from circular polarization) results in increased length and deteriorates the figure of merit (degrees of differential phase shift per db of loss) of the ferrite nonreciprocal phase-shift section. Thus, an ellipticity of 1.2 will reduce the figure of merit by 17 per cent. For an isolator it would limit the reverse-to-forward loss ratio to 20 to 1. The calculated ellipticity at the dielectric interface for our structure was from 1.1 to 1.3 in the frequency range of interest.

A slowing factor of 2.2 was measured over the desired frequency range, thereby reducing the length of the ferrite section by the same factor. To match the 16-ohm dielectric-loaded line to the 50-ohm input and output over the desired frequency band, three quarter-wave transformers which had a Tchebycheff response were used [11]. Matching was accomplished by using a 400- to 1200-Mc sweep oscillator and was checked point by point. The SWR of the dielectric line with the transformers averaged 1.15.

V. Hybrids

To construct a four-port phase-shift circulator, two hybrids are required to connect two 90-degree nonreciprocal phase-shift sections. For the best design, one hybrid should give a 90-degree phase difference and a 3-db power split; the other should give a 180-degree phase difference and a 3-db power split.

A 180° hybrid was developed based on previous work [12], [13]. This coaxial magic-tee is basically a broad-band four-port ring hybrid where all arms are $\lambda/4$ long. Reversing the inner and outer conductors on one of the arms introduces the extra 180 degrees of phase shift required for hybrid action. Since the 180° phase shift introduced in the crossover arm is not frequency sensitive, the bandwidth of the resulting hybrid is wider than the conventional ring hybrid. Neglecting the discontinuities caused by the reversal at the crossover arm and the wire connections, the calculation shows that for a 40-per cent bandwidth, an input SWR slightly less than 1.10 can be obtained at all ports. Since all line lengths in this hybrid are equal, we can obtain high isolation to the decoupled port and an even power split to the two coupled ports over a large frequency range.

The unit gave a power split of ± 0.10 db or better (from 700 to 1200 Mc), an isolation of 27 db or more, and an input SWR averaging 1.1.

For the 90° hybrid, we used a special unit supplied by Sage Laboratories that is a miniaturized version of a broad-band parallel strip-transmission-line hybrid [14].

VI. Circulator Package and Performance

Measurements on differential phase shift and loss on the ferrite section shows that good circulator operation can be obtained with 400-gauss material at 700 gauss (above resonance) or with 300-gauss material near 100 gauss (below resonance). This is shown in Table II. Operation below resonance is, of course, preferred because magnet weight is reduced substantially and broad-band operation can be readily achieved.

Fig. 5 shows the completely assembled circulator with the hybrids distinguishable at each end. The two nonreciprocal phase-shift sections are located one on top of the other (Fig. 4). This results in a compact and easily packaged geometry. The strip transmission lines have a 3.6° jog to obtain the proper physical locations for connecting the hybrids.

Performance data taken on the assembled circulator are shown in Fig. 6. The measured insertion loss was 0.5 db or less from 800 to 1150 Mc (with optimized magnetic field), and 1.0 db or less from 665 to 1320 Mc (with constant applied magnetic field).

Thus, a UHF/*L*-band circulator was realized that has an octave of coverage with constant magnetic field. The electromagnet can, of course, be replaced by a permanent magnet.

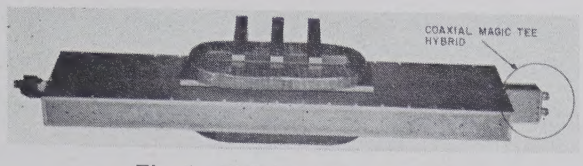

Fig. 5—UHF/*L*-band circulator.

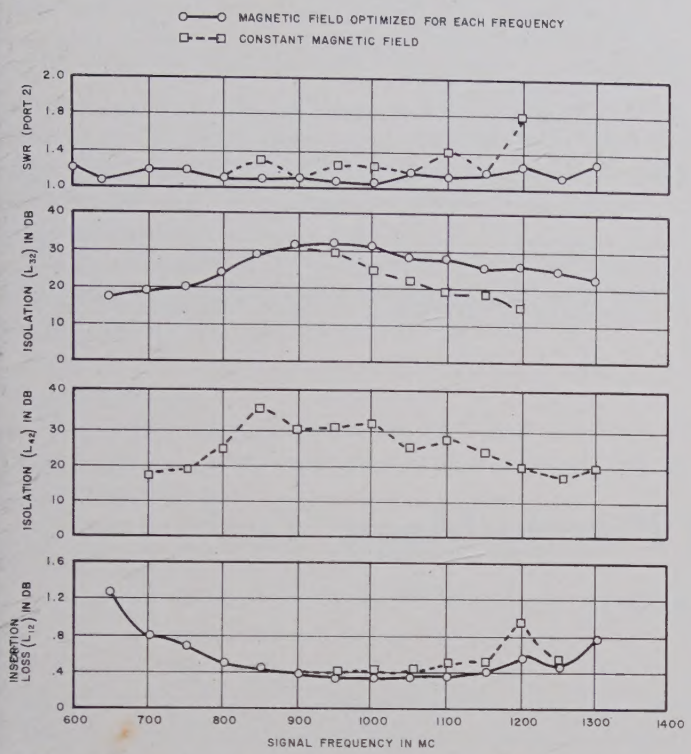

Fig. 6—Performance data for UHF/*L*-band circulator.

This circulator was tested with an experimental broadband parametric amplifier 15 and provided the large bandwidth necessary to accurately measure the low noise figures obtained. The amplifying region of the parametric amplifier is considerably greater than its 3-db bandwidth. Therefore, the circulator bandwidth should at least equal the gain-bandwidth product of the parametric amplifier so that a good match is provided to the amplifier until the gain drops to unity.

VII. Isolator Measurements

Isolator measurements of the 300-gauss material are shown in Fig. 7 with magnetic field optimized at each frequency. The measurements were obtained in the dielectric-loaded strip transmission line (Fig. 4) with a ferrite only 12 inches long. As is shown, high-reverse losses and good reverse-to-forward loss ratios (db) are obtained down to a frequency of 300 Mc. The figure of merit (reverse-to-forward loss ratio in db) was 38 at 800 Mc, 36 at 600 Mc, 20 at 400 Mc, and 12 at 300 Mc.

Since this structure is designed for higher frequencies,

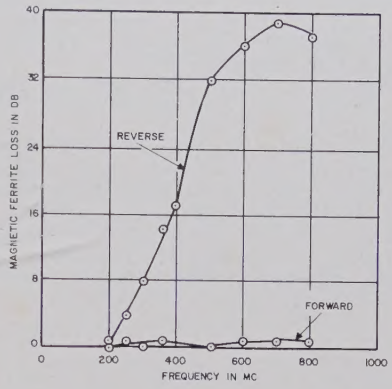

Fig. 7—Isolator performance at UHF/VHF frequencies.

it did not give optimum elliptical polarization below 500 Mc. Hence, substantial improvements should be possible over those previously reported [15] by optimizing the circuit design.

VIII. Conclusions

Measurements are reported on two aluminum-substituted YIG materials that can be used for ferrite devices in the VHF, UHF and L-bands.

One composition with a saturation magnetization of 300 gauss permits the extension of circulators and isolators to lower frequencies than has been possible in the past.

A four-port circulator has been developed using the 300-gauss material that can be operated over a 2-to-1 frequency band. An insertion loss of 1 db or less was obtained from 665 to 1320 Mc with constant magnetic field. Insertion loss with optimized magnetic field was 0.5 db or less from 800 to 1150 Mc.

A specially compact and favorable circulator package design was achieved that used coaxial hybrids and a dielectric-loaded strip-transmission-line ferrite structure.

Favorable reverse-to-forward loss ratios were obtained in isolator measurements to 300 Mc.

Acknowledgment

The authors wish to thank L. Van Uitert and H. Seidel of Bell Telephone Laboratories and J. Hanley of Sperry Gyroscope Company for discussions, and J. Wolczok for assistance in microwave and UHF measurements.

Bibliography

[1] C. L. Hogan, "Low-frequency problems in the design of microwave gyrators and associated elements," IRE Trans. on Antennas and Propagation, vol. AP-4, pp. 495–501; July, 1956.

[2] B. Lax, "Fundamental design principles of ferrite devices," *Proc. Symp. on Modern Advances in Microwave Techniques*, Polytechnic Institute of Brooklyn, Brooklyn, N. Y.; November, 1954.

[3] F. R. Arams, G. Krayer, and S. Okwit, "Low-loss *S*- and *L*-band circulators," 1959 IRE National Convention Record, pt. 3, pp. 126–133.

[4] G. Villers and J. Loriers, "Interpretation des propriétés magnétiques du grenat d'yttrium dans lequel des ions Al^{3+}, Ga^{3+}, et Cr^{3+} ont été substitués à des ions Fe^{3+}" *Comptes Rendus*, vol. 245, pp. 2033–2036; December, 1957.

[5] M. A. Gilleo and S. Geller, "Magnetic and crystallographic properties of substituted yttrium-iron garnet," *Physical Rev.*, vol. 110, pp. 73–78; April, 1958.

[6] G. P. Rodrigue, J. E. Pippin, W. P. Wolf, and C. L. Hogan, "Ferrimagnetic resonance in some polycrystalline rare earth garnets," IRE Trans. on Microwave Theory and Techniques, vol. MTT-6, pp. 83–90; January, 1958.

[7] P. Ahrens, D. Fleri, and M. Tanenbaum, "Final Engineering Report, Research and Development Program for Ferrite Microwave Switch," Sperry Gyroscope Company, Great Neck, N. Y., Rept. No. 7210–13014-4, April 10, 1959.

[8] B. J. Duncan, L. Swern, K. Tomiyasu, and J. Hannwacker, "Design considerations for broadband ferrite coaxial line isolators," Proc. IRE, vol. 45, pp. 483–490; April, 1957.

[9] K. Button, "Theory of nonreciprocal ferrite phase shifter in dielectric-loaded coaxial line," *J. Appl. Phys.*, vol. 29, pp. 998–1000; June, 1958.

[10] D. Fleri and G. Hanley, "Nonreciprocity in dielectric-loaded TEM mode transmission lines," IRE Trans. on Microwave Theory and Techniques, vol. MTT-7, pp. 23–27; January, 1959.

[11] L. Young, "Tables for cascaded homogeneous quarter-wave transformers," IRE Trans. on Microwave Theory and Techniques, vol. MTT-7, pp. 233–237; April, 1959.

[12] J. Lyons, A. Collard, and S. Blank, Airborne Instruments Lab., private communication.

[13] W. V. Tyminski and A. E. Hylas, "A wide-band hybrid ring for UHF," Proc. IRE, vol. 41, pp. 81–87; January, 1953.

[14] J. K. Shimizu and E. M. T. Jones, "Coupled-transmission-line directional couplers," IRE Trans. on Microwave Theory and Techniques, vol. MTT-6, pp. 403–410; October, 1958.

[15] P. Lombardo, "Low-noise widely-tunable microwave parametric amplifier," Proc. IRE, vol. 48, p. 4A; October, 1960.

[16] H. Seidel, "Compact passive non-reciprocal structures for UHF frequencies," *J. Appl. Phys.*, vol. 30, p. 156S; April, 1959.

A Five-Port Matched Pseudo-Magic Tee*

AKIRA OKAYA†

***Summary*—The five-port matched pseudo-magic tee consists of an input waveguide, two load arm waveguides which are coupled into the input waveguide with $+90°$ and $-90°$ phase shifts, respectively, and an output waveguide which is split into two load waveguides by a septum.**

The improvements include a much broader matching and isolation bandwidth, higher isolation between arms, better matching into arms, and a variety of modifications for different applications.

These characteristics have been obtained by employing frequency-insensitive phase shifters. Hence, frequency coverage is mainly limited by mechanical asymmetry and the characteristics of the directional coupler in the magic tee.

While this type of hybrid junction is not a true magic tee because the load arms are not used as the input arm, it does have several applications which an ordinary magic tee does not have.

***X*-, *K*-, and *M*-band models were examined experimentally, and highly sensitive and accurate impedance measurements were made.**

Introduction

CONVENTIONAL magic tees are not as well matched nor as well isolated over as broad a frequency range as one would like. The sensitivity and accuracy of impedance bridges and the sensitivity of microwave mixers are quite often limited by the aforementioned factors. Several attempts at modifying conventional matched magic tees have been made. However, the main difficulties, which arise from the fundamental restrictions of the structure itself, have remained.

A solution of this problem has been obtained in the following ways.

Principles of Operation

The new-type magic tee (type 1) is shown in Fig. 1(a) and 1(b) (page 218). Input-microwave power is split equally by a septum in the input waveguide and then introduced into load arm waveguides 1 and 2 through directional couplers. The waves reflected from loads 1 and 2 meet at the output arm.

One can see that the waves going into loads 1 and 2 are out of phase with each other, if the condition $L_{i1}=L_{i2}$ is satisfied. Hence, the wave coming from the output arm has zero amplitude if loads 1 and 2 are identical and $L_{o1}=L_{o2}$. The geometrical conditions $L_{i1}=L_{i2}$ and $L_{o1}=L_{o2}$ are satisfied independently of the input frequency. This condition has enabled us to build a frequency-insensitive magic tee.

The matching conditions of the input waveguide depend mainly upon the matched load of the directional couplers. The necessity for the matched loads at waveguide junctions of the load arms is easily seen by circuit theory.[1] The mismatches at the junction cause fre-

* Received by the PGMTT, October 28, 1960; revised manuscript received, January 9, 1961. Supported jointly by the U. S. Army Signal Corps, the Office of Naval Research, and the A. F. Office of Scientific Research. USA Patent No. 2,949,587, issued August 16, 1960.

† Radiation Lab., Dept. of Physics, Columbia, University, New York, N. Y.

[1] C. G. Montgomery, R. H. Dicke, and E. M. Purcell, "Principles of Microwave Circuits," M.I.T. Rad. Lab. Ser., McGraw-Hill Book Co., Inc., New York, N. Y., p. 285; 1948.

quency-sensitive reflections. Although the basic principle of this tee is simple, there are several construction difficulties.

Another version of the magic tee, as sketched in Fig. 2(a) (type 2), was much more practical and easier to build. Here an input waveguide, which was separated by a septum in the first model, is replaced by a single waveguide and a single directional coupler, and is coupled to the two load arms by two lines of coupling holes symmetrically arranged about the A-A plane, as shown in Fig. 3. The holes are located at the position of maximum H field of the input waveguide so that the input wave couples to the load arms magnetically with $+90°$ and $-90°$ phase shifts, as shown in Fig. 2(a) and Fig. 4.

In this case, one can see that the phase shifts are obtained only by one directional coupler, instead of by the complicated waveguide bends of Type 1.

This hybrid circuit can be analyzed with the use of the scattering matrix.

The scattering matrix of the five-port network of Fig. 3, which is symmetric about the A-A plane, can be written as follows:

$$\begin{pmatrix} S_{11} & S_{12} & iS_{13} & -iS_{13} & iS_{15} \\ S_{12} & S_{22} & iS_{23} & -iS_{23} & iS_{25} \\ iS_{13} & iS_{23} & S_{33} & S_{34} & S_{35} \\ -iS_{13} & -iS_{23} & S_{34} & S_{44} & S_{35} \\ iS_{15} & iS_{25} & S_{35} & S_{35} & S_{55} \end{pmatrix}$$

where $V_{01}=S_{11}V_{i1}+S_{12}V_{i2}+S_{13}V_{i3}+S_{14}V_{i4}+S_{15}V_{i5}$.

V_{0n} is the voltage amplitude of the wave out of test arm n, and V_{im} is the voltage amplitude of the wave incident on test arm m.

From reciprocity, it follows that $S_{ij}=S_{ji}$. From the symmetry of the tee we obtain

$$S_{35} = S_{45}.$$

Finally, from the phase relations and the symmetry of the tee, we deduce the conditions

$$S_{13} = -S_{14}$$

$$S_{23} = -S_{24}.$$

Here the phase relations are included in the matrix elements. From column 3, row 4, the following relations are obtained:

$$+S_{13}^2 \quad +S_{23}^2 \quad +S_{33}^2 \quad +S_{34}^2 \quad +S_{35}^2 \quad =1.$$

$$+S_{13}^2 \quad +S_{23}^2 \quad +S_{34}^2 \quad +S_{44}^2 \quad +S_{35}^2 \quad =1.$$

Therefore,

$$S_{33} = S_{44}.$$

From column 1, row 2,

$$S_{11}S_{12} + S_{12}S_{22} + 2S_{13}S_{23} + S_{15}S_{25} = 0.$$

If $S_{11}=S_{22}=0$, then

$$2S_{13}S_{23} + S_{15}S_{25} = 0.$$

From the geometrical symmetry of a tee and field symmetry of arms 3 and 4, one can see immediately that

$$S_{15} = S_{25} = 0.$$

Hence,

$$S_{13}S_{23} = 0.$$

From column 1, row 3,

$$S_{11}S_{13} + S_{12}S_{23} - S_{13}S_{33} + S_{13}S_{34} - S_{15}S_{15} = 0.$$

If $S_{11}=S_{33}=0$, then $S_{12}S_{23}+S_{13}S_{34}=0$.

Suppose the coupling is directive:

$$S_{13} \neq 0 \quad \text{and} \quad S_{23} = 0,$$

then

$$S_{34} = 0.$$

The opposite directivity, $S_{13}=0$, $S_{23}\neq 0$, is not allowed because $S_{12}\neq 0$ should be satisfied in any case. One can summarize the results as follows:

Directive coupling is required such that $S_{23}=0$, $S_{13}\neq 0$, as in a magic tee. Complete isolation between load arms 3 and 4 is obtained if ports 1, 2, 3, and 4 appear matched looking out of the tee.

Experimental Results

X-, K- and M-band tees of type 2 shown in Fig. 2(a) were built and tested. Photographs of those tees are shown in Fig. 2(b).

A K-band tee of type 1, shown in Fig. 1(a), was also built and tested. Fig. 1(b) is a photograph of the part of this K-band magic tee which does not include directional couplers.

One of the type 2 X-band tees was analyzed in detail by a reflectometer setup which covered the frequency range from 8.2 kMc to 12.5 kMc. The isolation between ports 1 and 5, with matched loads at ports 2, 3, and 4, was examined. The results are shown in Fig. 5. The small leakage, which appeared on the low-frequency end of Fig. 5, was due to imperfect matching of the loads at port 2. The reflectometer was too insensitive to measure a real value of isolation at which unbalanced signals were far below the noise signal. The voltage standing wave ratios at input and output arms were less than 1.3 and 1.10, respectively, over the frequency range from 8 kMc to 11 kMc.

A more severe test of isolation was made by shorting ports 3 and 4. This test serves to emphasize any unbalancing in the two load arms, even though the tee would never be used this way in practice. As the data in Table I shows, the isolation is extremely high, even in this case.

The detailed characteristics of the tee are shown in Table I. In this case, slight adjustment of the balancing,

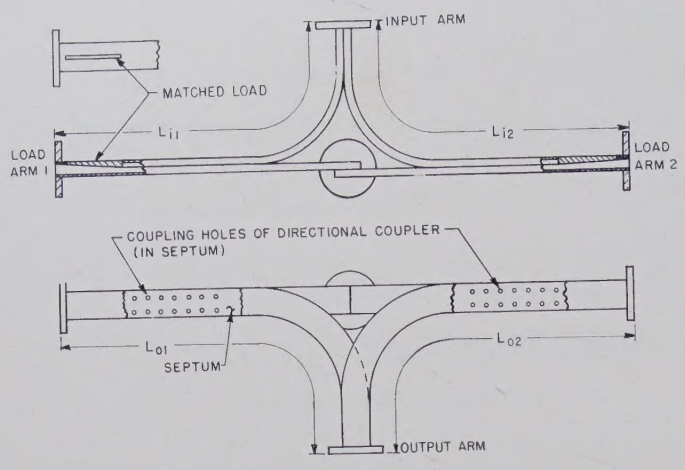

(a)

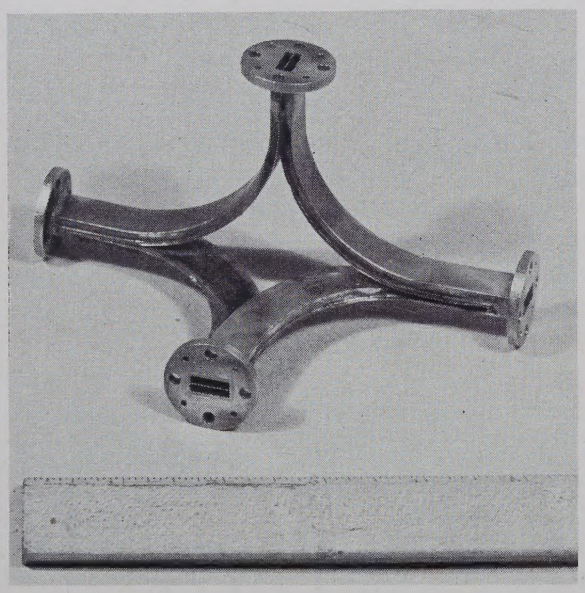

(b)

Fig. 1—(a) Structure of split waveguide-type matched magic tee (type 1). (b) Photograph of split waveguide-type magic tee.

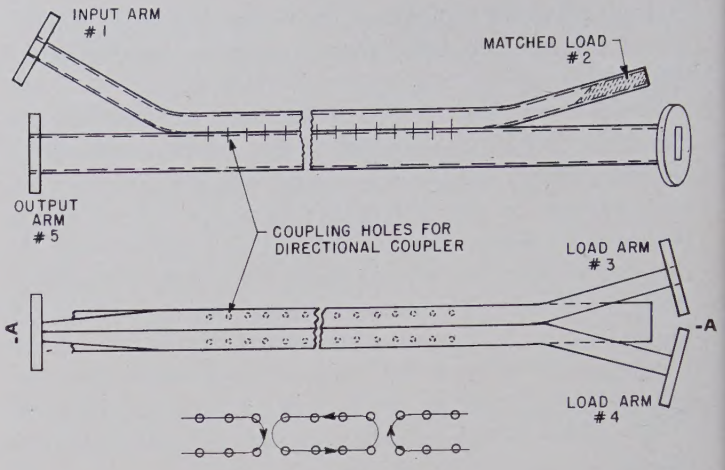

(a)

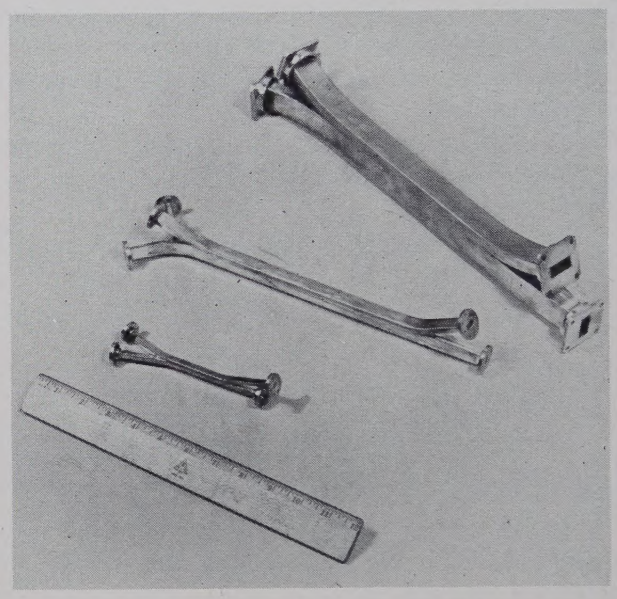

(b)

Fig. 2—(a) Structure of five-port split waveguide-type matched magic tee (type 2). (b) Photograph of five-port split waveguide-type matched magic tee.

which compensated for the mechanical asymmetry (less than 60 mils), was made for each frequency. An isolation 30 db better than the conventional magic tee was obtained.

The same type of test on the type 1 K-band tee was made. Fig. 6 shows the results of this test.

An M-band tee, which is shown in Fig. 2(b), was made, and quite uniform characteristics over the frequency range 45–58 kMc were obtained. The isolation between the input and output arms was greater than 35 db.

Conclusion

Experiments show no reason to prevent the use of this type of magic tee in the shorter millimeter wave region. Furthermore, this type of magic tee is no more difficult to build than directional couplers and matched loads at the same frequencies.

The tee is well matched in any arm, particularly in the load arm, if arm 1 is used as the input. But if one of the load arms 3 or 4 is used as an input, there is no longer isolation between arms 3 and 4. This is different from the usual magic tee.

It does have power dissipation at the matched load of arm 2. However, it need not be 11.5 db as in our test model. The circuits with 3-db directional couplers are easy to design and build.

The characteristics of the circuit are independent of the coupling loss. Hence, the coupling loss must be chosen to meet the application.

The directivity of the directional couplers contributes to the isolation between the load arms, as one can see from the previous discussion. However, the balancing characteristics do not depend upon the directivity. They depend only on the symmetric arrangement of coupling holes.

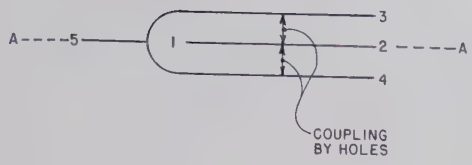

Fig. 3—A simplified schematic of the five-port magic tee.

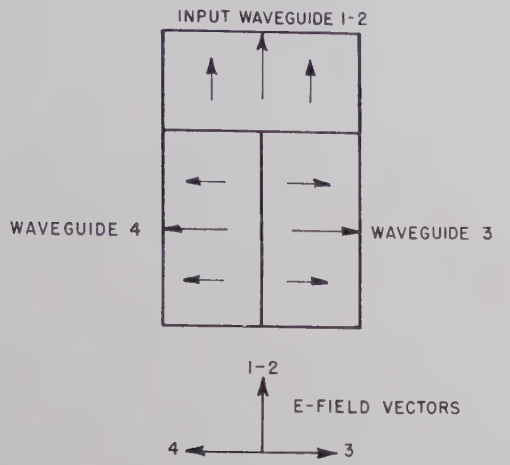

Fig. 4—Electric field phase relation in the cross section of a tee.

The standard magic tee can be converted to a very-broadly-banded matched magic tee using a lossy pad as a matching device. If we compare the modified regular magic tee with our pseudo-magic tee, we can see the following differences.

The modified standard magic tee has as big a loss between output and load arms as between input and load arms. On the other hand, the loss in our pseudo-tee is almost entirely between input and load arm and there is very little loss between the load arms and the output arm.

Furthermore, since the coupling loss in the directional coupler effectively contributes to the isolation between load arms 3 and 4, much greater isolation could be achieved in this way than by the regular magic tee.

This type of pseudo-tee was therefore effectively used to make an extremely sensitive impedance bridge, and measurements were made rapidly and accurately for the various impedances.

In several applications, the coupling loss in the input arm is even desirable. For example, in a balanced mixer, the local oscillator is normally isolated from the rest of the circuit with an attenuator. Here, the attenuator is already included in the tee.

One can modify the five-port tee in several ways. For example, the modification shown in Fig. 7 enables us to introduce simultaneously two signals of different frequencies from different waveguides.

This circuit is effectively used to monitor a high-power balanced circuit. The input power from port 5 is divided equally into arms 3 and 4. Only a fraction of unbalanced power from arms 3 and 4 is detected at arm 1 through small coupling holes.

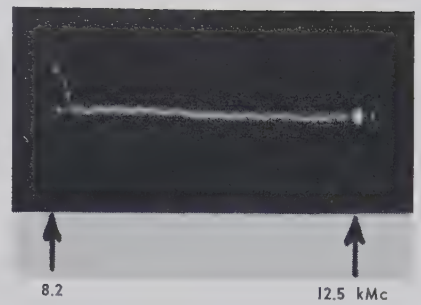

Fig. 5—The frequency characteristics of isolation between ports 1 and 5, with matched loads at ports 2, 3, and 4.

TABLE I

CHARACTERISTICS OF THE FIVE-PORT MATCHED PSEUDO-MAGIC TEE

Frequency in KMC	Isolation* (excluding the coupling loss)† Between Ports 1 and 5 (ports 3 and 4 are shorted) in db	VSWR Port 5‡	Port 1§
8.0	40	1.10	1.3
8.6	75	1.10	1.25
9.0	75	1.09	1.25
9.5	70	1.08	1.20
10.0	75	1.07	1.02
10.5	70	1.14	1.20
10.9	70	1.05	1.00
11.1	70	1.14	1.07

* 70~75 db was the limit of measurement by our instruments.
† The total coupling loss of the directional coupler was 11.5 db in this specific model.
‡ Matched loads at ports 3 and 4.
§ Match load at port 2 and short circuit at ports 3 and 4.

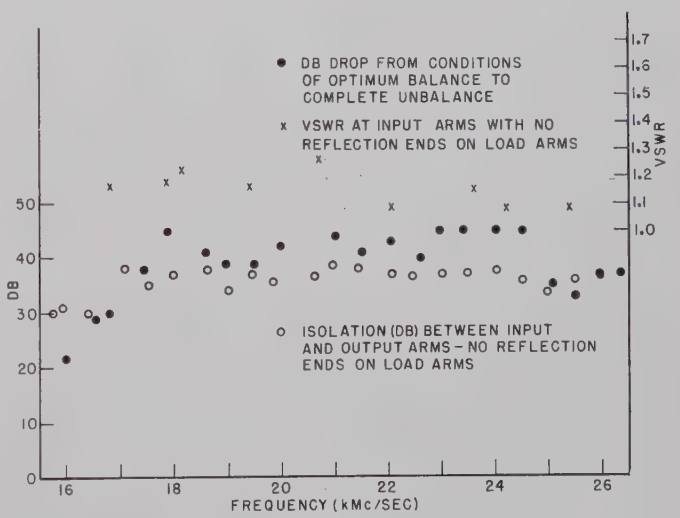

Fig. 6—The frequency characteristics of split waveguide-type magic tee (type 1).

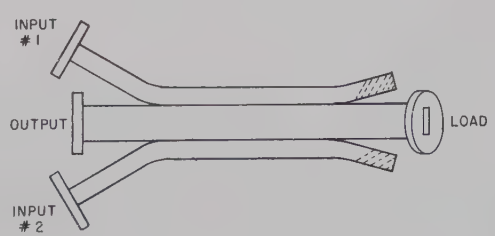

Fig. 7—Modified magic tee.

Theory of Dielectric-Loaded and Tapered-Field Ferrite Devices*

R. F. SOOHOO†, SENIOR MEMBER, IRE

Summary—Loading a ferrite resonance isolator or differential phase shifter with a dielectric or biasing the ferrite with an inhomogeneous dc magnetic field are very useful ways of improving the performance of these ferrite devices. Whereas these methods are very commonly used in transverse-field ferrite devices, no extensive analytical treatment of the subject has appeared in the literature. It is the purpose of this paper to present a theoretical analysis of the problem, chiefly by means of combined boundary-value and perturbation-theory approach. It will be shown that dielectric-loading and tapered-field techniques increase the bandwidth of isolators and phase shifters, the isolation-to-insertion loss ratio of the former, and the phase shift of the latter.

Introduction

TWO of the most important contributions to the improvement of the characteristics of ferrite devices are 1) loading a ferrite resonance isolator or phase shifter with a dielectric, and 2) biasing the ferrite with an inhomogeneous dc magnetic field. Whereas these methods are in general use in present-day ferrite devices, the reasons for their remarkable success are not well understood. It is the purpose of this paper to investigate these problems analytically by means of a combined boundary-value and perturbation-theory approach. In the following sections, we will show that dielectric loading improves the ellipticity ratio and concentrates more energy in the ferrite over a large frequency band as compared with the unloaded case. We will also show that biasing the ferrite by a spatial varying dc magnetic field would give rise to a continuum rather than a single-resonance frequency, thereby increasing the bandwidth of the particular ferrite device.

Fig. 1(b) is the most common configuration used in dielectric-loaded ferrite devices. Because of the large number of boundaries at which the continuity of the tangential components of $\boldsymbol{E}$ and $\boldsymbol{h}$ must be satisfied, the exact solution of the problem is most difficult to obtain. The problem is further complicated by the fact that the ferrite and dielectric do not extend across the entire height of the waveguide, thus requiring the existence of other than the TE_{10} mode, even if the composite structure has such dimensions that all other modes are beyond cutoff. However, the problem is more amenable to treatment by the perturbation theory. In this case, we make the plausible assumption that the ferrite and dielectric cross sections are so small that the electromagnetic field outside the vicinity of the ferrite is not appreciably disturbed. For the configuration of Fig. 1(a), a more realistic solution to the problem may be obtained by solving a combined boundary-value and perturbation problem. Here, we first solve the exact boundary-value problem with only the dielectric slab present; then, the presence of the ferrite is treated as a perturbation.

Since the dc magnetic field is inhomogeneous in the ferrite in Fig. 1(c), the permeability of the ferrite is a function of x, thus rendering any exact boundary-value solution unfeasible. Furthermore, since $b \neq b'$, a pure TE_{10} mode can never exist. Here again, the perturbation theory could be advantageously used to get some physical insight into the behavior of this kind of device.

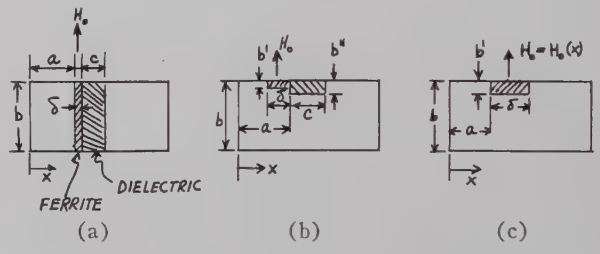

Fig. 1—Configuration of ferrite derives. (a) and (b) Dielectric-loaded devices. (c) Tapered-field devices.

Dielectric Loading

Consider first the case of Fig. 1(a) without the ferrite slab. If the dielectric is centrally located, we may plot $h_{x,y}(x)/\sqrt{P}$, where P is the waveguide power flow, by using the expressions given by Vartanian, *et al.*[1] as is done in Fig. 2 for $\epsilon_d = 9\epsilon_0$, and $kL = 5$ where $k = \omega\sqrt{\mu_0\epsilon_0}$ is the free-space wave number. For comparison, $h_{x,y}(x)$ for an empty waveguide is also shown. From Fig. 2, we note a drastic change in the RF magnetic field distribution due to the presence of the dielectric. In particular, we note that there is a high concentration of electromagnetic field near the dielectric where the ferrite is to be placed. Thus, other things being equal, the absorption and phase shift due to the presence of the ferrite should increase with dielectric loading.

* Received by the PGMTT, September 6, 1960; revised manuscript received, January 13, 1961. A brief account of some of the results of this paper was reported at the PGMTT Natl. Convention, Harvard University, Cambridge, Mass., June, 1959. The research for the paper was carried out while the author was with Cascade Res., Los Gatos, Calif.

† Lincoln Lab., Mass. Inst. Tech., Lexington, Mass.

[1] P. H. Vartanian, W. P. Ayres, and A. L. Helgesson, "Propagation in dielectric slab loaded rectangular waveguide," IRE TRANS. ON MICROWAVE THEORY AND TECHNIQUES, vol. MTT-6, pp. 215–222; April, 1958.

We note further that $h_x \simeq h_y$ over a large portion of the unfilled region of the guide. This result can best be illustrated by plotting h_{x1}/h_{y1} as is done in Fig. 3, again for a centrally-located slab. We note immediately that the ellipticity is remarkably close to unity over most of the unfilled portion of the guide. To emphasize this point, we have plotted in Fig. 3, also, the ellipticity in the same portion of an empty guide.

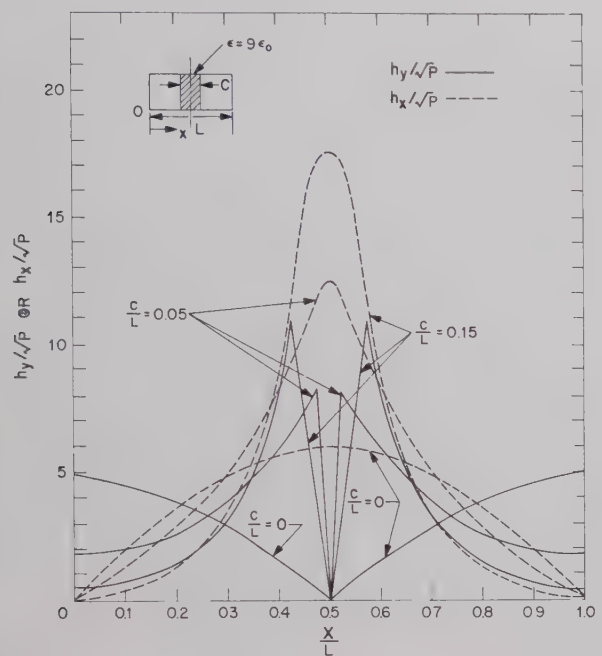

Fig. 2—Normalized RF magnetic-field component vs normalized distance from guidewall of a waveguide loaded by a centrally located dielectric slab at $kL=5$.

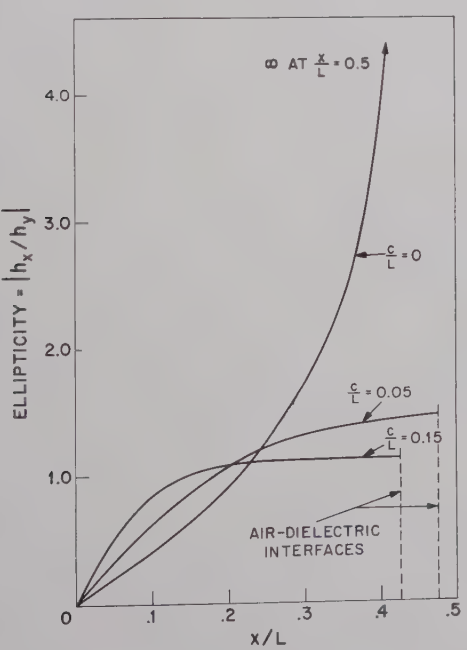

Fig. 3—Ellipticity vs normalized distance from guidewall of a waveguide loaded by a centrally-located dielectric slab at $kL=5$.

From the above discussion, we conclude that the most important effects of dielectric loading are:

1) *The concentration of the electromagnetic field in and near the dielectric*, and

2) *The two planes of circular polarization in an empty guide are smeared into two regions of near circular polarization.*

Next, we should like to investigate the dependence of ellipticity with frequency as is done in Fig. 4. For comparison, we have shown the ellipticity of the empty guide at a location x_0, so chosen that the ellipticity is equal to 1 at midband ($kL=5$). We note here that the variation of ellipticity with frequency may be greatly reduced by dielectric loading.[2]

Ferrite Perturbation

Now, if a thin ferrite slab is placed against the dielectric as shown in Fig. 1(a), a calculation of the propagation constant may be achieved by means of the perturbation formula:[3]

$$\gamma + \gamma_0^* = \frac{j\omega \int_{\Delta s} [(\Delta \underline{\mu} \cdot \boldsymbol{H}) \cdot \boldsymbol{H}_0^* + (\Delta \epsilon \boldsymbol{E}) \cdot \boldsymbol{E}_0^*] ds}{\int_s l_y \cdot (\boldsymbol{E} \times \boldsymbol{H}_0^* + \boldsymbol{E}_0^* \times \boldsymbol{H}) ds}, \quad (1)$$

where $\Delta \underline{\mu} = \mu_0(\underline{\mu} - 1)$ and $\Delta \epsilon = \epsilon_0(\epsilon_r - 1)$. The Polder permeability tensor[4] is $\underline{\mu}$, and $\epsilon_0 \epsilon_r$ is the dielectric constant

[2] We must bear in mind here the difference between internal and external fields, especially with regard to configuration 1(a). For a detailed discussion, see R. F. Soohoo, "Theory and Application of Ferrites," Prentice-Hall, Inc., Englewood Cliffs, N. J., pp. 170–172; 1960.

[3] For derivation, see R. F. Soohoo, *op. cit.*, pp. 264–265.

[4] D. Polder, "On the theory of ferromagnetic resonance," *Phil. Mag.*, vol. 40, pp. 99–115; February, 1949.

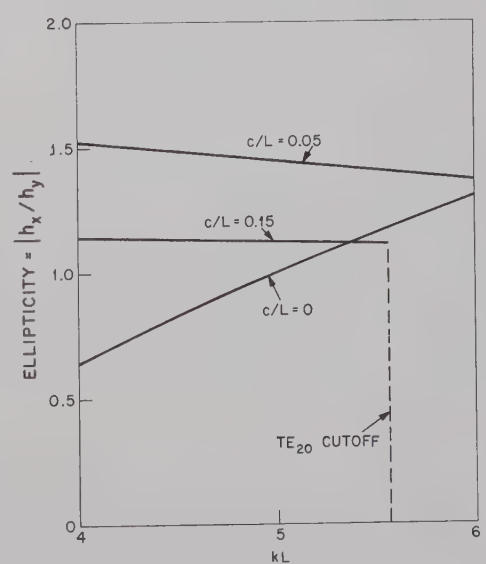

Fig. 4—Ellipticity at the dielectric-air interfaces vs normalized frequency (kL) for a waveguide loaded by a centrally located dielectric slab.

of the ferrite. The cross-sectional areas of the ferrite and guide are Δs and s, respectively. The quantities with and without the zero subscript refer to the electromagnetic fields in the waveguide without and with the ferrite slab, respectively. From (1), we find for the case where the dielectric is centrally located:

$$\frac{\gamma+\gamma_0^*}{j\beta_0}=\frac{A_1\frac{\delta}{2}+A_2\sin k_{ca}(L-c-2\delta)+A_3\sin k_{ca}(L-c)+A_4[\cos k_{ca}(L-c)-\cos k_{ca}(L-c-2\delta)]}{L-c-\frac{1}{k_{ca}}\sin k_{ca}\frac{(L-c)}{2}+\left(\frac{k_{ca}}{k_{cd}}\right)^2\left(c+\frac{\sin k_{cd}c}{k_{cd}}\right)\left\{\frac{\cos k_{ca}\frac{(L-c)}{2}}{\sin k_{cd}\frac{c}{2}}\right\}}, \quad (2)$$

where

$$A_1=\chi_1+\left(\frac{k_{ca}}{\beta_0}\right)^2\chi_2-\frac{\omega^2\mu_0\epsilon_0(\epsilon_r-1)}{\beta_0^2}$$

$$A_2=\frac{1}{4k_{ca}}\left[\chi_1-\left(\frac{k_{ca}}{\beta_0}\right)^2\chi_2-\frac{\omega^2\mu_0\epsilon_0(\epsilon_r-1)}{\beta_0^2}\right]$$

$$A_3=\frac{1}{4k_{ca}}\left[-\chi_1+\left(\frac{k_{ca}}{\beta_0}\right)^2\chi_2+\frac{\omega^2\mu_0\epsilon_0(\epsilon_r-1)}{\beta_0^2}\right]$$

$$A_4=\frac{K}{2\beta_0},$$

and

$$\chi_1=\frac{\gamma_e^2M_0\left(H_0-\frac{i\alpha\omega}{\gamma_e}\right)}{[\gamma_e^2H_0(H_0+M_0)-\omega^2]-i\alpha\omega\gamma_e(2H_0+M_0)}$$

$$\chi_2=\frac{\gamma_e^2M_0\left(H_0+M_0-\frac{i\alpha\omega}{\gamma_e}\right)}{[\gamma_e^2H_0(H_0+M_0)-\omega^2]-i\alpha\omega\gamma_e(2H_0+M_0)} \quad (3)$$

$$K=\frac{\gamma_eM_0\omega}{[\gamma_e^2H_0(H_0+M_0)-\omega^2]-i\alpha\omega\gamma_e(H_0+M_0)},$$

where H_0 and M_0 are dc magnetic field and magnetization, while γ_e and α are the gyromagnetic ratio and damping constant, respectively.

Noting that $A_{1,2,3}$ all contain terms that involve β_0^2, we conclude that these terms cannot give rise to anisotropic effects. On the other hand, A_4 is inversely proportional to the first power of β_0, thus representing anisotropic effects. Thus, it follows that the differential propagation constant is:

$$\gamma_+-\gamma_-=jK\frac{\cos k_{ca}(L-c)-\cos k_{ca}(L-c-2\delta)}{L-c-\frac{\sin k_{ca}\frac{(L-c)}{2}}{k_{ca}}+\left(\frac{k_{ca}}{k_{cd}}\right)^2\left(c+\frac{\sin k_{cd}c}{k_{cd}}\right)\frac{\cos k_{ca}\frac{(L-c)}{2}}{\cos k_{cd}\frac{c}{2}}}. \quad (4)$$

If $\delta/L\ll 1$, the numerator of (15) may be replaced by $-(K''+jK')k_{ca}2\delta\sin k_{ca}(L-c)$. To appreciate the broadbanding effects of dielectric loading, we have plotted the real part of (4) in Fig. 5 for a ferrite whose $\delta=L/100$, $4\pi M_s=2000$ gauss and $\Delta H=450$ oersteds biased to resonance at a frequency corresponding to $kL=4$. The calculation shows that K'' decreases as kL is increased or decreased from a frequency corresponding to $kL=4$, while the remainder of (4) increases with frequency. Thus, for $kL>4$, it is possible to adjust the values of ϵ_d and c so that $\alpha_+-\alpha_-$ would be less sensitive to frequency over a band of frequencies.

An even more instructive comparison would be to place the ferrite slab at $a=L/4$ of an otherwise empty guide. This location corresponds to the plane of maximum differential propagation in a guide loaded only by a thin ferrite slab, as can be shown from (1). In this case, we find that:

$$\gamma_+-\gamma_-\doteq -j2\pi K\delta/L^2. \quad (5)$$

Thus, the bandwidth of the device is solely determined by the line width of the ferrite. This is in contrast to the dielectric-loaded case whereby (4) indicates that the possibility of compensation exists so that $\gamma_+-\gamma_-$ may vary slowly with frequency. Eq. (5) has also been plotted in Fig. 5 for comparison with the dielectric-loading case. The two curves have been normalized at $kL=4$ by dividing $\alpha_+-\alpha_-$ of the dielectric-loaded case by 144, showing that d_+-d_- is some 150 times larger for the dielectric-loaded case due to the concentration of RF field in the ferrite.

For the case where the ferrite and dielectric configuration is as shown in Fig. 1(b), the boundary-value problem with the dielectric alone is extremely difficult to solve exactly. However, if we assume that the RF field just adjacent to the dielectric is nearly the same as that of the case of a guide loaded by a dielectric slab extending completely across the guide, but that the RF field elsewhere is essentially the same as that of the unloaded

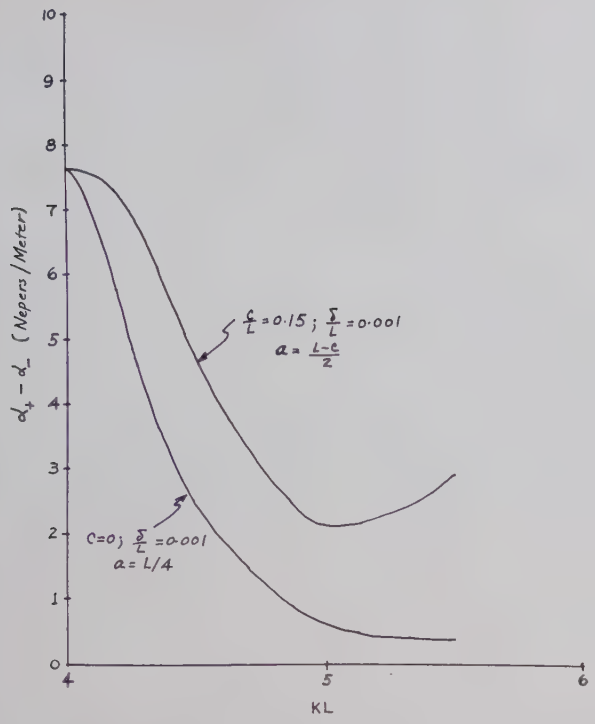

Fig. 5—Differential attenuation vs normalized frequency (kL) for a ferrite isolator loaded and unloaded by a dielectric slab. The normalization factor $(d_+-d_-)_{c=0.15}/(d_+-d_-)_{c=0}$ is equal to 144.

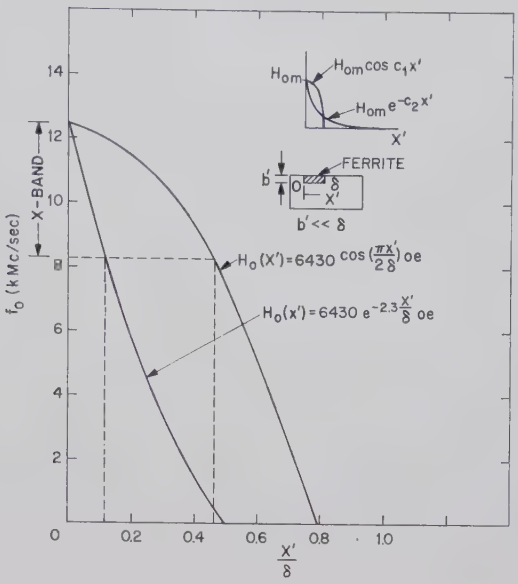

Fig. 6—Resonance frequency of a ferrite sample biased by a tapered dc magnetic field. H_{0m} has been so chosen that $f_0=12.4\ KM_s$ at $x'=0$, while c_1 and c_2 were so chosen that $H_0(x')=0$ and $H_0(x')=0.1\ H_{0m}$ at $x'=\delta$ for the cosine and exponential variations, respectively.

case, we can easily show from (1) that:

$$\gamma_+ - \gamma_- = 2jKk_{ca}(\delta/L)(b'/b)\sin k_{ca}2a. \tag{6}$$

Tapered-Field Theory

If the ferrite sample is biased by a spatially varying static magnetic field as shown in Fig. 1(c), we would expect the resonance frequency of different parts of the ferrite to be different. This should give rise to a *distribution of resonance frequencies* and consequently to broadbanding of the device. In Fig. 6, we have plotted the resonance frequency of the ferrite as a function of distance with both a cosine and an exponential variation of the static magnetic field with the distance x'. It is noted that a large portion of the ferrite has its resonance frequency outside x band, and this portion would act essentially as a dielectric, providing $4\pi M_s$ is not so high that low field losses might occur.

The propagation constant of the structure shown in Fig. 1(c) could again be obtained by the perturbation formula (1). For a given static field distribution, we find:

$$\gamma+\gamma_0^* = \frac{j\omega b'}{Lb\left(\frac{f}{f_c}\right)\sqrt{\left(\frac{f}{f_c}\right)^2-1}\sqrt{\frac{\mu_0}{\epsilon_0}}}\left\{\int_a^{a+\delta}[\chi_3(|h_x|^2+|h_y|^2)+jK(h_xh_y^*-h_yh_x^*)]dx\right.$$
$$\left.-\mu_0\left(\frac{\epsilon_r-1}{\epsilon_r}\right)\left(\frac{f}{f_c}\right)^2\left[\frac{\delta}{2}-\frac{L}{4\pi}\left(\sin\frac{2\pi(a+\delta)}{L}-\sin\frac{2\pi a}{L}\right)\right]\right\} \tag{7}$$

where

$$\chi_3=\frac{\gamma M_0[\gamma H_0(x)+j\omega\alpha-\gamma M_0]}{[\gamma H_0(x)+j\omega\alpha-\gamma M_0]^2-\omega^2}$$
$$K=\frac{\omega\gamma M_0}{[\gamma H_0(x)+j\omega\alpha-\gamma M_0]^2-\omega^2}. \tag{8}$$

In principle, if $H_0(x)$ is specified, (7) could be integrated to obtain $\gamma+\gamma_0^*$. However, the integration is usually difficult except for the very simple distribution of $H_0(x)$.

As a simple example to illustrate the application of (7) to tapered-field problems, we consider the case where $H_0(x)=H_{0m}(1-c_3(x'/\delta))$. To be definite, we may let $H_{0m}=6430\ oe$, as is done in Fig. 6, and let $c_3=4430/6430$ so that $H_0(x)=2000=4\pi M_s$ at $x'=\delta$, such that the entire ferrite slab is saturated. From (7) we find the differential propagation:

$$\gamma_+-\gamma_-=\frac{-j\omega b'\gamma M_0\delta}{Lb\left(\frac{f}{f_c}\right)\sqrt{\frac{\mu_0}{\epsilon_0}}H_{0m}c_3}\left[\log\frac{\frac{\omega}{\gamma_e}+M_0}{\frac{\omega}{\gamma_e}-M_0}-\log\frac{\frac{\omega}{\gamma_e}+H_{0m}-M_0}{\frac{\omega}{\gamma_e}-H_{0m}+M_0}\right]. \tag{9}$$

In the derivation of (9), we have assumed that $K=K'-j0$ for simplicity, so that $\gamma_+-\gamma_-$ will become infinite at resonance. Also, we have assumed that δ is small enough that sin $2\pi x/L$, which occurs in the $h_xh_x^*-h_x^*h_y$ expression, can be replaced by 1 inside the integral, *i.e.*, by setting $x=L/4$ so as to locate the ferrite at the plane of maximum differential propagation.

Further Discussion

From Fig. 3, we observe that the ellipticity for the $c/L=0.15$ case is nearly equal to 1.2, over half of the air-filled region of the waveguide. Thus, a thin slab of ferrite with a width of $x/L\simeq 0.2$ may be placed against the top wall of the waveguide, and adjacent to the dielectric, to obtain good isolation-to-loss ratio or large differential phase shift with low loss over a broad band of frequencies. This configuration has the advantage of higher power-carrying capacity than that of Fig. 1(a). If more isolation or differential phase shift per unit length is desired, two or four ferrite slabs may be placed against the top and/or bottom guide walls on either side of the dielectric slab. In this case, the ferrite slabs on the opposite sides of the dielectric should be oppositely magnetized.

When $\omega<|\gamma_e|(H_a+M_s)$, where H_a is the anisotropy field, low field losses may occur when the ferrite is not saturated. Thus, in the design of tapered-field devices, care should be taken so that the ferrite is saturated at all points, if low field losses would otherwise occur. If the dc magnetic-field configuration is such that this cannot be achieved, it would be best to eliminate the unsaturated portion or to replace that portion by a dielectric of about the same dielectric constant.

Theory of TEM Diode Switching*

ROBERT V. GARVER†, MEMBER, IRE

Summary—**The theory of TEM diode switching is presented for the purpose of understanding and designing TEM microwave diode switches. A few experimental results are reported for the purpose of supporting the theory and demonstrating the exceptional bandwidth possible.**

An analysis is given of the switching action of one and of two or more diodes as well as the biasing of the center conductor of a TEM transmission line over broad-frequency bandwidths without interacting with the RF signal. The use of point-contact germanium, varactor, and gold-bonded germanium diodes for TEM switching is discussed. Some considerations of switching speed and maximum power-handling capacity are given.

A coaxial transmission line switch has been constructed in which two gold-bonded diodes provide 26-db or greater isolation and insertion loss ranging from 1.6 db to less than 1 db from 40 Mc to 4000 Mc. The addition of a bias lead should increase the insertion loss 0.4 db or less over the 100-to-1 bandwidth, the maximum increase being at the upper and lower bounds.

I. Introduction

FOR SOME years a technique for switching microwaves in X-band waveguide with semiconductor diodes has been in use [1]. Attempts to understand this switching action led to a theory of semiconductor diode microwave switching by use of point-contact germanium diodes [2]. Other investigators found a more direct theory for isolation [3] and proved the good possibilities of using varactor diodes [4] and gold-bonded diodes [5] in coaxial transmission lines for switching. This report covers a more thorough investigation of the theory of TEM microwave diode switching and presents some modes of operation heretofore unreported.

When discussing diode switching it is necessary to define certain terms. RF power incident on an ideal attenuating device is either absorbed in or transmitted past the device, with no power reflected. The attenuation α of the device is defined as the ratio in decibels of the incident power to the transmitted power. If the attenuation of the device can be changed from some low value to some high value the device is called a switch. The insertion loss δ is defined as the minimum attenuation, and the isolation η is defined as the maximum attenuation.

When a diode is inserted in series or in shunt in a transmission line, RF power incident on the diode is reflected by, absorbed in, or transmitted past the diode. A diode is different from an attenuating device in that most of the incident RF power not transmitted is reflected rather than absorbed. In fact, in an ideal diode switch, the incident power is either completely reflected or completely transmitted. The definitions of attenuation, insertion loss, and isolation are the same for a diode switch as for an absorption switch.

* Received by the PGMTT, September 20, 1960.
† Diamond Ordnance Fuze Laboratories, Washington 25, D. C.

II. Basic Concepts

To obtain attenuation by use of a single diode element in a TEM wave transmission line, the diode is mounted either in series with the center conductor or in shunt across the center and outer conductors. The derivation of attenuation will be briefly reviewed. For a more thorough treatment see Riebman [3].

The RF power transmitted past the diode is, in all cases, the power delivered to the matched load. The incident RF power must be visualized as the forward traveling wave incident on the diode, considered for the moment to be in a holder which is a four-terminal transmission line device [6]. For the purpose of deriving the attenuation resulting from diode impedance and admittance, the diode is visualized as a two-terminal device whose RF impedance can be varied by changing the applied voltage. The equivalent circuits are shown in Fig. 1. If the diode is considered to be of zero thickness and in a bilaterally matched transmission line, then the equivalent circuits are valid for most calculations.

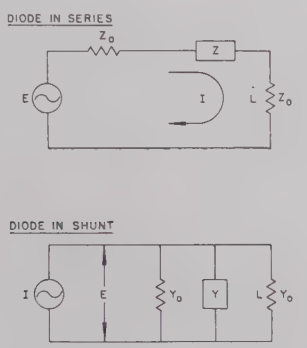

Fig. 1—The equivalent circuits of a diode impedance Z in series and admittance Y in shunt in a transmission line.

In the equivalent circuit of a series-connected diode (Fig. 1), E is the peak amplitude of the sinusoidal voltage source which is assumed to have an output impedance Z_0; Z represents the diode, and $L(=Z_0)$ is the matched load behind it. I is the peak amplitude of the resulting sinusoidal current. The power P_L in L is given by

$$P_L = \tfrac{1}{2}II^*Z_0. \tag{1}$$

If $Z=R+jX$ then the power P_T transmitted to the load is given by

$$P_T = \frac{1}{2}\,\frac{E^2Z_0}{(R+2Z_0)^2+X^2}. \tag{2}$$

The power P_i incident on the diode is the power in the forward traveling wave going toward L. This is attained in the series equivalent circuit by setting Z equal to zero. So

$$P_i = \frac{E^2}{8Z_0} \tag{3}$$

and the resulting attenuation is

$$\alpha = 10\log\frac{P_i}{P_T} = 10\log\frac{\left(\frac{R}{Z_0}+2\right)^2+\left(\frac{X}{Z_0}\right)^2}{4}. \tag{4}$$

For a diode in shunt having an admittance $Y=G+jB$, the derivation of attenuation is the same as above with the substitution of Y for Z, I for E, etc. Thus,

$$P_L=\tfrac{1}{2}EE^*Y_0 \tag{5}$$

and

$$\alpha = 10\log\frac{\left(\frac{G}{Y_0}+2\right)^2+\left(\frac{B}{Y_0}\right)^2}{4}. \tag{6}$$

Equi-attenuation curves are circular arcs on a rectangular grid plot of normalized impedance or admittance with their centers at $-2+j0$ and radii of $2\times10^{\alpha/20}$, or circular arcs on the Smith Chart as shown in Fig. 2.

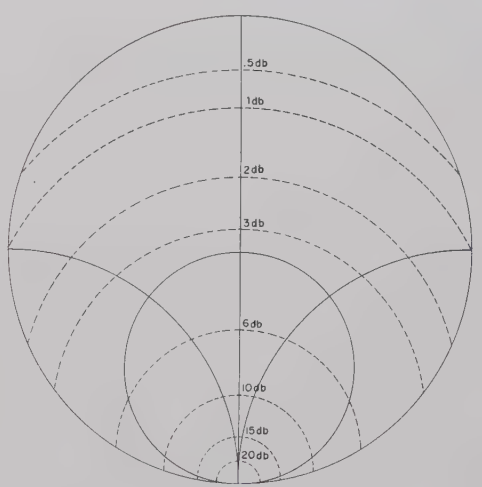

Fig. 2—Smith Chart plot of equal attenuation curves.

The diodes most suited for switching at high frequencies are the point-contact germanium, gold-bonded, and varactor diodes by virtue of their low spreading resistance (R_s) at forward bias and small depletion layer capacitance (C_d) at reverse bias (Fig. 3). In the fabrication of these diodes use is made of a fine wire, or whisker, that makes contact with the active region of the diode. The whisker and semiconductor are each attached to pieces of metal that are supported by a ceramic or glass tube, and to which the diode connecting leads are attached. This whisker introduces a small but not negligible series inductance (L_W). An appreciable capacitance exists between these metal end pieces, denoted as the cartridge capacitance C_c in Fig. 3. This capacitance is 0.16 pf for the 1N23 and 1N263 microwave cartridges, and is much less for the glass cartridge used with gold-bonded diodes. L_w varies from 2 to 10 nh depending on

the length and diameter of the whisker. C_d ranges from 0.05 to 0.2 pf, some good gold-bonded diodes giving 0.2 pf and the best varactors giving 0.05 pf. For point-contact germanium diodes, C_d varies from 0.2 pf at low frequencies to 0.015 pf at UHF. In available diodes, R_s ranges from 3 ohms for gold-bonded diodes to 10 ohms for varactors and point-contact germanium diodes. The reactance of these parameters in the frequency range of interest is plotted in the reactance frequency chart of Fig. 4.

At forward bias, the equivalent circuit (Fig. 3) is valid for all three types of diodes. At reverse bias, the equivalent circuit is valid for varactors and gold-bonded diodes, but is invalid for point-contact germanium diodes because C_d has a resistance in parallel with it which is about 5000 ohms [2].

In Fig. 5, the attenuation from a diode shunting a 50-ohm transmission line is plotted as a function of diode impedance. The R_s of forward-biased diodes will allow 10- to 20-db isolation at frequencies below 200 Mc, since the reactance of L_w will generally be less than 5 ohms below this frequency.

At reverse bias, the capacitance C_c+C_d is the dominant impedance. The insertion loss for $C_c+C_d=0.2$ pf is less than 0.1 db for all frequencies below 5 Gc. Note from Fig. 5 that if $R_s=50$ ohms and $L_w=2$ nh, which may be found in a gold-bonded diode, it is possible to have a constant isolation of 3 db with a very low insertion loss for all frequencies up to that corresponding to $2\pi fL_w=30$ ohms, which is 2 Gc. A very flat, low-insertion loss, 3-db modulator is then possible. Other values of isolation are possible by selecting the proper R_s.

For a diode in series in a 50-ohm transmission line the attenuation is depicted in Fig. 6 as a function of the diode impedance. The diode impedances at forward bias for frequencies below 2 Gc result in insertion loss in the 1-db region. In conjunction with Fig. 4, Fig. 6 reveals that a capacitance C_d+C_c of 0.2 pf results in isolation of approximately 20 db up to about 1 Gc. Figs. 5 and 6 in conjunction with Fig. 4 are useful for quickly determining the frequency range and basic configuration in which a diode can be made to switch. From these figures it is apparent that the available diodes give greater isolation at higher frequencies without considerable sacrifice in insertion loss when used in the series configuration in a 50-ohm TEM transmission line. In general, if the diode impedance is variable from $1/20Z_0$ to $4Z_0$, the shunt configuration is indicated; and if the diode impedance is variable from $1/4Z_0$ to $20Z_0$,

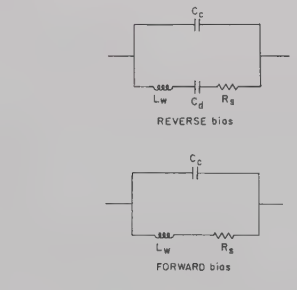

TYPICAL VALUES

	POINT CONTACT GER. DIODES	GOLD BONDED DIODES	VARACTOR DIODES
R_s—Ω	6	4	10-2
L_w—nh	5	2	5
C_d—pf	.015	.2	2-.05
C_c—pf	.16	.05	.16

Fig. 3—Equivalent circuits of a diode at reverse bias and forward bias.

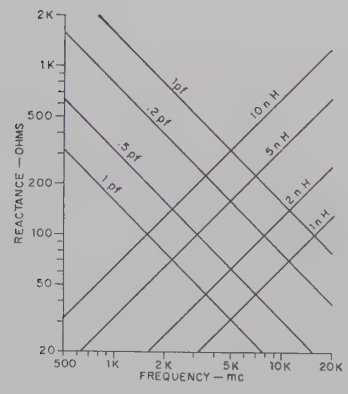

Fig. 4—Enlarged reactance-frequency plot.

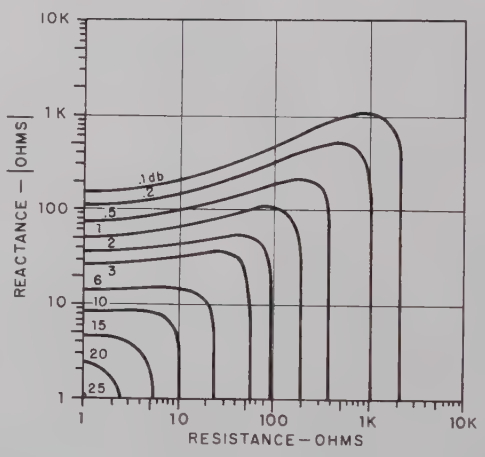

Fig. 5—Attenuation resulting from a diode shunting 50-ohm transmission line as a function of diode impedance.

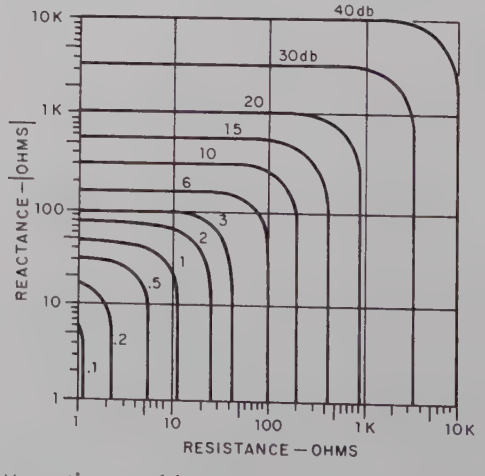

Fig. 6—Attenuation resulting from a diode in series in 50-ohm transmission line as a function of diode impedance.

the series configuration is indicated. Note also that switching improves as frequency decreases, indicating broad-band switching down to any desired frequency.

III. Diode Modes

A. Series Diode

As a function of frequency, the computed attenuation of a series diode in a 50-ohm transmission line is shown in Fig. 7. The equivalent circuit parameters shown in Fig. 3 are $C_c=0.2$ pf, $L_w=5$ nh, $C_d=0.2$ pf, and $R_s=5$ ohms. It is assumed that these parameters do not change drastically with frequency. From Fig. 7 it is seen that high isolation is available at three frequencies, which are labeled Modes 1, 2, and 3. In Mode 1, the insertion loss is low, as previously discussed. The isolation of Mode 2 is the result of parallel resonance between C_c and L_w at forward bias, and the insertion loss is the result of a series resonance between L_w and C_d at reverse bias. By picking $C_c=C_d$, these resonances are made to occur at the same frequency so that Mode 2 has a low insertion loss. Mode 3 is caused by the reverse bias parallel resonance between C_c and L_w in combination with C_d.

1) Mode 1: Expanded curves for Mode 1 are shown in Fig. 8. Here it is assumed for the C_c+C_d curves that the diode is at reverse bias and $R_s=L_w=0$. For the L_w curves it is assumed that the diode is at forward bias and $C_c=0$ and $R_s=5$ ohms. One sees that the combination of $C_c+C_d=0.2$ pf and $L_w=5$ nh allows for 10 db or greater switching up to 2 Gc. It is also seen how with a given C_c+C_d the isolation increases with decreasing frequency. This increase continues until the reactance of C_c+C_d becomes greater than the depletion region resistance, at which point the resistance becomes the predominant factor in determining the isolation.

With Mode 1 operation, the insertion loss becomes undesirably large at higher frequencies due to L_w; at 2 Gc, 5 nh already results in 2-db insertion loss. Another effect of L_w is to decrease isolation slightly by lowering the reactance presented by C_c+C_d. Because the whisker is of nonzero length it can be more accurately described as a short length of high-impedance TEM-wave transmission line, and the effect of L_w will be slightly less than depicted in Fig. 8.

A method of decreasing the effect of L_w is to increase the distributed capacitance from the inner conductor to the outer conductor in the region of the diode, thus maintaining $Z_0=\sqrt{L/C}=50$ ohms. A technique for attaining this without greatly increasing C_c is shown in Fig. 9. The length of the abrupt 50-ohm tapers is controlled to provide the desired amount of shunt capacitance.

2) Mode 2: Mode 2 will normally exist for most diodes, but the maximum isolation and minimum insertion loss may not occur at the same frequency. To cause them to occur at the same frequency, C_c can be increased as illustrated in Fig. 10 so that $C_c=C_d$. To reduce the frequency of the maximum isolation, it is necessary to apply less than maximum reverse bias which increases C_d. To increase this frequency it is necessary to decrease L_w. Riebman [4] found Mode 2 to be useful between 8 and 12 Gc.

3) *Mode 3:* As seen from Fig. 7, Mode 3 has an associated high insertion loss. One method of decreasing the insertion loss is to increase the separation between Modes 2 and 3. When this is done by increasing C_c, both modes move down in frequency as the separation increases and the maximum isolation of Mode 3 decreases. Attempts to increase the operating frequency of Mode 3 result in a decrease of separation between Modes 2 and 3, plus a higher insertion loss for Mode 3. A more suitable method for decreasing the insertion loss is to place an inductor in series with the diode. The diode at forward bias at Mode 3 is capacitive, and a series resonance results in reduced insertion loss. The series inductance may be a short length of high-impedance transmission line immediately adjacent to the diode.

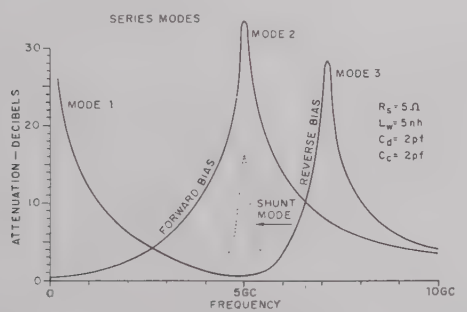

Fig. 7—Switching modes of a diode in series in 50-ohm transmission line.

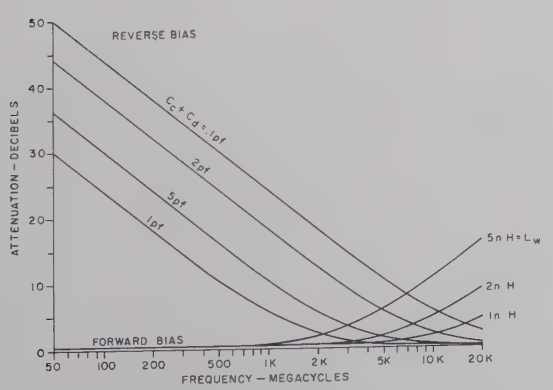

Fig. 8—Detailed presentation of Mode 1 operation. For the "C_c+C_d" curves it is assumed that the diode is at reverse bias and that $R_s=L_w=0$. For the "L_w" curves it is assumed that $C_c=0$ and $R_s=5$ ohms. These same curves describe the bandwidth of the isolation and insertion loss of the diode operating in the other series modes.

B. Shunt Diode

Fig. 11 shows the computed attenuation of a shunt diode in a 50-ohm transmission line as a function of frequency. The diode equivalent circuit parameters are the same as those picked for the series diode of Fig.

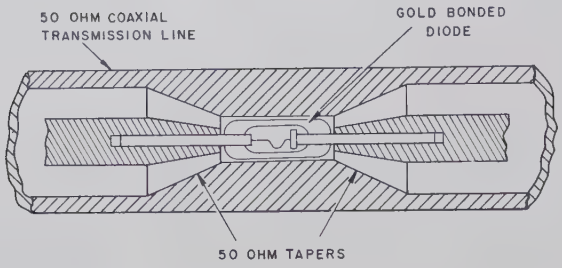

Fig. 9—Phantom view of a diode in a configuration for increasing the capacitance to the outside conductor (without increasing C_c) to reduce the effect of L_w.

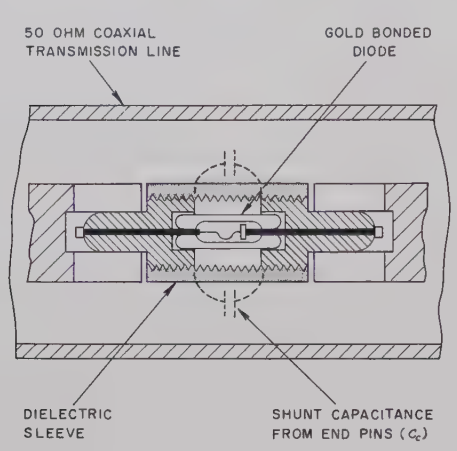

Fig. 10—Phantom view of a diode in a configuration for controlling Mode 2 operation by increased cartridge shunt capacitance.

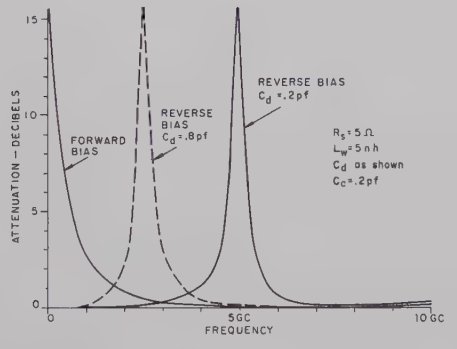

Fig. 11—Switching modes of a diode shunting 50-ohm transmission line.

7. At forward bias, high isolation occurs only at low frequencies. At reverse bias, high isolation occurs only at the frequency corresponding to the series resonance between L_w and C_d. The insertion losses associated with the low and high isolation frequencies are very low because of the high reactances of C_c+C_d, and L_w, respectively. A curve for the resonant shunt mode is also given in Fig. 7 for comparison with the curve for series Mode 2 with respect to bandwidth and maximum isolation.

A very efficient switch can be made using a varactor as a shunt diode. If it is assumed that the varactor capacitance C_d can increase to 0.8 pf before conduction starts, then the resonant shunt mode will appear as shown by the dashed curve in Fig. 11. The switch behaves as a voltage-tunable, band-rejection filter, drawing practically no current and able to cause switching at any frequency in its tunable range. At the two frequencies shown, 2.5 and 5 Gc, the attenuation can be varied from 15 db to less than 0.2 db. Section V below will show that the use of more than one diode will increase the isolation and bandwidth beyond that attainable with a single diode. The frequency range of this configuration can be further controlled by placing additional inductance in series with the diode. The insertion loss resulting from C_c can be decreased by making the center conductor diameter smaller, which increases the coaxial line inductance per unit length, keeping $Z_0=\sqrt{L/C}=50$ ohms constant. This configuration provides a very efficient switch for low-power microwaves since the switching occurs entirely at reverse bias, drawing essentially no current.

C. A Modified Series Mode

1) Mode 1½: Riebman [4] has developed a technique for extending the range of Mode 1-type operation by placing an inductor L_T in parallel with C_c+C_d to resonate with their reactance and restore high isolation. This technique will be called Mode 1½ operation. Here the technique of reducing the effect of L_w is useful to maintain low forward bias insertion loss at these higher frequencies. The equivalent circuit for Mode 1½ operation is shown in Fig. 12. L_T is the inductor used in tuning C_c+C_d to the desired operating frequency range. C_b prevents L_T from shunting out the dc switching voltage. It was shown by Riebman [4] that the design frequency should be the geometric mean of the minimum and maximum frequencies of the desired operating range. The isolation is then equal at the extremes. A Mode 1½ diode switch can be fabricated easily by wrapping eight turns of fine enameled wire around the 1N263 glass tube with several closely packed tight turns around the pin ends of the diode. The insulation is left on the fine wire to provide C_b at the ends. The wire can then be anchored with Q dope. Such a configuration will be optimum at about 1 Gc. Based upon C_d+C_c of 0.2 pf, calculated isolations for Mode 1½ are shown in Fig. 13 for several design frequencies. Average isolation values for two AEL Model CM/2/4 diode switches are shown as the plotted points in Fig. 13. The operation can be shifted down in frequency by applying less than maximum reverse bias voltage on the diodes. (Note that for a given isolation, the bandwidth in Mc remains constant for a given C_d+C_c rather than the ratio of upper frequency to the lower frequency remaining constant.) The bandwidth and maximum isolation at the resonant frequency are given in Section IV. The bandwidth is exactly the bandwidth of Mode 1 which is plotted in Fig. 8. It is seen that for lower C_d+C_c greater bandwidth is possible. Lowering the operating frequency by reducing the reverse bias thus reduces the bandwidth as well. For lower frequency operation of Mode 1½, a resonance between L_T and

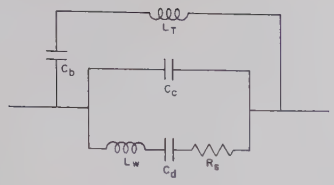

Fig. 12—Equivalent circuit for Mode 1½ operation.

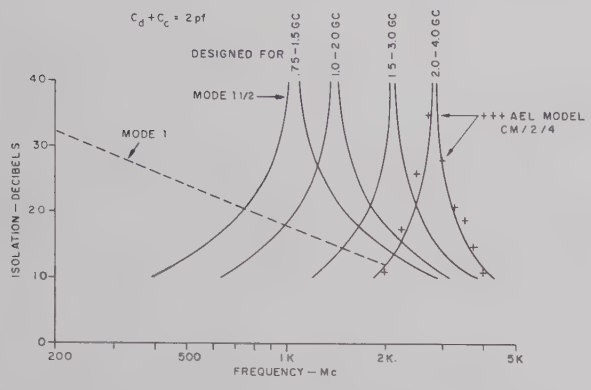

Fig. 13—Isolation for Mode 1½ switching for various tunings.

C_b must be avoided by making C_b large. The construction used in the CM/2/4 attains this as well as being rugged. The Mode 1 curve for $C_d+C_c=0.2$ pf is given in Fig. 13 to show the improvement at higher frequencies afforded by Mode 1½.

IV. Bandwidth

A. Isolation

The isolation of a series diode switch results from the high reactive impedance of the diode. In a 50-ohm transmission line, when $R/Z_0 \ll 1$ and $X/Z_0 \geq 6$, the isolation given by (4) reduces to

$$\eta \approx 20 \log \frac{|X|}{100} \tag{7}$$

with an error of less than 5 per cent. This relation is valid for isolation greater than 10 db and frequencies slightly away from any resonances. Thus, for a specified isolation, the required series reactance is

$$|X| = 100 \times 10^{\eta/20}. \tag{8}$$

If X is due to a parallel combination of L and C (such as L_T and C_c+C_d in Fig. 12), the susceptance of the pair is

$$\frac{1}{X} = 2\pi fC - \frac{1}{2\pi fL}. \tag{9}$$

Solving for f:

$$f = \frac{1}{4\pi CX} + \frac{1}{2\pi}\sqrt{\frac{1}{4C^2X^2} + \frac{1}{LC}}. \tag{10}$$

Given a value of X, the isolation will increase as the parallel resonant frequency is approached and then decrease to the same isolation as $-X$ is approached. The bandwidth is the difference between the frequencies that correspond to X and $-X$. Over the bandwidth, the isolation is maximum at parallel resonance and minimum at the extremes which correspond to X and $-X$. Substituting $-X$ for X in (10) and then subtracting from the same, the bandwidth is obtained:

$$\Delta f = f(X) - f(-X) = \frac{1}{2\pi C|X|} = [200\pi C \times 10^{\eta/20}]^{-1}. \tag{11}$$

Note that L does not appear in the equation and that the isolation bandwidth is a function of specified isolation and C (and Z_0) only.

For Mode 1, L is assumed to be infinite. The isolation results from a capacitor alone in series in the transmission line. Thus Fig. 8 shows not only an extended plot of Mode 1 operation, but also shows the plot of isolation bandwidth, (11).

The resonance causing Mode 2 isolation is between C_c and L_w (Fig. 3). In this case C_c rather than C_c+C_d determines the bandwidth. If $C_c=C_d$, Mode 2 bandwidth is twice that of Mode 1 (Fig. 7).

Mode 3 is the result of a series-parallel antiresonance of C_c, L_w, and C_d, which occurs at $\sqrt{2}$ times the center frequency of Mode 2 when $C_c=C_d$ and has the same bandwidth as Mode 1.

Mode 1½ (Fig. 13) is a resonance between L_T and C_c+C_d; thus, the bandwidth is determined by C_c+C_d. The Mode 1½ technique can be visualized as simply causing Mode 1 operation to be shifted to higher frequencies, since their bandwidths are exactly the same.

At and near the parallel resonance between L and C, the isolation is limited by any R in series with L or C. At resonance, the impedance of the diode is $Z \approx X^2/R+j0$ where X is the reactance of the L or C in series with R. The isolation from this impedance in a 50-ohm transmission line is

$$\eta \approx 20 \log \frac{X^2}{100R}. \tag{12}$$

For Mode 1½, C_d is in series with R_s. For Mode 2, L_w is in series with R_s. For Mode 3, the inductive reactance of the L_w, C_d combination is in series with R_s; and at resonance, their reactance is equal to that of C_c.

The bandwidth of a diode switch shunting the transmission line is similar in derivation to that of the series diode. The isolation results from the low impedance of a series resonance between an L and a C. Isolations above 10 db in a 50-ohm transmission line are given approximately by

$$\eta = 20 \log \left(\frac{25}{|X|}\right), \tag{13}$$

where X is the shunting reactance.

Solving for $|X|$:

$$|X| = 25 \times 10^{-\eta/20}. \tag{14}$$

The reactance of the shunting series LC is

$$X = 2\pi fL - \frac{1}{2\pi fC}. \tag{15}$$

Solving for f,

$$f = \frac{X}{4\pi L} + \frac{1}{2\pi}\sqrt{\frac{X^2}{4L^2} + \frac{1}{LC}}. \tag{16}$$

Substituting $-X$ for X as before, and subtracting:

$$\Delta f = f(X) - f(-X) = \frac{|X|}{2\pi L} = \frac{25}{2\pi L} \times 10^{-\eta/20}. \tag{17}$$

It is seen here that the bandwidth is dependent only on L and η (and Z_0).

Comparison is made between the bandwidths of series and shunt switches at the 20-db points. They are, respectively, $1/2000\pi C$ and $25/20\pi L$. Assuming R_s is low enough to allow good shunt switching, L must be no larger than $2500C$ for equal bandwidths. A capacitance of 0.2 pf is readily available. For an equal bandwidth, then, an inductance of 0.5 nh is needed. Such a small inductance is obtainable in pill-type diode cartridges designed for stripline applications. With a whisker inductance of 2 nh, the bandwidth of the shunt switch is only one fourth that of the series switch. If the frequency of the resonant shunt mode is lowered by increasing the series inductance, the bandwidth is decreased. Electrically tuning the resonant shunt mode as in Fig. 11 does not alter the bandwidth.

B. Insertion Loss

The insertion loss of a series diode switch results either from the low impedance of R_s and L_w for Mode 1, or a series resonance between C_d and L_w for Mode 2.

$$Z = R_s + j\left(2\pi fL_w - \frac{1}{2\pi fC_d}\right) = R_s + jX. \tag{18}$$

From Section II, the insertion loss in a 50-ohm transmission line is given by the relation

$$\delta = 10 \log \left[\left(1 + \frac{R_s}{100}\right)^2 + \left(\frac{X}{100}\right)^2\right]. \tag{19}$$

Solving for X:

$$|X| = 100\left[10^{\delta/10} - \left(1 + \frac{R_s}{100}\right)^2\right]^{1/2}. \tag{20}$$

Solving for the bandwidth as before:

$$\Delta f = \frac{|X|}{2\pi L_w} = \frac{50}{\pi L_w}\left[10^{\delta/10} - \left(1 + \frac{R_s}{100}\right)^2\right]^{1/2}. \tag{21}$$

The insertion-loss bandwidth is not a function of C_d and is also plotted in Fig. 8.

The insertion loss of a shunting diode in the frequency range of interest (Fig. 11) is less than some maximum value δ from zero to a maximum frequency f_{max} at reverse bias; at forward bias it is below δ for frequencies above a minimum frequency f_{min}. The insertion loss of a shunting diode comes from low susceptance and negligible conductance. From (6):

$$\delta = 10 \log\left[1 + \left(\frac{B}{2Y_0}\right)^2\right] \approx 4.35\left(\frac{B}{2Y_0}\right)^2 \tag{22}$$

for a small insertion loss.

Solving for B in a 50-ohm transmission line:

$$B = \frac{\sqrt{\delta}}{52}. \tag{23}$$

At reverse bias:

$$B = 2\pi fC, \quad \text{and} \quad f_{max} = \frac{\sqrt{\delta}}{327C}. \tag{24}$$

The insertion loss is less than δ up to f_{max}. At forward bias:

$$B = \frac{1}{2\pi fL_w} \tag{25}$$

and

$$f_{min} = \frac{1}{2\pi BL_w} = \frac{8.28}{\sqrt{\delta}\, L_w}. \tag{26}$$

The insertion loss is less than δ above f_{min}. If a resonant shunt diode switch is to be made by using pill-type diodes in stripline, C_c may have to be increased to cause the insertion loss to be reduced at the switching frequency.

C. Diode Quality Factor, f_c

The bandwidth of the series diode switch (Mode 1) for given values of isolation η and insertion loss δ can be derived in terms of the diode quality factor, or the so-called cut-off frequency f_c.

$$f_c = \frac{1}{2\pi CR_s}. \tag{27}$$

From (11), the derived expression for bandwidth is

$$\begin{aligned}\Delta f &= [200\pi C \times 10^{\eta/20}]^{-1} \\ &= [(2\pi C)(2Z_0 \times 10^{\eta/20})]^{-1} \\ &= f_c \frac{R_s}{2Z_0} 10^{-\eta/20}.\end{aligned} \tag{28}$$

The insertion loss is usually more broadband than the isolation, and this will be considered to be frequency independent, as expressed by (4);

$$\delta = 20 \log \left(1 + \frac{R_s}{2Z_0}\right)$$

$$\approx 8.7 \frac{R_s}{2Z_0}. \tag{29}$$

Rearranging (29), and substituting into (28), we obtain

$$\Delta f = f_c \frac{\delta}{8.7} 10^{-\eta/20}. \tag{30}$$

A diode of $f_c = 200$ Gc can give 30-db or greater isolation and 0.2-db insertion loss over 147-Mc bandwidth, or it can give 20-db or greater isolation and 0.5-db insertion loss over 1150-Mc bandwidth. The transmission line characteristic impedance Z_0 is varied to give the desired combination.

V. Multiple Switching Elements

Where higher isolation is required than is possible with one diode, two or more diodes may be used [7]. The total isolation from multiple diodes is a function of the spacing between them. At optimum spacing, the total isolation is larger than the sum of individual isolations. For theoretical analysis, the diodes in the isolating state are considered to be equal, lossless reactances. The spacing between two equal reactances for minimum reflected power is a function of their normalized reactance [9]. For maximum reflected power, the spacing l/λ_g is a quarter wavelength different from that for minimum reflection (Appendix I),

$$\frac{l}{\lambda_g} = \frac{1}{4} + \frac{1}{2\pi}\left[\tan^{-1}\frac{2}{X/Z_0}\right]. \tag{31}$$

Eq. 31 is plotted in Fig. 14 as the curve intersecting the l/λ axis at 0 and 0.5. The curve for minimum reflection is shown as the curve intersecting the l/λ axis at 0.25. The relations are the same whether the reflectors are in series or in shunt. The spacing for mismatch is optimum not only for two elements but also for any number of elements. Using the transmission line equation, the attenuation of two equal reactances was calculated as a function of separation and plotted as equi-attenuation curves in Fig. 14. A Mode 1 series diode and a nonresonant mode shunt diode are a negative reactance and susceptance, respectively. For example, assume they are represented by the point at -4 on the maximum reflection curve in Fig. 14. For a maximum isolation at some high frequency, l/λ is made 0.175. As the frequency is decreased, l/λ decreases for a fixed l and the reactance or susceptance increases, causing the plot of the parameters to follow a hyperbola. Following the hyperbola, increasingly higher equi-attenuation curves are intersected, indicating not only improved isolation at the highest frequency but ever increasing attenuation at lower frequencies. The calculated isolation of two elements for a fixed spacing follows closely a curve for a smaller capacitance as in Fig. 8. Thus, the series Mode 1 and the nonresonant shunt mode can be extended up in frequency with no sacrifice in isolation at lower frequencies.

When equal reactive elements are spaced for maximum attenuation, the total attenuation is greater than the sum of individual attenuations. This is termed extra attenuation α_{xn}. In Appendix I, α_{x2} is derived and a simplified calculation for other α_{xn} is described. The extra attenuation for $n = 1, 2, 3, 4$ and ∞ is plotted in Fig. 15. If one diode gives α_1-db attenuation, then the total attenuation α_T of N optimum spaced identical diode is

$$\alpha_T = N\alpha_1 + \sum_{n=1}^{N} \alpha_{xn}. \tag{32}$$

As an example of the use of multiple diodes, suppose it is desired to extend Mode 1 operation to 4 Gc, using two gold-bonded diodes having a $C_c + C_d$ of 0.2 pf, and R_s of 5 ohms, and an L_w that is negligible. At 4 Gc the capacitive reactance is 200 ohms (Fig. 4), which corresponds to an X/Z_0 of -4. Then, according to Fig. 14, the spacing should be 0.175 λ_g. In an air dielectic coaxial line, this spacing is 0.519 inch. Now, by Fig. 8, the isolation with 0.2 pf at 4 Gc is 7 db. By Fig. 15 and (32), the total isolation at 4 Gc is 19.2 db. The isolation

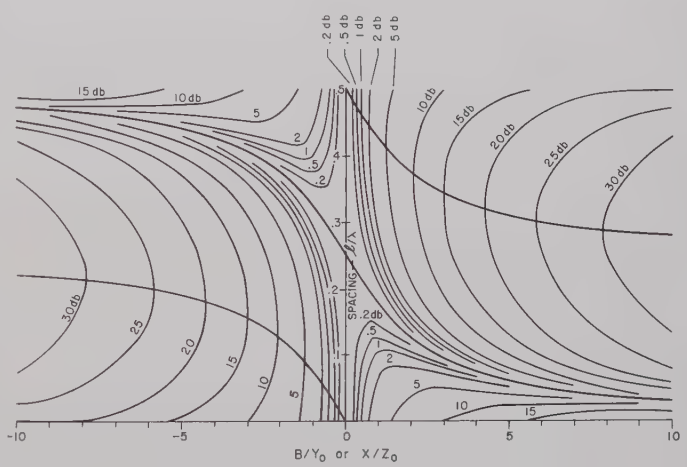

Fig. 14—Attenuation of two equal reactive (or susceptive) elements as a function of their separation and normalized reactance (or susceptance). The curve for match intersects the l/λ axis at 0.25 while the mismatch curves intersect it at 0 and 0.5.

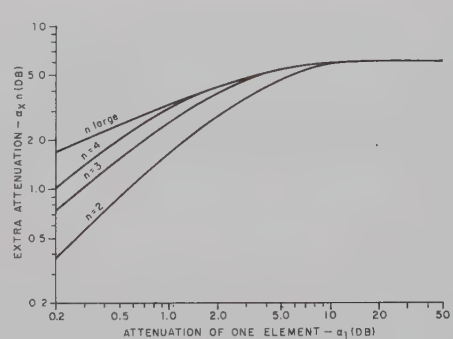

Fig. 15—Extra attenuation resulting from a second, third, and fourth equal element and the limit approached for many equal elements, as a function of the attenuation of one element.

of these two diodes with a fixed spacing was calculated for decreasing frequency and was found to behave approximately as that of $C_c+C_d=0.04$ pf. If L_w is sufficiently small, each diode will have about 0.5-db insertion loss at forward bias. Being nonreactive, the insertion loss adds with no extra attenuation; thus, the insertion loss of two of these diodes should be about one db.

As another example, the calculated isolation of four 0.2-pf diodes at 10 Gc with optimum spacing is 20 db. If L_w is reduced below 0.5 nh, the insertion loss would be about 2 db.

Data from a switch made by using one and two gold-bonded diodes is shown in Fig. 16. Photographs of the switch assembled and unassembled are shown in Fig. 17. For one diode, the insertion loss is less than one db for all frequencies shown, and the isolation is a minimum of 17 db at 4 Gc. For two diodes it was difficult to obtain a low insertion loss at all frequencies. To obtain the insertion loss shown, the spacing for maximum isolation could not be used. The isolation at 4 Gc is 26 db. The insertion loss is a maximum of 1.6 db at two frequencies, and less than one db at other frequencies. It is believed that the design could be improved to more closely approach the theoretical isolation and insertion losses of 40 db and one db, respectively, at 4 Gc.

One might think that if C_b in Fig. 12 can be made large enough for Mode $1\frac{1}{2}$ operation, the use of one

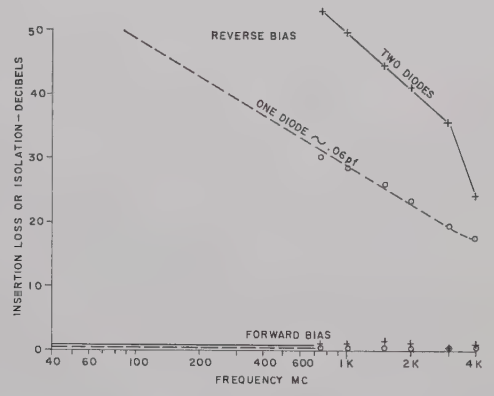

Fig. 16—Experimental characteristics of a 40-Mc to 4-Gc switch using one and two gold-bonded diodes.

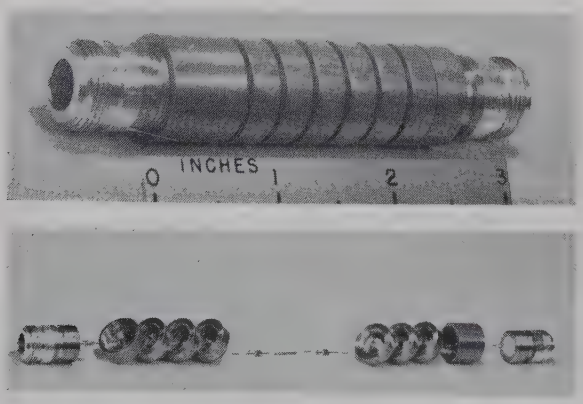

Fig. 17—Photograph of 40-Mc to 4-Gc diode switch.

Mode 1 diode and one Mode $1\frac{1}{2}$ diode separated by some calculated spacing would give a broad-band switch with better performance at the higher frequencies than is obtained with two Mode 1 diodes. However, below the parallel resonant frequency of the Mode $1\frac{1}{2}$ diode, the diode impedance is inductive, and this would be in series with a capacitive Mode 1 diode. A series resonance would then occur at some lower frequency. Below the resonance, the isolation would be less than that of one Mode 1 diode. For a broad-band switch, this is not desirable. Such a configuration might be useful, however, as a tunable narrow band-pass filter or efficient narrow-band switch. This is to be compared with shunt mode diodes producing tunable narrow-band rejection.

Many combinations of diode modes are possible for a great variety of switching results. It is believed, however, that the most broad-band configuration is obtained by placing Mode 1 diodes in series.

VI. Biasing Circuitry

To produce switching action with a diode, it is necessary to supply a switching signal to the diode. It is most desirable to have no interaction between the biasing circuitry and the microwave circuitry. For a diode in series or in shunt, all of the components for the needed isolation between circuits are shown in Fig. 18. C_2 and C_3 can be omitted in many applications or they can be built into the end connectors [4]. An 0.0005-inch gap in a center conductor of 0.25-inch diameter has a capacitance of about 20 pf, which results in 1-db insertion loss at 160 Mc and less than 0.1 db above 600 Mc. L_2 and C_3 are not used if a ground return exists in some other component in the line. At the lowest frequency to be used, the reactance of C_1 should be less than one tenth of the impedance of L_1 for the series switch or of the diode for the shunt arrangement.

The diode switching element is broad band. The capacitors just discussed are broad band. The biasing

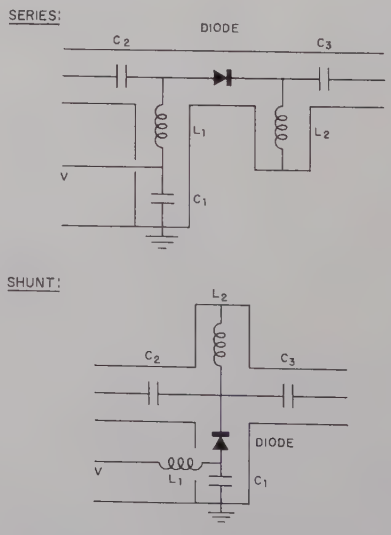

Fig. 18—Equivalent circuit of the biasing components needed for series diode switching and shunt diode switching.

inductors must therefore be made broad band in order to have a broad-band switch. At lower frequencies prewound RF inductors are satisfactory. Since the reactance of an inductor decreases with decreasing frequency, a sufficiently large inductance must be selected for a given minimum operating frequency. For higher frequencies, however, the self-resonance in a large prewound RF inductor may cause trouble. Also, for high-speed switching a large inductor is undesirable. Therefore, another approach to the design of the biasing lead is needed.

In prior designs, the center conductors in coaxial waveguides were supported by shorted quarter wavelength coaxial sections. These supports had little effect on the microwave transmission over considerable bandwidths. By substituting a capacitance for the short and making the characteristic impedance of the quarter-wavelength line section equal to that of the main guide (Z_0), a bias can be applied to this lead with an attenuation of $\frac{1}{4}$ db or less over a 2-to-1 frequency range. Greater bandwidth can be obtained by using shorted quarter-wavelength biasing leads having higher characteristic impedance as shown below.

The impedance of a shorted length of lossless transmission line of characteristic impedance Z_g is

$$Z = jX = jZ_g \tan\left(\frac{2\pi l}{\lambda}\right). \tag{33}$$

This is plotted in Fig. 19. For a lossless shunting reactance $G/Y_0=0$. From (6)

$$\alpha = 10 \log\left[1+\left(\frac{B}{2Y_0}\right)^2\right]$$

or, since

$$\left(\frac{B}{Y_0}\right)^2 = \left(\frac{Z_0}{X}\right)^2,$$

$$\alpha = 10 \log\left[1+\left(\frac{Z_0}{2X}\right)^2\right]. \tag{34}$$

Now by (34), as long as the reactance is greater than some minimum value, the attenuation will be lower than some maximum value. From Fig. 19, this is possible from l/λ_1 to l/λ_2. If λ_1 corresponds to f_1, λ_2 corresponds to f_2, and $f_2=Nf_1$ (where N is the bandwidth factor), then $\lambda_2=\lambda_1/N$. To find N, set $X_1=X_2$; then

$$N = \frac{\lambda_1}{2l} - 1. \tag{35}$$

Combining (33)–(35) gives

$$N = \pi\left[\arctan\left(2\,\frac{Z_g}{Z_0}\sqrt{10^{\alpha/10}-1}\right)^{-1}\right]^{-1} - 1. \tag{36}$$

The equation is plotted in Fig. 20. For $Z_g/Z_0>5$ and $\alpha\leq 1$,

$$N \approx 3\,\frac{Z_g}{Z_0}\sqrt{\alpha}. \tag{37}$$

Modifying a $Z_0=50$-ohm coaxial T so that one arm has a 42 AWG wire for a center conductor, a Z_g of 325 ohms is possible, which gives a $Z_g/Z_0=6.5$ and $N=20$ for $\alpha=1$ db. Thus, one biasing lead can be made to work from 4000 Mc down to 200 Mc. It is pointed out that the 1-db reflection will exist only at the upper and lower limits. Between these limits, the insertion loss of the biasing lead will be less than 0.1 db over a 6-to-1 frequency range. Knowing N, l can be found from (35). More precisely, l can be determined by using the upper frequency and (33) and (34) for a given α. If a 1-db attenuation is allowed and some other reactive element is causing 1-db insertion loss (by itself), these can at worst add up to 3.6 db as in Fig. 15. By observing tuning procedures such as the spacing in Fig. 14, the biasing lead insertion losses can cancel at a frequency. As the frequency is decreased, the spacing will cross optimum mismatch, but the insertion loss of each element will be reduced at the lower frequency.

The bandwidth attainable by using a straight center conductor is limited by the smallest diameter of wire that can be tolerated. Greater bandwidth can be attained with helical center conductor (coaxial) transmission line because of its higher characteristic im-

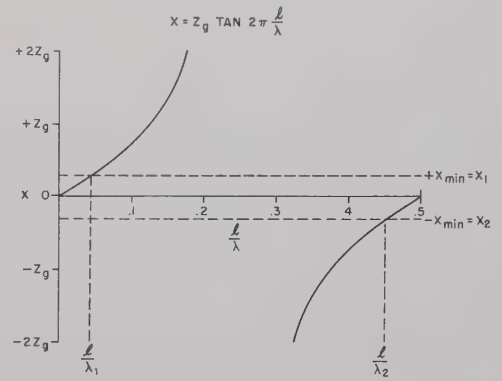

Fig. 19—Reactance of a straight biasing lead as a function of physical length, wavelength, and characteristic impedance Z_g.

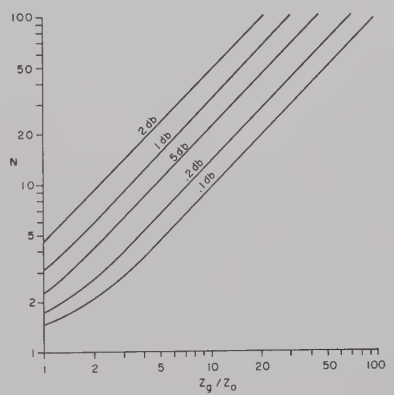

Fig. 20—Bandwidth of one biasing lead as a function of maximum insertion loss and the ratio of biasing lead characteristic impedance Z_g to main transmission line characteristic impedance Z_0.

pedance. Expressions for this type of line are derived in Appendix II, and the results are plotted in Fig. 20. From Fig. 21, it is seen that characteristic impedances on the order of 2000 ohms are easily obtained. Also from Fig. 21, a biasing lead with such a characteristic impedance, when used with a 50-ohm transmission line switch, would allow a 100-to-1 bandwidth with 0.4-db insertion loss (due to the biasing lead) at the extremes. An inductor of this type could be used profitably with the switch shown in Figs. 16 and 17.

VII. Power

It was shown that X-band diode switches could be made to isolate microwave power as high as one watt by choosing diodes having a high reverse breakdown voltage, E_b [10]. The reverse breakdown voltage, however, is not the only factor determining the maximum incident power the diode can switch; it limits only the peak power the diode can control. The diode series resistance R_s and the power the diode can dissipate $\overline{P}_d$ determine the average power the diode can switch.

As shown in Fig. 22(a), the peak RF voltage which can be applied to a diode without appreciable conduction is $E = E_b/2$. If the impedance of the series diode is high, then the maximum available peak power $\hat{P}_i$ which the switch can isolate is, approximately,

$$\hat{P}_i = \frac{E^2}{8Z_0} = \frac{E_b^2}{32Z_0} \cdot \tag{38}$$

Since the highest E_b available (in gold-bonded diodes) is about 125 volts, such a diode can isolate a peak incident power of about 10 watts in a 50-ohm transmission line, provided the power dissipated in the diode under these conditions is within the dissipation rating of the diode.

The maximum average incident power that a series diode can switch to the load is limited by the power $\overline{P}_d$ dissipated in R_s. Referring to Fig. 22(c), $P_L/P_d = Z_0/R_s$. If very little power is reflected, then

$$\overline{P}_i \approx \overline{P}_L + \overline{P}_d = \overline{P}_d\left(1 + \frac{Z_0}{R_s}\right) \approx \overline{P}_d \frac{Z_0}{R_s} \cdot \tag{39}$$

The dissipation rating of available switching diodes ranges from 0.08 − 0.2 watt. For example, assuming that $\overline{P}_d = 0.1$ watt, $Z_0 = 50$ ohms, and $R_s = 5$ ohms, results in $\overline{P}_i = 1.1$ watts.

It is noted that for modulated incident power, the incident power may be greater than the maximum permissible average power provided the repetition rate of the modulation is sufficiently high to permit thermal averaging by the diode. In the event that the maximum power ratings of the diode are exceeded somewhat, the diode will not suddenly be destroyed but the switching characteristics will be temporarily degraded. In some applications, the degraded switching characteristics may still be satisfactory in which case the diode can switch larger RF incident power than indicated above.

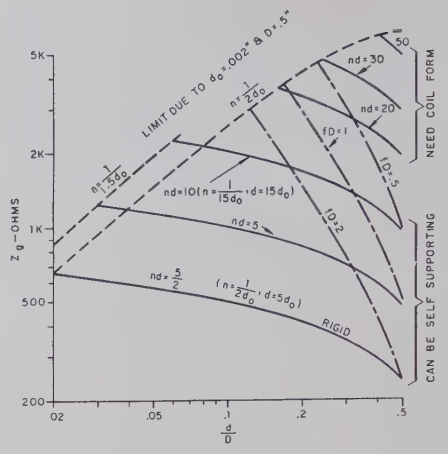

Fig. 21—Characteristic impedance of a helical center coaxial transmission line as a function of d/D, helix diameter to outer conductor diameter, from (60) for various values of nd.

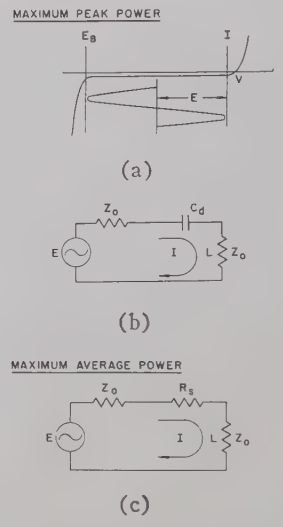

Fig. 22—Voltage-current characteristic of a diode and series equivalent circuits for determining maximum peak and average power the diode can switch.

For applications in which the diode is in the isolation state part of the time, incident CW power greater than the rated average power can be switched. The power dissipation of the diode in the isolation state (40) is usually less than in the ON state

$$\overline{P}_d \approx 4\frac{R_s Z_0}{X^2}\overline{P}_i. \tag{40}$$

The value of X is related to the isolation as indicated in Fig. 6. Higher power can be controlled by use of more than one diode.

To obtain the peak power which a shunt diode can switch, reference is made to Fig. 1, in which Y is replaced by C_d. The maximum voltage is just E, as shown in the equivalent circuit.

$$P_L = \frac{1}{2}E^2 Y_0 = \frac{E_b^2}{8Z_0} \tag{41}$$

A 125-volt shunt diode in 50-ohm transmission line can switch 40 watts of incident peak power in this configuration. Higher peak power would result in increased insertion loss, and more diodes would only make the insertion loss greater.

The average power a shunting diode can isolate is determined by making Y equal to $1/R_s(=G_s)$ in Fig. 1. Then as in the case of the series diode,

$$\overline{P}_i' = \overline{P}_d'\left(\frac{Z_0}{4R_s}+1\right) \approx \frac{Z_0}{4R_s}\overline{P}_d'. \tag{42}$$

In a 50-ohm transmission line, a 5-ohm, gold-bonded diode can switch average power of about 0.3 watt in this configuration.

To determine the highest CW power that a diode can switch, the transmission line impedance is varied so that the peak power rating of the diode and average power rating of the diode are equal. Assuming for the shunt diode that

$$\hat{P}_i' = \frac{E_b^2}{8Z_0} \quad \text{and} \quad \overline{P}_i' = \overline{P}_d\frac{Z_0}{4R_s},$$

for the series diode that

$$\hat{P}_i = \frac{E_b^2}{32Z_0} \quad \text{and} \quad \overline{P}_i = P_d\frac{Z_0}{R_s},$$

and that the optimum characteristic impedance is used in each case, then the diode in both configurations can switch the same amount of CW power

$$\overline{P}_i = E_b\sqrt{\frac{\overline{P}_d}{32R_s}}.$$

A 5-ohm, 125-volt, gold-bonded diode can switch 2.8 watts CW power in a 180-ohm transmission line.

VIII. Further Techniques

A. Alternate Switch Configuration

Another technique of switching warrants mention. If the diode terminates a quarter-wavelength arm of a T, the whisker can be made part of the length of line; and the contact impedance Z_c is transformed by virtue of the transforming action of a quarter-wavelength line section to an admittance

$$\frac{Y}{Y_0} = Z_c\left(\frac{Z_0}{Z_{0,\lambda/4}^2}\right),$$

in which $Z_{0,\lambda/4}$ and Z_0 are characteristic impedances, respectively, of the quarter-wavelength section and the main transmission line. This configuration is illustrated in Fig. 23. If $Z_{0,\lambda/4}=Z_0$, the series diode impedance of Fig. 6 dictates the switching behavior in spite of the configuration being in shunt with the main guide. Also,

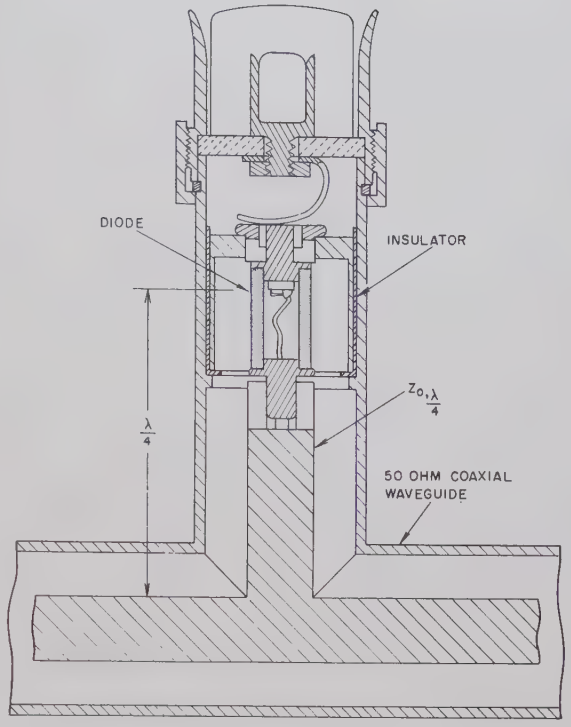

Fig. 23—Phantom view of a diode in a quarter wavelength T arm.

the diode contact impedance rather than the entire diode impedance describes the switching since the cartridge is part of the $\lambda/4$ configuration. Using a 1N263, greater than 20-db isolation has been attained over a 5 per cent bandwidth at 1 Gc, with an associated 1-db insertion loss. Isolation greater than 10 db was available over a 20 per cent bandwidth with little change from 1 db in insertion loss.

B. Switching Speed

It has been found that a germanium point-contact diode causing switching in X-band waveguide can provide about half of maximum isolation in about 0.2×10^{-9} second. Later observations indicate the diode provides full isolation in about 20×10^{-9} second. Varactors and gold-bonded diodes may differ from these point-contact diodes if forward conduction is used for part of the switching. The makers of gold-bonded diodes claim switching times of about 0.5 μsec. If germanium point-contact diodes are used in a switch, or these other diodes are found to be faster, the biasing lead inductance must be small to avoid increasing the switching time or decreasing the maximum modulation rate. To attain this the bandwidth of the biasing leads is made no larger than it has to be, using the lowest possible characteristic impedance. It is noted that similar precautions should be taken with the detector.

RF leakage out the biasing network (Fig. 18) will be small by virtue of the network needed to prevent interaction between the RF and bias circuits for optimum

switching. If high-speed switching is not needed, C_1 can be increased and additional inductance can be placed in series with V to provide any desired broad-band RF leakage suppression.

C. Whisker Inductance, L_w

In addition to the technique mentioned in Section III, another suggested method of reducing the effect of L_w is to actually reduce L_w by surrounding the wire whisker with soft, high-conductivity rubber epoxy as shown in Fig. 24. The soft rubber would allow the whisker to flex for thermal variations of the cartridge and yet provide low inductance. The whisker could be encapsulated by drilling a hole in the cartridge near the base of the whisker and forcing the required amount of uncured epoxy into the cartridge. With the above technique for reducing L_w, it should be possible to make Mode 1 switches operable up to 10 Gc.

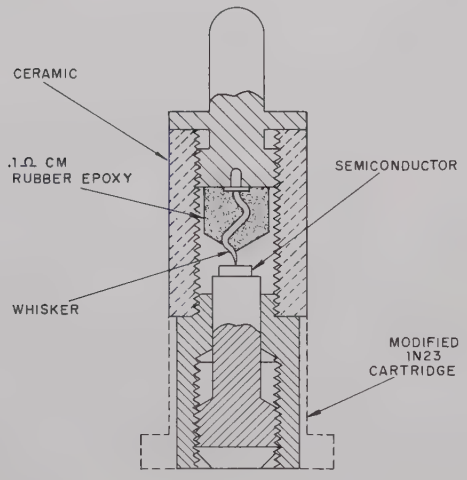

Fig. 24—Phantom view of a diode filled with conducting rubber epoxy for the purpose of reducing L_w.

IX. Conclusions

Comparison of the series and shunt connected diodes reveals that the best whisker-type diodes, when used in series configuration, provide higher isolation and wider bandwidth over that of the shunt configuration by a factor of 4. It is anticipated that pill-type diodes with low R_s will allow competitive isolation and bandwidth in the shunt configuration.

It is concluded that Mode 1 operation with multiple diodes affords the greatest bandwidth. The addition of L_T in parallel with C_c+C_d moves Mode 1 to a higher frequency. Mode 2 is useful at even higher frequencies. Mode 3 is useful at the highest frequencies, but adding the series inductor to reduce the insertion loss provides a narrow-band insertion loss (approximately that which would result from the total inductance) and reduces the bandwidth of the isolation. Most efficient low-power switching is obtained with the resonant shunt mode.

Broad-band biasing is obtained by using helical center conductor coaxial transmission lines, which are equally useful in detectors, coaxial transistors, and (in eliminating lower frequencies) as a form of high-pass filter.

In addition to using the single-pole, single-throw basic switching configurations as switches, they may be utilized as the basic element for making attenuators, multipole switches [5], phase modulators, and frequency translators [11]. Present diodes can switch incident peak power of 10 watts and incident average power of 1 watt.

Appendix I

Multiple-Element Spacing and Isolation

One shunt susceptance element with a matched load behind it results in a normalized admittance of

$$\frac{Y}{Y_0} = 1 + j\frac{B}{Y_0} .$$

This can be matched out (or compensated) by placing a second equal shunt susceptance a distance l toward the generator, which would render the first admittance

$$\frac{Y}{Y_0} = 1 - j\frac{B}{Y_0} .$$

This distance is [9]

$$l = \frac{\lambda_g}{2\pi} \tan^{-1} \frac{2}{B/Y_0} . \tag{43}$$

Similarly, for one series reactive element,

$$\frac{Z}{Z_0} = 1 + j\frac{X}{Z_0}$$

is transformed to

$$\frac{Z}{Z_0} = 1 - j\frac{X}{Z_0}$$

by a displacement of

$$l = \frac{\lambda_g}{2\pi} \tan^{-1} \frac{2}{X/Z_0} . \tag{44}$$

A second equal reactive element, spaced a distance l from the first, would result in minimum insertion loss, or match. Eqs. (43) and (44) are plotted in Fig. 14, as the curve for match. For maximum attenuation, the second equal reactive element is placed where the impedance of the first is transformed to

$$\frac{1}{1 - j\dfrac{X}{Z_0}}$$

which is

$$l = \frac{\lambda_g}{2\pi}\left(\tan^{-1}\frac{2}{X/Z_0}\right) + \frac{\lambda_g}{4} . \tag{45}$$

This is plotted in Fig. 14 as the curve for mismatch.

Power loss due to reflection [12] is

$$\alpha = 10 \log \frac{\left(\frac{R}{Z_0}+1\right)^2 + \left(\frac{X}{Z_0}\right)^2}{4\left(\frac{R}{Z_0}\right)}. \quad (46)$$

One series reactive element gives

$$\frac{Z}{Z_0} = 1 + j\left(\frac{X}{Z_0}\right),$$

$$\alpha_1 = 10 \log \left[\frac{4 + \left(\frac{X}{Z_0}\right)^2}{4}\right] \quad (47)$$

and

$$\left(\frac{X}{Z_0}\right)^2 = 4(10^{\alpha_1/10} - 1). \quad (48)$$

Two series reactive elements optimumly spaced give

$$\frac{Z}{Z_0} = \frac{1}{1 - j\left(\frac{X}{Z_0}\right)} + j\left(\frac{X}{Z_0}\right)$$

or

$$\frac{Z}{Z_0} = \frac{1 + j\left(\frac{X}{Z_0}\right)\left[2 + \left(\frac{X}{Z_0}\right)^2\right]}{1 + \left(\frac{X}{Z_0}\right)^2}. \quad (49)$$

Then,

$$\alpha_2 = 10 \log \left[\frac{\left\{\frac{1}{1 + \left(\frac{X}{Z_0}\right)^2} + 1\right\}^2 + \left\{\frac{\frac{X}{Z_0}\left(2 + \frac{X^2}{Z_0^2}\right)}{1 + \left(\frac{X}{Z_0}\right)^2}\right\}^2}{4 \frac{1}{1 + \left(\frac{X}{Z_0}\right)^2}}\right]$$

or

$$\alpha_2 = 20 \log \frac{2 + \left(\frac{X}{Z_0}\right)^2}{2}, \quad (50)$$

$$\alpha_{x2} = \alpha_2 - 2\alpha_1$$

$$= 20 \log \left[\frac{2 + \left(\frac{X}{Z_0}\right)^2}{2}\right] - 20 \log \left[\frac{4 + \left(\frac{X}{Z_0}\right)^2}{4}\right]$$

or

$$\alpha_{x2} = 20 \log \left[\frac{4 + 2\left(\frac{X}{Z_0}\right)^2}{4 + \left(\frac{X}{Z_0}\right)^2}\right] = 20 \log \left[2 - 10^{-\alpha_1/10}\right]. \quad (51)$$

For $\alpha_1 \geq 20$ db, $\alpha_{x2} = 6$ db.

For $\alpha_1 \leq 0.5$ db, $\alpha_{x2} \approx 2\alpha_1$.

For the maximum α from 2 or more, N_d, small shunt susceptances

$$Y_2 = \frac{1}{1 - j\left(\frac{B}{Y_0}\right)} + j\left(\frac{B}{Y_0}\right) \approx 1 + j2\left(\frac{B}{Y_0}\right)$$

$$Y_{N_d} = 1 + jN_d\left(\frac{B}{Y_0}\right) \quad (52)$$

$$\alpha = 10 \log \frac{\left(\frac{G}{G_0}+1\right)^2 + \left(\frac{B}{Y_0}\right)^2}{4\left(\frac{G}{Y_0}\right)}$$

$$= 10 \log \left(1 + \frac{N_d^2 \frac{B^2}{Y_0^2}}{4}\right). \quad (53)$$

Log $(1+\delta) = 0.435\delta$ for $\delta \leq 0.1$. So,

$$\alpha = \frac{4.35}{4} N_d^2 \frac{B^2}{Y_0^2} \quad \text{for } N_d^2 \frac{B^2}{Y_0^2} \leq 0.5. \quad (54)$$

The calculation for the extra attenuation resulting from the third, or higher, additional identical optimum-spaced elements is simplified by the fact that the addition of equal reactance (or susceptance) results in a total impedance (or admittance) which has repeatedly the same reflection coefficient angle, and that the corresponding reciprocal of the complex conjugate of the impedance has another repeating reflection coefficient angle. Thus, the total impedance (or admittance) for one more element can be found by taking the reciprocal of the complex conjugate of the total impedance (or admittance) from the addition of the last element and then adding the new element. The extra attenuation for the second, third, and fourth additional elements as well as the limit for large numbers of elements is plotted in Fig. 15. The total attenuation α_T from N elements is

$$\alpha_T = N\alpha_1 + \sum_{n=2}^{N} \alpha_{xn}. \quad (55)$$

Appendix II

Helical Center Conductor [13]

When a helix of average diameter d (inches), n turns per inch, wire diameter d_0 (inches), and length l (inches)

is centered coaxially in a hollow cylinder of inside diameter D (inches), the inductance in microhenries per axial foot is

$$L \approx 0.30n^2d^2[1 - (d/D)^2] \tag{56}$$

and the capacitance in picofarads per axial foot is

$$C \approx \frac{7.4\epsilon}{\log_{10}(D/d)}, \tag{57}$$

where ϵ is the relative dielectric constant of the material separating the helix and the outer conductor. In the present application, the dielectric is air, for which ϵ is unity. Eqs. (56) and (57) are most accurate when

$$1.0 \leq l/D < 4.0$$
$$0.45 < d/D < 0.6$$

and

$$n \approx \frac{1}{2d_0},$$

but they can be used as an approximate guide outside these limits.

The characteristic impedance of this line is

$$Z_0 = \sqrt{\frac{L}{C}} \times 10^3 \cdot \tag{58}$$

and the propagation constant is

$$T = \sqrt{LC} \times 10^{-9}. \tag{59}$$

Substituting (56) and (57) in (58) and (59), Z_0 and T are, respectively,

$$Z_0 = 202nd\sqrt{[1 - (d/D)^2]\log(D/d)} \tag{60}$$

$$T = 1.49nd\sqrt{\frac{1 - (d/D)^2}{\log(D/d)}} \times 10^{-9}. \tag{61}$$

Eq. (60) is plotted in Fig. 21 for various values of nd. The limits imposed by $d_0 = 0.002$ inch and $D = 0.5$ inch for

$$n = \frac{1}{2d_0} \quad \text{and} \quad n = \frac{1}{1.5d_0}$$

are shown as the dashed curves. For larger d_0 or smaller D this limit is lower. Another limit is imposed by the requirement that $l/d > 1.0$.

It is desired that the line be $\frac{1}{2}$ wavelength long electrically at some frequency slightly higher than f_2 (Fig. 19). The electrical length K in wavelengths at the frequency f in gigacycles is defined as

$$K = \frac{fTl}{12} \times 10^9. \tag{62}$$

Assuming $l/d = 1$ and $K = \frac{1}{2}$ and solving (60) by substituting (61) and (62) in it, the following limit is placed on Z_0:

$$Z_0 = \left[\frac{(202)(12)(10^9)\sqrt{[1 - (d/D)^2]\log(D/d)}}{(1.49)(2)(10^9)fd}\right] \cdot \left[\sqrt{\frac{\log(D/d)}{1 - (d/D)^2}}\right]$$
$$= \frac{813}{fD}\left(\frac{D}{d}\right)\log\left(\frac{D}{d}\right) \cdot \tag{63}$$

Eq. (63) is plotted for various values of fD as the dot-dash curves in Fig. 21. Above each curve l/d is less than 1.0, which is undesirable. If D is 0.5 inch and f is 4 Gc, then the highest possible characteristic impedance is 3000 ohms. d/D is outside of the desirable limits; but coils fabricated and tested with $d/D \approx 0.2$ demonstrate higher impedance and resonate at 5 per cent to 10 per cent higher frequency than predicted, which provides a margin of safety.

X. Acknowledgment

The author would like to express his appreciation to B. Haimowitz and L. Riebman of American Electronic Laboratories, Inc. for helpful discussions and for supplying several Mode $1\frac{1}{2}$ switches.

Bibliography

[1] M. A. Armistead, E. G. Spencer and R. D. Hatcher, "Microwave semi-conductor switch," Proc. IRE, vol. 44, p. 1875; December, 1956.
[2] R. V. Garver, J. A. Rosado and E. F. Turner, "Theory of the germanium diode microwave switch," IRE Trans. on Microwave Theory and Techniques, vol. MTT-8, pp. 108–111; January, 1960.
[3] L. Riebman, "Study of Wide-Open Receiver Detection Capabilities Interim Report," American Electronic Labs., Inc., Philadelphia, Pa., AEL Tech. Rept. 57052-3, Signal Corps Contract DA-36-039-sc-74813; July–December, 1958.
[4] L. Riebman, "Study of Wide-Open Receiver Detection Capabilities Final Progress Report," American Electronic Labs., Inc., Philadelphia, Pa., AEL Tech. Rept. 57052-F, Signal Corps Contract DA-36-039-sc-74813; October–June, 1959.
[5] M. Bloom, "Single-Pole Double-Throw Wideband Microwave Switch," presented at the PGMTT Natl. Symp., Harvard University, Cambridge, Mass.; June 2, 1959.
[6] R. V. Garver and J. A. Rosado, "Microwave diode cartridge impedance," IRE Trans. on Microwave Theory and Techniques, vol. MTT-8, pp. 104–107; January, 1960.
[7] R. V. Garver, E. G. Spencer and M. A. Harper, "Microwave semi-conductor switching techniques," IRE Trans. on Microwave Theory and Techniques, vol. MTT-6, pp. 378–383; October, 1958.
[8] R. V. Garver, "High-speed microwave switching of semiconductors—II," IRE Trans. on Microwave Theory and Techniques, vol. MTT-7, pp. 272–276; April, 1959.
[9] G. C. Southworth, "Principles and Applications of Waveguide Transmission," D. Van Nostrand Co., Inc., New York, N. Y., p. 220; 1950.
[10] R. V. Garver, E. G. Spencer and R. C. LeCraw, "High-speed microwave switching of semiconductors," *J. Appl. Phys.*, vol. 28, pp. 1336–1338; November, 1957.
[11] E. M. Rutz and J. E. Dye, "Frequency Translation by Phase Modulation," 1957 IRE Wescon Convention Record, pt. 1, pp. 201–207.
[12] T. Moreno, "Microwave Transmission Design Data," Sperry Gyroscope Co., Inc., Great Neck, N. Y., p. 22; 1944.
[13] H. P. Westman, "Reference Data for Radio Engineers," IT&T, New York, N. Y., 4th ed., p. 600; 1956.

Measurement of Small Dielectric Losses in Material with a Large Dielectric Constant at Microwave Frequencies*

R. O. BELL† AND G. RUPPRECHT†

Summary—A method is described for measuring dielectric losses at microwave frequencies in materials with a large dielectric constant. By observing a dielectric resonance in a sufficiently large sample, the loss tangent of the material can be obtained. Results on $SrTiO_3$ single crystals at 20 kMc are presented.

Introduction

ACCURATE measurement of small dielectric losses in a material with a large dielectric constant is difficult at microwave frequencies. If a cavity perturbation method[1] is used, it is hard to strike a balance in sample size so that the frequency shift of the cavity caused by the large dielectric constant is not too large, while the losses are large enough to be readily measurable. For a metallic cavity filled with the dielectric material, the skin losses may obscure the dielectric losses. Coaxial measurements are not free from skin losses and it also becomes more and more difficult with increasing frequency to avoid losses associated with the generation of higher-order modes.[2] An appreciable reduction of skin losses has been achieved with a dielectric cavity proposed by Hakki and Coleman,[3] but here the coupling to the cavity, the identification of the modes, and the mechanical requirements complicate the use of this method.

We propose a method which uses a sample large enough to support a dielectric resonance. The shape of the sample is not critical for the measurement of the microwave losses, and the physical size can be small compared to the dimensions of the waveguide in which it is suspended. Thus the dielectric sample, which is the resonant structure, is entirely surrounded by the exciting electromagnetic wave. It will be shown that the observed losses represent the Q of the dielectric material itself. This method has been applied successfully to measure the loss tangent of $SrTiO_3$ between 3 kMc and 37 kMc in a temperature range from -180°C to 250°C.

Theory

Strontium titanate has a relative dielectric constant of about 300 at room temperature and 1500 at -180°C. This large dielectric constant presents an appreciable discontinuity for the propagation of electromagnetic waves. Since the characteristic feature of a resonant structure is the existence of discontinuities, an almost arbitrary piece of $SrTiO_3$ can be used as a resonant structure provided that at least two dimensions are greater than $\lambda_0/\sqrt{\epsilon}$. This makes it possible to work with small samples. A $SrTiO_3$ sample at room temperature with dimensions the order of one millimeter is large enough to resonate at 20 kMc, since the wavelength in the sample is only about 0.9 mm.

In this section of the paper the problem of dielectric resonances in general will be considered; in the Appendix the theory for the particular case of a spherically shaped dielectric resonator will be developed in more detail, and it will be shown that the approximations made here are valid for a sphere in particular.

Let us consider a finite piece of material with a relative dielectric constant ϵ and loss tangent $\tan\delta$ in free space. For a dielectric resonance Q_0 will be defined as

$$Q_0 = \frac{2\pi \times \text{stored energy}}{\text{energy loss per cycle}} = \frac{\omega U}{W}, \tag{1}$$

$$U = \frac{\epsilon\epsilon_0}{2}\int_{\text{inside}} |E|^2 d\tau + \frac{\epsilon_0}{2}\int_{\text{outside}} |E|^2 d\tau, \tag{2}$$

where the first integral is taken over the electric field inside the dielectric sample and the second integral over the electric field associated with the dielectric resonance outside the sample. ω is the characteristic frequency of the dielectric resonance.

The dielectric loss will be given by

$$W = \frac{\omega\epsilon\epsilon_0 \tan\delta}{2}\int_{\text{inside}} |E|^2 d\tau, \tag{3}$$

where the integral is taken over the electric field inside the dielectric sample. With $\epsilon \gg 1$ and a rapidly decaying electromagnetic field outside the sample, the second term of the stored energy, U, becomes negligible compared to the energy stored inside the sample. With these

* Received by the PGMTT, October 18, 1960; revised manuscript received, January 27, 1961. Supported in part by the U. S. Air Force under Contract AF 19(604)-4085.

† Raytheon Co., Research Div., Waltham, Mass.

[1] See for example, W. Von Aulock and J. H. Rowen, "Measurements of dielectric and magnetic properties of ferromagnetic materials at microwave frequencies," *Bell Sys. Tech. J.*, vol. 36, pp. 427–448; March, 1957.

[2] See W. S. Gemulla, "Measuring Microwave Properties of Ferroelectrics," Sylvania Electric Products, Inc., Mountain View, Calif., Tech. Memo. No. EDL-M246, pp. 2–11; February 10, 1960, for a review of dielectric constant and loss tangent measurements as applied to ferroelectrics.

[3] B. W. Hakki and P. D. Coleman, "A dielectric resonator method of measuring inductive capacities in the millimeter range," IRE TRANS. ON MICROWAVE THEORY AND TECHNIQUES, vol. MTT-8, pp. 402–410; July, 1960.

approximations,

$$Q_0 = \frac{1}{\tan \delta}. \tag{4}$$

In practice the sample is placed inside a waveguide; therefore, skin losses can also contribute to losses of the dielectric resonance, but because of the rapid decay of the electromagnetic fields outside the sample, this source of loss may be neglected.

It is possible to measure the cavity Q by the usual frequency variation methods,[4] but because of the special problems encountered with $SrTiO_3$, a different method was developed. $SrTiO_3$ is a paraelectric whose dielectric constant obeys a Curie-Weiss law.

$$\epsilon = \frac{C}{T - T_c} \tag{5}$$

where $C \approx 8.5 \times 10^4$ is the Curie constant and $T_c = -240°C$ is the Curie temperature. For a lossless resonant structure the frequency varies inversely with the square root of the dielectric constant, so that for $\omega_0 \gg \Delta\omega$,

$$\frac{\Delta\omega}{\omega_0} = \frac{1}{2} \frac{\Delta T}{T - T_c},$$

where ΔT is the width of a resonant peak in the temperature scale. The loaded Q, Q_L, is related to the unloaded Q_0 by the coupling constant β:

$$Q_0 = (1 + \beta)Q_L.$$

Therefore,

$$\tan \delta = \frac{1}{2} \frac{\Delta T}{(T - T_c)(1 + \beta)}. \tag{6}$$

Measurement

Fig. 1 shows the experimental set up used to measure the losses of $SrTiO_3$ at 20 kMc. At this frequency the samples were either rough cubes or spheres with dimensions the order of one millimeter. The sample was supported on a piece of polyfoam for measurements below room temperature and on fiberglass for measurements above room temperature (Fig. 2). Even though the sample was partially surrounded by polyfoam or fiber glass, convection heating kept the sample close to the temperature of the waveguide. The temperature of a resonance as measured by the thermocouple with slowly increasing and with slowly decreasing temperature, varied by less than two degrees. The sample temperature differs, therefore, at most by one degree from the thermocouple reading. From (6) this will contribute about 2 per cent to the error at $-200°C$ and much less at higher temperatures.

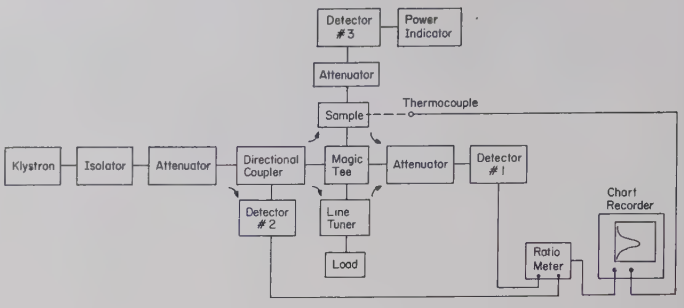

Fig.1—Block diagram for measurement of the loss tangent at K band.

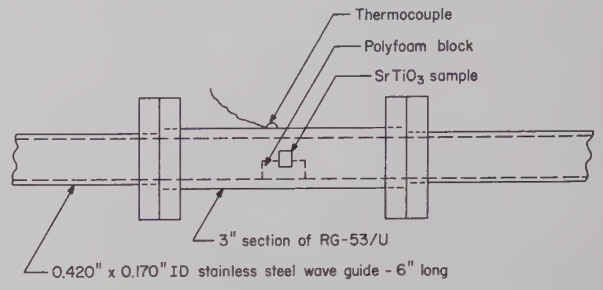

Fig. 2—Sample holder.

The sample and attenuator (which was set at 15- to 20-db attenuation to appear as a load) were placed in one arm of a hybrid tee, and a line tuner and a load were placed in the opposite arm. The line tuner was adjusted to cancel any reflections from the sample arm when the sample was not resonant. For measurements below room temperature the section of waveguide with the sample was cooled to liquid nitrogen temperature and then allowed to warm slowly. Above room temperature a coil heater was used to heat the sample. A thermocouple was soldered to the waveguide wall next to the sample and used to drive the x axis of an x-y chart recorder. The relative signal at detector 1 (Fig. 1) was plotted as a function of temperature on the chart recorder. From this plot of reflection vs temperature, ΔT and T were obtained. By observing the power received at detector 3, the coupling coefficient can be determined.[5] In particular, if we assume the sample behaves as a reaction cavity, it can be shown that

$$(1 + \beta) = \sqrt{\frac{P_0}{P_{\min}}},$$

where P_0 is the power transmitted off resonance and $P_{\min}$ is the minimum power transmitted as the sample goes through resonance.

Measurements have also been made at various frequencies between 3 kMc and 37 kMc using similar methods.

[4] E. L. Ginzton, "Microwave Measurements," McGraw-Hill Book Co., Inc., New York, N. Y.; 1957.

[5] C. G. Montgomery, "Technique of Microwave Measurements," McGraw-Hill Book Co., Inc., New York, N. Y.; 1947.

Results and Discussion

Measurements have been made on various rough cubes and spheres. Fig. 3 shows measurements made on two different samples of $SrTiO_3$. Because of the large variation of the dielectric constant in the temperature range of $-180°C$ to $250°C$, there are many temperatures at which the samples were resonant. From these resonances the loss tangent can be determined as a function of temperature for a constant frequency.

When the relative orientation of the sample in the waveguide was changed, different resonances were excited, but the same value of the loss tangent was observed. The measured value of the loss tangent was also independent of the surface finish and the size of the sample.

The main problem encountered with the cube was that resonances were partially superimposed. Because of the symmetry of a cube a large number of resonances are degenerate, but since the samples were not quite perfect this degeneracy is lifted and some peaks are split. Care must be taken to insure that there is only one peak. This problem can be reduced by using a parallelepiped with three (3) unequal sides, or spheres.

The microwave power incident on the sample must be kept at a low level to reduce any heating effects. The linewidths are only about 0.2°C near liquid nitrogen temperature. Slight heating can alter the line shape or width. In all measurements the power was reduced until the line shape and width were independent of the power level.

Obviously, this or a similar method of measuring the loss tangent can be extended to any frequency where $SrTiO_3$ or any other material with a large dielectric constant can be placed inside a section of waveguide.

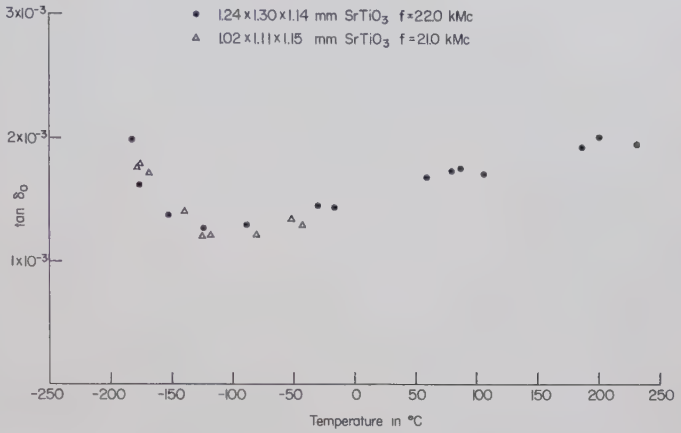

Fig. 3—Loss tangent vs temperature.

Appendix

The problem of a dielectric resonator of anything but the simplest shape is quite complicated. Because of its symmetry the sphere is the easiest shape to solve exactly.[6,7] Several other types of dielectric resonators such as the dielectric circular ring resonator[7] and rectangular resonators[8] have also been studied. The sphere is used here as an example to validate some of the statements made in the section on Theory. An attempt will be made to show principally that the energy associated with the dielectric resonance outside the sphere can be neglected compared to the energy stored inside the sphere, and that the skin losses can be neglected compared to the dielectric losses.

Richtmyer[7] has shown in general that energy cannot be confined in a finite region of space by a dielectric alone because energy is always lost by radiation. Under certain conditions, though, this energy loss can be quite small compared to the dielectric losses. The electromagnetic fields outside the dielectric sample initially decay rapidly but then at large distances from the sample they oscillate. Because of the presence of this radiation field, the integral over the total energy density outside the dielectric resonator does not converge. A related problem with dielectric resonators is how much of the energy outside the sample should be included in the stored energy of the resonator.

Because of these problems we will consider the dielectric resonator in a slightly different way. Experimentally we know the spherical dielectric sample is not radiating since it is surrounded by waveguide. We will consider the problem of a dielectric sphere of radius a and relative dielectric constant ϵ at the center of a spherical metal cavity of radius $b>a$. For estimating the skin losses, b will be some number the order of the waveguide dimensions. We will consider the modes which are little different from the modes which would exist if the sample were in free space.

The electromagnetic fields can be expressed in terms of the vector potential in spherical coordinates, which inside and outside the dielectric sphere will be

$$\boldsymbol{A}_{\text{in}} = j_n(k_1 r) e^{im\phi} \left[\hat{\theta} \frac{im}{\sin\theta} P_n^m - \hat{\phi} \frac{dP_n^m}{d\theta} \right] e^{-i\omega t},$$

$$\boldsymbol{A}_{\text{out}} = \left[B_n j_n(k_2 r) + C_n n_n(k_2 r) \right] e^{im\phi} \cdot \left[\hat{\theta} \frac{im}{\sin\theta} P_n^m - \hat{\phi} \frac{dP_n^m}{d\theta} \right] e^{-i\omega t}.$$

j_n and n_n are spherical Bessel functions of the first and second kind, P_n^m are the associated Legendre functions,[9]

[6] P. Debye, "Der Lichtdruck auf Kugeln von Beliebigem Material," *Ann. Phys.*, ser. 4, vol. 30, pp. 57–136; 1909.

[7] R. D. Richtmyer, "Dielectric resonators," *J. Appl. Phys.*, vol. 10, pp. 391–398; June, 1939.

[8] N. M. Kroll, *et al.*, "Millimeter Wave Measurements," Columbia University, New York, N. Y., Radiation Lab. Quart. Rept., June 16 to September 15, 1959.

[9] For the properties of spherical Bessel function and associated Legendre functions, see J. A. Stratton, "Electromagnetic Theory," McGraw-Hill Book Co., Inc., New York, N. Y., 1941, or a similar work.

$k_1=(2\pi/\lambda)\sqrt{\epsilon}$, $k_2=2\pi/\lambda$, and ω is the angular frequency. B_n and C_n are determined by the boundary condition that the tangential components of $\boldsymbol{A}$ and its curl must be continuous at $r=a$, and that the tangential components of $\boldsymbol{A}$ must vanish at $r=b$. A characteristic equation is obtained which determines the resonant frequencies of the system.

$$\frac{[k_1 a j_n(k_1 a)]'}{j_n(k_1 a)} = \frac{[(k_2 a n_n(k_2 a)]' - \dfrac{n_n(k_2 b)}{j_n(k_2 b)}[k_2 a j_n(k_2 a)]'}{n_n(k_2 a) - \dfrac{n_n(k_2 b)}{j_n(k_2 b)} j_n(k_2 a)}.$$

The prime indicates differentiation with respect to the argument. The damping because of skin losses can be computed and expressed in terms of a Q_{skin}.[10]

$$Q_{\text{skin}} = \frac{b}{\delta} + \frac{a}{\delta}(\epsilon - 1)(k_2 a)^2 (k_2 b)^2 \cdot \{ n_n(k_2 a) j_n(k_2 b) - j_n(k_2 a) n_n(k_2 b) \}^2,$$

where δ is the skin depth $(2/\omega\mu\sigma)^{1/2}$ and σ is the conductivity of the walls. We have assumed that the relative permeability of the cavity and of the dielectric sphere is one.

The radius of the samples measured at 20 kMc was of the order of 5×10^{-4} meters. If we assume that $b=15\times10^{-4}$ meters, which is roughly $\frac{1}{2}$ the smallest dimension of the waveguide, we find that $\epsilon=150$ and $\epsilon=750$ for the first two roots of the characteristic equation for $n=1$. The characteristic equation is almost independent of b for values of a, b, and ω of this order. If we assume that the metal cavity is copper ($\sigma\approx5.8\times10^{-7}$ mhos/meter), we find $Q_{\text{skin}}\approx10^5$ and $Q_{\text{skin}}\approx5\times10^5$ for $\epsilon=150$ and 750, respectively. For larger values of n, Q_{skin} is still larger. Since the loss tangent of the material being measured was the order of 10^{-3} which corresponds to an unloaded $Q=10^3$, the skin losses may be neglected.

The ratio of the energy stored inside the dielectric sphere to the energy stored outside the dielectric sphere can be calculated. Considering roots of the characteristic equation such that the electric field decreases outside the dielectric sphere, it is found that for any reasonably small value of b the energy stored inside the dielectric sphere is much greater than the energy stored outside. For instances for $n=1$, $\epsilon=300$, $a=5\times10^{-4}$ meters, and a frequency of 20 kMc, we find that b must be about 0.8 meter before the energy stored externally equals the energy stored inside the dielectric sphere.

If we assume that $a=5\times10^{-4}$ meters and $b=15\times10^{-4}$ meters and $n=1$, then the ratio of the energy stored outside the dielectric sphere to the energy stored inside is 0.03 for $\epsilon=150$ and 0.007 for $\epsilon=750$. For larger values of n and larger values of the dielectric constant, the ratio of the energies is still smaller.

Other shapes of dielectric resonators such as cubes or parallelepipeds will behave in a similar manner in regard to skin losses and the relative energy stored inside and outside the sample; although the details will depend on the specific geometry. Some of the possible uses of dielectric resonators have been pointed out by Okaya.[11]

[10] W. R. Smythe, "Static and Dynamic Electricity," McGraw-Hill Book Co., Inc., New York, N. Y., p. 531; 1950.

[11] A. Okaya, "The rutile microwave resonator," PROC. IRE, (Correspondence), vol. 48, p. 1921; November, 1960.

On the Existence of Leaky Waves Due to a Line Source Above a Grounded Dielectric Slab*

E. S. CASSEDY†, MEMBER, IRE AND M. COHN‡, MEMBER, IRE

Summary—**The existence of a particular type of leaky wave is verified experimentally. The leaky wave considered is that due to an electric line source above a dielectric slab. Since such a leaky wave cannot exist by itself, it must be detected in the presence of the remainder of the continuous spectrum and often in the presence of a surface wave (or waves). This was done by probing the fields and observing an interference pattern between the leaky wave and the existing surface wave, as predicted by the theory. These results emphasize a need to take leaky waves into account in the design of surface wave components and antennas.**

INTRODUCTION

A LEAKY wave is broadly characterized as a wave which has a continuous leakage of energy away from the surface with which its propagation is associated. The most familiar case in which this arises is that of a long slot perturbing a normally closed waveguide.

A more careful enumeration of the characteristics of the leaky waves puts them in sharp contrast to surface waves, with which there has been considerable confusion in the past. A leaky wave is not a proper modal solution, whereas the surface wave is. The surface wave propagates unattenuated parallel to the guiding surface and has pure attenuation transverse to the surface. The leaky wave, in contrast, has complex propagation constants in both longitudinal and transverse directions, attenuating in the forward phase direction along the surface and growing transverse to the surface. The surface wave is a slow wave, whereas the leaky wave has a longitudinal phase velocity greater than that of light. Finally, the surface wave cannot radiate, whereas the leaky wave is not bound to the surface and may therefore contribute to the radiation field of the structure.

Although, in general, leaky waves exist on structures that are quite different from those supporting surface waves, there are some structures that support both types of waves. The existence of leaky waves on a surface interface structure has been postulated by Zucker.[1] It was subsequently found that, in the absence of sources at finite distances, leaky waves would exist in a physical sense only if the guiding structure were modulated periodically.[2–4]

In the presence of a source, it has been found that leaky waves also exist on unmodulated structures. Marcuvitz[5] has predicted the existence of nonmodal waves due to a source exciting a uniform guiding surface, which have characteristics identical in form to the waves referred to above. Marcuvitz[5] points out that such waves are, in reality, part of the continuous spatial spectrum of the source and are distinct from the discrete (modal) spectrum of surface waves. Furthermore, these waves are exponentially attenuated along any radius from the source within their domain of existence and therefore comprise a part of the near field, so to speak, of the source.

Interest in such waves should not be limited to the theoretical since the design of excitation structures for surface-wave transmission lines, antennas and cavities should take these waves into account if there are obstructions to or changes in the surface-wave structure anywhere but at great distances from the source (or launcher).

A particular case of leaky waves due to sources has been worked out in detail by Barone.[6] Barone has found the resonances, both proper and improper, for the case of an electric line source over a dielectric slab and has made numerical calculations for several typical cases of parameters.

The present paper takes the odd solutions of Barone (the "short circuit bisection"), which apply to the case of a grounded dielectric slab, and reports experimental verification of his results through use of the physically realizable dielectric loaded trough waveguide. The dielectric loaded trough waveguide, with spacing be-

* Received by the PGMTT, December 13, 1960; revised manuscript received, January 1, 1961. This research was supported by the USAF through WWRNGW of the Wright Air Dev. Div. of the Air Res. and Dev. Command.

† Microwave Res. Inst., Polytechnic Inst. of Brooklyn, Brooklyn, N. Y.

‡ Electronic Communications, Inc., Timonium, Md.

[1] F. J. Zucker, "The guiding and radiation of surface waves," *Proc. Symp. on Modern Advances in Microwave Techniques*, Polytechnic Inst. of Brooklyn, Brooklyn, N. Y., November 8–10, 1954, vol. 4, pp. 403–435; November, 1954.

[2] A. S. Thomas and F. J. Zucker, "Radiation from modulated surface wave structures—I," 1957 IRE NATIONAL CONVENTION RECORD, pt. 1, pp. 153–160.

[3] R. L. Pease, "Radiation from modulated surface wave structures," 1957 IRE NATIONAL CONVENTION RECORD, pt. 1, pp. 161–165.

[4] A. A. Oliner and A. Hessel, "Guided waves on sinusoidally-modulated reactance surfaces," IRE TRANS. ON ANTENNAS AND PROPAGATION, vol. AP-7, pp. S201–S208; December, 1959.

[5] N. Marcuvitz, "On field representations in terms of leaky modes or eigen modes," IRE TRANS. ON ANTENNAS AND PROPAGATION, vol. AP-4, pp. 192–194; July, 1956.

[6] S. Barone, "Leaky Wave Contributions to the Field of a Line Source Above a Dielectric Slab," Microwave Res. Inst., Polytechnic Inst. of Brooklyn, Brooklyn, N. Y., Rept. R-532-56, PIB-462; November, 1956.

tween side walls small compared to the wavelength, supports TE waves which are the sole wave type excited in the infinite configuration. The spacing between side walls may be made small enough so that a single conductor, fed by a coaxial line through one wall, will approximate the uniform line source to any degree of accuracy desired.

The results of the present work show the correspondence of experimental data with calculations for one of the cases of Barone. The most striking aspect of the results is an interference pattern, primarily between surface wave and leaky wave, existing out along the line several wavelengths from the source.

Theoretical Background

The structure being investigated and the coordinate system used are shown in Fig. 1. The expression for the total electric field in Region II (E_{y2}) due to an electric line source over a grounded dielectric slab has been found previously[6,7] and may be written as follows:

$$E_{y2}(x, z) = \frac{i\omega\mu_0}{2\pi}\int_{-\infty}^{\infty}\frac{1}{-2i\kappa}\cdot\left[e^{i\kappa|x-h|} + \Gamma e^{i\kappa(x+h-2d)}\right]e^{i\zeta z}d\zeta, \quad (1)$$

where

$$\Gamma = \frac{\kappa - i\kappa_\epsilon \cot \kappa_\epsilon d}{\kappa + i\kappa_\epsilon \cot \kappa_\epsilon d}, \quad (2)$$

$$\kappa = \sqrt{k^2 - \zeta^2}, \quad (3)$$

$$\kappa_\epsilon = \sqrt{k^2K_1 - \zeta^2}, \quad (4)$$

$$k^2 = \omega^2\mu_0\epsilon_0 = (2\pi/\lambda_0)^2, \qquad K_1 = \epsilon_1/\epsilon_0.$$

In (1), the integral has been written so that the first term in the bracket may be seen to be the field due to the line source alone. We shall now show, following Barone, that the total field can be expressed as the sum of three types of terms: leaky-wave terms, surface-wave terms, and radiative terms. The radiative terms will be found to represent the far fields of the source and its image in the dielectric. Eq. (1) may be rewritten in the following form:[6]

$$E_{y2}(r, \theta) = \frac{-\omega\mu_0}{4}H_0^{(1)}(k\rho) - \frac{\omega\mu_0}{4\pi}\int_{-\infty}^{\infty}\Gamma e^{i\kappa(x+h-2d)+i\zeta z}d\zeta, \quad (5)$$

where

$x-h=\rho\cos\psi$ and $z=\rho\sin\psi$,

$H_0^{(1)}$ is the Hankel function of zero order and first kind.

The second part of this expression evidently is due to an image source of strength Γ at $x=2d-h$, $z=0$. The two parts of this expression may also be called the "incident wave" and the "reflected wave," respectively, having reference to the transverse transmission line analysis of Barone.[6]

[7] C. T. Tai, "The effect of a grounded slab on the radiation from a line source," *J. Appl. Phys.*, vol. 22, pp. 405–414; April, 1951.

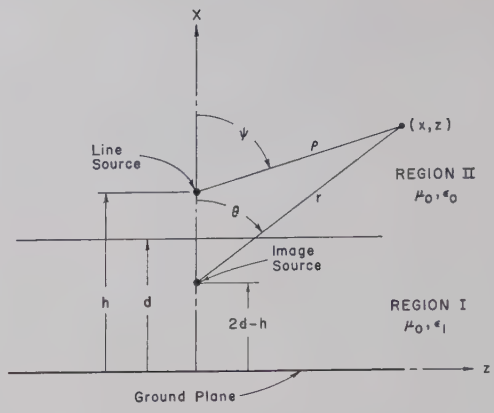

Fig. 1—End view of the line source over a grounded dielectric slab.

The integrand of the second part of (5) has a branch point at $\zeta=k$ and an infinite number of poles. The poles, some pure real and others complex, have been found graphically for parameters of the geometry (Fig. 1) and the dielectric constant by Barone.[6] In the original contour of integration of Tai,[7] it would be found that there are residues due to the real poles and a contribution due to integration around the branch cut, but the complex poles are not included within the contour. The real-pole residues are surface-wave contributions and the branch-cut contribution may be called the "entire space-wave" contribution. The latter is discussed more fully below.

The branch-cut contribution is integrated by using steepest-descent methods, which yields the familiar radiation terms. Prior to performing the steepest-descent integration, the following change of variables is made:

$$\zeta = k\sin\phi, \qquad \phi = \xi + i\eta. \quad (6)$$

When the path of integration is deformed to the path of steepest descent, it is found that some of the complex poles are now included within the contour. Residues due to the complex poles have been shown by Barone[6] to be of the leaky-wave form,

$$E_y^L(r, \theta) = Ae^{\alpha k_\theta' r}e^{i\beta k_r' r}, \quad (7)$$

where

A = a constant specified by h, d, and K_1,
$\alpha=\sinh\eta'$,
$\beta=\cosh\eta'$,
$k_r'=k\cos(\theta-\xi')$,
$k_\theta'=-k\sin(\theta-\xi')$,
$x+h-2d=r\cos\theta$,
$z=r\sin\theta$,
$\phi'=\xi'+i\eta'$ = location of the complex pole in the ϕ plane.

It should be emphasized that these leaky-wave contributions are merely a part of the particular field representation of the entire space wave chosen by using the steepest-descent method of integration and are to be included with the radiation and higher-order terms obtained from the saddle point or steepest-descent integration.

The surface-wave contributions (*i.e.*, residues of real

poles) have been indicated by Barone.[6] Complete data on the lower-order surface waves of the trough line has been given by Cohn.[8,9] The excitation of the lowest order of these modes by a current element in the physical situation, depicted in Fig. 1, has been studied by Cohn, Cassedy and Kott.[10] The expression for this lowest-order mode (the TE_{20} mode, in Cohn's designation) may be written as follows:[9,10]

$$E_y^s(x, z) = \omega\mu_0 \frac{(k_{10}d)\sin^2 k_{10}d}{(\zeta_p d)(\tan k_{10}d - k_{10}d)} e^{-k_{20}(h-2d+x)+j\zeta_p z}, \quad (8)$$

where

$$\zeta_p = \sqrt{\omega^2\mu_0\epsilon_1 - k_{10}^2} = \sqrt{\omega^2\mu_0\epsilon_0 + k_{20}^2}$$

= values of the propagation constant at the pole.

The values of $k_{10}d$ and $k_{20}d$ are given by Cohn[8,9] for various K_1.

The steepest-descent evaluation of the second part of (5) yields an asymptotic series in "kr," the leading term of which is:

$$f(r, \theta) = \frac{i}{4\pi}\sqrt{\frac{\pi}{kr}}\, G(\theta)e^{ikr} \quad (9)$$

where

$$G(\theta) = \frac{\cos\theta - i\sqrt{K_1 - \sin^2\theta}\cot\left[kd\sqrt{K_1 - \sin^2\theta}\right]}{\cos\theta + i\sqrt{K_1 - \sin^2\theta}\cot\left[kd\sqrt{K_1 - \sin^2\theta}\right]}.$$

Higher-order terms of the expansion are readily evaluated[11] and will be mentioned below.

The addition of (9) and the first term of the (Hankel type) asymptotic expansion of the line source yields

$$E_y^R(x, z) = -\frac{\omega\mu_0}{4}\sqrt{\frac{2}{\pi}}\frac{(i)^{-1/2}}{(k\rho)^{1/2}}e^{ik\rho} + \omega\mu_0 f(r, \theta), \quad (10)$$

where r, θ and ρ were given previously as functions of x, y. This may be termed the radiative term of the entire space wave of the structure.

The entire space wave, which includes all saddle-point terms and leaky-wave terms given in this representation, has been shown to be orthogonal to each of the surface-wave terms,[12] but no orthogonality exists between individual terms of the space wave. The entire space wave, arising from the branch-cut contribution, is seen to be a continuous spectrum of spatial frequencies.[5,12] The surface-wave terms correspond to discrete spatial frequencies, obeying all orthogonality requirements of proper modes. The leaky waves, on the other hand, do not have these properties and are thus termed "improper modes."[5,12]

Calculations

One of the complex poles found by Barone[13] corresponded to $2d/\lambda = 1.08$, $h/d = 1.10$ and $K_1 = 2.56$. The computation of the residue for that pole then completes the data necessary to specify the constant A in (7). Barone[6] has shown that this is by far the strongest leaky wave present for these physical parameters, due to the greater rate of attenuation of all others.

It also may be seen that only one surface wave exists[6,8,9] for the above-specified parameters. The expression (8) for this mode is completely specified for the above parameters.

In order to specify the total electric field for the above parameters, we need to add the fields of the leaky waves, the surface waves, the line source [first term of (5)] and the complete asymptotic expansion for the saddle-point contribution of the image source [second part of (5)]. For the computation we start with the first terms only of these space-wave terms (10), yielding the following approximate expression for the total field:

$$E_{y2}(x, z) \simeq E_y^L(x, z) + E_y^S(x, z) + E_y^R(x, z). \quad (11)$$

It was found that a particularly striking manner to present the computed results, was to make plots of $E_y(x, z)$ vs z for parameters of constant x. This method of presentation shows marked interference patterns in the range

$$2 < z/\lambda_0 < 6, \qquad 0.6 < x/\lambda_0 < 0.75.$$

This interference, it turns out, is primarily between surface wave and leaky wave, with $E_y^R(x, z)$ modifying the result only slightly. Furthermore, investigation of the second-order terms of the primary and image source space waves show them to be at least an order of magnitude smaller than the sum of the three terms of (11) everywhere in the above specified range. The second-order terms were therefore not included in the data presented below. The results are shown in Fig. 2.

Fig. 3 shows a plot of constant amplitude lines for each of the three components of (11) for the case $2d/\lambda_0 = 1.08$, $h/d = 1.10$ and $K_1 = 2.56$. The region in the neighborhood of the critical angle[14] is not accurate since there the saddle-point contribution is modified by the proximity of the complex pole to the path of steepest

[8] M. Cohn, "Propagation in a dielectric loaded parallel plane waveguide," IRE Trans. on Microwave Theory and Techniques, vol. MTT-7, pp. 202–208; April, 1959.

[9] M. Cohn, "TE modes of the dielectric loaded trough line," IRE Trans. on Microwave Theory and Techniques, vol. MTT-8, pp. 449–454; July, 1960.

[10] M. Cohn, E. S. Cassedy, and M. A. Kott, "TE mode excitation on dielectric loaded parallel plane and trough waveguides," IRE Trans. on Microwave Theory and Techniques, vol. MTT-8; pp. 545–552; September, 1960.

[11] L. Felsen and N. Marcuvitz, "Modal Analysis and Synthesis of Electromagnetic Fields," Microwave Res. Inst., Polytechnic Inst. of Brooklyn, Brooklyn, N. Y., Rept. R776-59; October, 1959.

[12] L. Felsen and N. Marcuvitz, "Modal Analysis and Synthesis of Electromagnetic Fields," Microwave Res. Inst., Polytechnic Inst. of Brooklyn, Brooklyn, N. Y., Rept. R726-59; June, 1959.

[13] $N = 3$ resonance of Barone.[6]

[14] It is shown by Barone[6] that the leaky wave does not exist above a certain critical angle "θ_c." Briefly, this is due to the path of steepest descent's being a function of the angle of observation (θ). Only for angles of θ_c and greater is the leaky-wave pole captured within the closed path of integration and, therefore, add its residue to the solution.

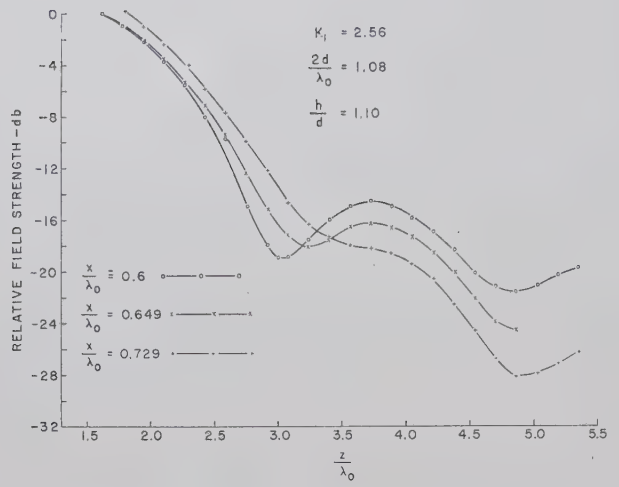

Fig. 2—Calculated curves of the total electric field vs normalized horizontal distance from the line source (z/λ_0) for various values of normalized distance above the ground plane (x/λ_0).

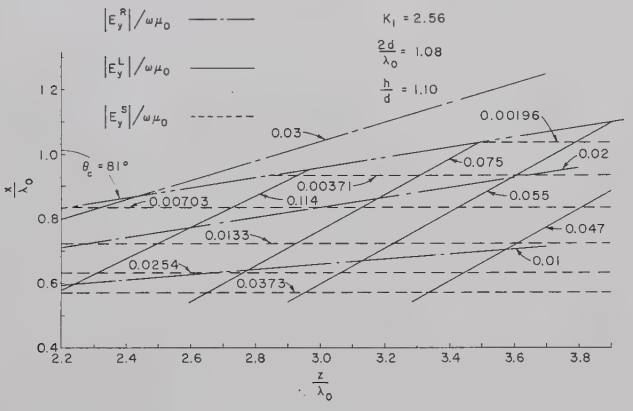

Fig. 3—Calculated constant amplitude lines of radiation field $|E_y^R|$, leaky-wave field $|E_y^L|$, and surface-wave field $|E_y^S|$.

descents.[11] The necessary correction to the saddle-point contribution has not been made here. This correction should make the field everywhere continuous in the region of the critical angle to satisfy the physical requirement of continuity.

Measurements and Apparatus

As stated in the Introduction, the mathematical formulation of this problem assumes a physically unrealizable geometry and excitation condition. If two parallel conducting planes, spaced a distance "b" apart, are located on the above structure so as to be perpendicular to the current source, then the physically realizable dielectric loaded trough waveguide results. The fields which would exist on the unrealizable structure of Fig. 1 are undisturbed by the addition of the two conducting planes, but the total power emanating from the unit current source is now finite.

The trough waveguide, in which the fields were explored, and the method of exciting the current source have been previously reported.[9,10,15] The measurements reported in this paper were made at a frequency of 4.86 Gc. The trough line and current source are specified by the following parameters: $K_1 = 2.56$, $d = 3.33$ cm, $b = 0.79$ cm, and $h = 3.70$ cm. The geometric parameters were those existing on the trough line previously built to determine the properties of the TE_{20} mode and to measure the efficiency with which the TE_{20} mode could be launched from a current source.[9,10] The frequency was chosen to provide a value of $(2d/\lambda_0)$, which yielded a large amplitude leaky wave as determined from Barone's computations.[6]

Matched loads were placed along the top of the trough line and on one side of the current source in order to provide reflectionless terminations for both the radiating fields and any waves which have a component of propagation in the negative z direction. These loads consisted of tapered sections of white pine wood, which were impregnated with a liquid containing suspended carbon.

The probe used to sample the fields in the interior of the trough guide is shown in Fig. 4. This probe is held

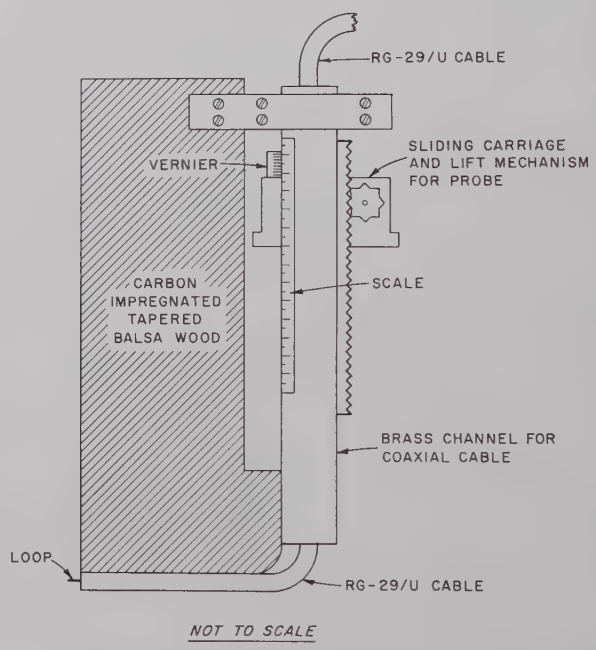

Fig. 4—Side view of the probe used to sample the fields in the trough line.

in place by a carriage assembly which in turn slides along the top edges of the side walls of the trough. The vertical position of the probe can be changed by the rack and pinion arrangement shown. In order to insure accurate motion of the probe, the top edges of the side walls were carefully machined to be parallel to the inside of the bottom of the trough. Scales with 1-mm graduations and verniers were mounted on the probe and trough line so that horizontal and vertical positions of the probe could be read to an accuracy of 0.1 mm.

The probe consists of a length of RG-29/U coaxial cable terminated by a small loop. This cable runs through a rectangular cross-section brass block and around the underside of a matched load, with only the loop extending ahead of the matched load. The entire

[15] M. Cohn, "Propagation in Partially Dielectric Loaded Parallel Plane and Trough Waveguides," Radiation Lab., The Johns Hopkins University, Baltimore, Md., Tech. Rept. No. AF-78; July, 1960.

probe assembly thus appears to be a reflectionless termination to the impinging wave. The loop was formed by bending the extended center conductor of the cable into a circle of approximately 1/8 inch diameter and connecting it to the cable's outer conductor. This loop lies in a horizontal plane (x = constant) and couples to the x component of the magnetic field.

The probe was set at a fixed height above the bottom of the trough guide ($x/\lambda_0 = 0.60$) and the relative field strength was measured as a function of distance along the guide from the current source (z/λ_0). This procedure was repeated for two other probe heights ($x/\lambda_0 = 0.649$ and $x/\lambda_0 = 0.729$) to determine if the theoretically predicted field distributions of Fig. 2 existed. The results of these measurements are shown in Fig. 5. The predicted interference between the leaky and surface waves, as manifested by the decrease in field strength near the predicted values of (z/λ_0) is clearly shown. Possible causes of the discrepancy in the depths of the measured nulls compared to the predicted nulls will be discussed below.

The probe was also used in conjunction with a phase-sensitive bridge to determine constant phase contours in the vicinity of the first amplitude null ($2.3 < z/\lambda_0 < 3.2$). The measured constant phase contours are shown in Fig. 6. It should be noted, from the calculated constant amplitude surfaces of Fig. 3, that the constant phase contours of Fig. 6 were measured in a region where the leaky wave is the principal contributor to the total field. The slope of these constant phase contours is in good agreement with the calculated slope of the leaky wave phase fronts. The center phase front, having the large wiggles, is the one which occurs at the null of the interference pattern. It is hence the least accurate, since the field amplitude is very low at that point. There is no discontinuity of the phase fronts at the critical angle ($\theta = \theta_c$), but rather there is a smooth blending of the phase fronts of the leaky wave with the radiation field.

Also measured but not shown in this paper were the constant amplitude contours in the region where the leaky wave is the principal wave. The slope of these measured constant amplitude contours was in good agreement with the calculated leaky-wave amplitude contours of Fig. 3. The change of amplitude between adjacent contours was also in good agreement with the predicted values.

There are a number of possible sources of error in the above measurements. One such source of error is due to reflected waves coming from the certainly imperfect matched loads at the top of the trough line and on the negative z side of the current source. The error caused by these reflections would probably be greatest in the vicinity of the amplitude nulls. Another source of error is the low signal-to-noise ratio obtainable near the amplitude nulls. The ratio of source height to dielectric slab thickness (h/d) used for the measurements was 1.11 rather than 1.10 as used for the calculations. A further source of error is that the normalized spacing between the parallel walls of the trough guide ($b/\lambda_0 = 0.128$), though small, is not negligible.

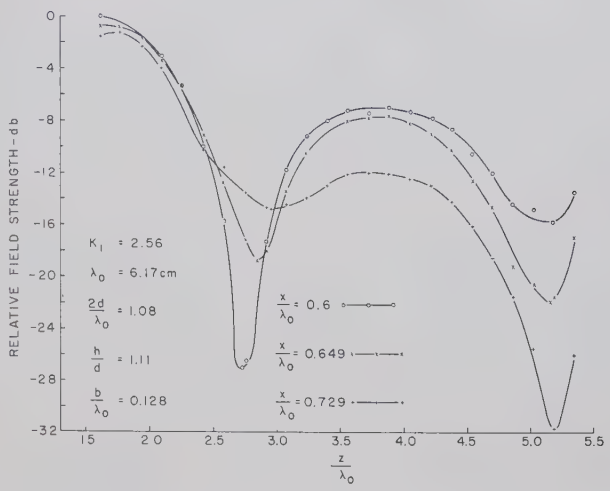

Fig. 5—Measured values of the total electric field in the trough line vs normalized horizontal distance from line source (z/λ_0) for various values of normalized distance above ground plane (x/λ_0).

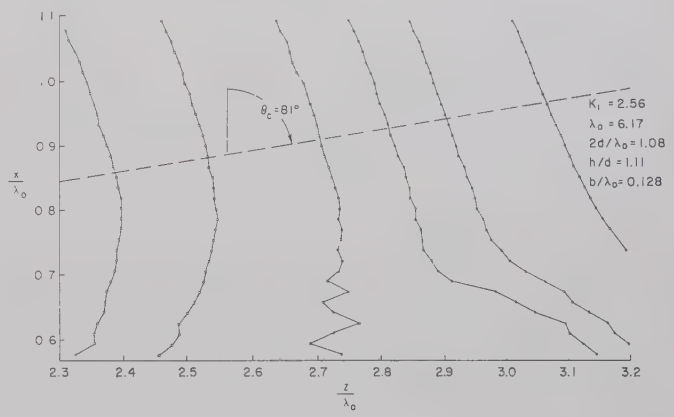

Fig. 6—Measured constant phase contours in the trough line.

Conclusions

Since a leaky wave can never exist by itself, but must be detected in the presence of the remainder of the continuous spatial spectrum and often in the presence of surface waves as well, it is difficult to measure its characteristics. The measurements reported above, however, confirm the existence and predicted characteristics of leaky waves due to a line current source above a grounded dielectric slab.

The predicted and subsequently measured interference between the leaky wave and surface wave strongly emphasizes the need to take leaky waves into account in the design of surface waveguide components and antennas. The particular surface-wave structure and excitation configuration should be investigated to determine if leaky waves exist and what effect they may have on the field distribution.

Acknowledgment

The authors are indebted to Prof. A. A. Oliner and Dr. A. Hessel of the Polytechnic Institute of Brooklyn for stimulating and informative discussions of leaky waves. The authors would also like to thank I. E. Pakulis, who made the measurements reported herein; and Miss M. D. Velten, who performed the numerical calculations.

A Broad-Band Glass-to-Metal Coaxial Vacuum Seal*

W. M. NUNN, JR.†, SENIOR MEMBER, IRE AND L. E. PAUL†, MEMBER, IRE

Summary—The design procedure for a broad-band glass-to-metal seal is described, and experimental results are presented for a structure examined over the frequency range of 100 to 11,000 Mc. The seal described is capable of operating at bakeout temperatures as high as 450°C, with higher temperatures being attainable by the use of other materials.

Introduction

THE fabrication of electron beam devices has led to the requirement for a glass-to-metal vacuum seal in a coaxial transmission system possessing a low standing wave ratio over a wide frequency range. Of the several configurations containing discontinuities[1] the majority involve an abrupt transition with its accompanying bandwidth limitations. It is the purpose of this paper to describe the design and experimental characteristics of a broad-band glass-to-metal vacuum seal developed in this laboratory.

Mathematical Analysis

The basic geometry of the transmission system consists of a coaxial line constructed from Kovar tubing and round stock. The inner conductor is undercut along a circular arc of prescribed radius in the region where the glass-to-metal seal is to be obtained, as shown in Fig. 1.

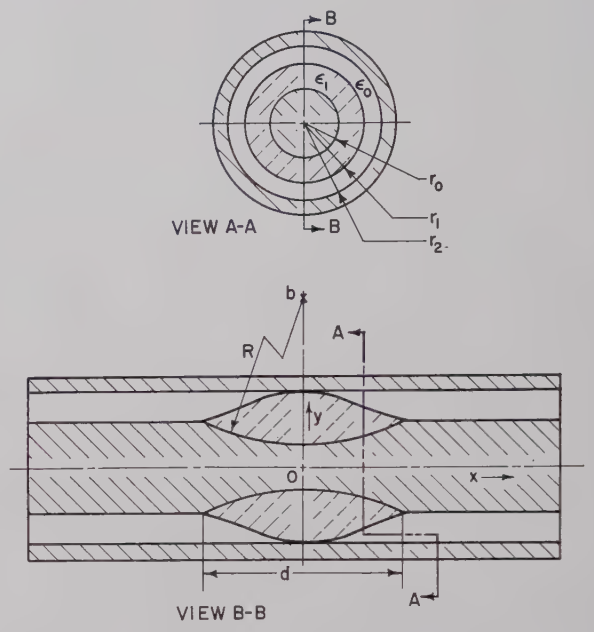

b = center of undercut circle
R = radius of undercut circle
d = length of center-conductor undercut section
r_0 = outside radius of inner conductor
r_1 = radius of glass seal
r_2 = inside radius of outer conductor
ϵ_0 = free-space permittivity
ϵ_1 = permittivity of glass

Fig. 1—Geometry of coaxial transmission system.

Since only the TEM mode is presumed to exist in the lossless coaxial line, the characteristic impedance of the air-glass dielectric region (such as view A-A) of Fig. 1 can be computed by means of[2,3]

$$Z_0 = \sqrt{\frac{L}{C}}, \tag{1}$$

where L = inductance per unit length of the transmission line in henry per meter, and C = capacitance per unit length of the transmission line in farad per meter. Subject to the assumption that the permeability of the glass is the same as that of air, the inductance per unit length is found to be[2]

$$L = 2 \cdot 10^{-7} \ln\left(\frac{r_2}{r_0}\right) \text{ henry per meter}, \tag{2}$$

where $\ln(r_2/r_0)$ designates the natural logarithm of the ratio of radii defined in Fig. 1. The capacitance per unit length can be determined for a typical transverse plane containing the two types of dielectric by noting first that the "RF voltage" V, in that plane, is equal to

$$V = \int_{r_0}^{r_1} \frac{Q dr}{2\pi\epsilon_1 r} + \int_{r_1}^{r_2} \frac{Q dr}{2\pi\epsilon_0 r}. \tag{3}$$

It follows that

$$C = \frac{2\pi k \epsilon_0}{\ln\left(\frac{r_1}{r_0}\right) + k \ln\left(\frac{r_2}{r_1}\right)} \tag{4}$$

where Q designates the charge per unit length and k denotes the relative dielectric constant of the glass seal.

* Received by the PGMTT, July 13, 1960; revised manuscript received, February 17, 1961. Supported by the Diamond Ordnance Fuze Labs. under Contract No. DA-49-186-502-ORD-720.

† Electron Phys. Lab., Dept. of Elec. Engrg., The University of Michigan, Ann Arbor.

[1] G. L. Ragan, "Microwave Transmission Circuits," M.I.T. Rad. Lab. Ser., McGraw-Hill Book Co., Inc., New York, N. Y., vol. 9; 1948.

[2] W. C. Johnson, "Transmission Lines and Networks," McGraw-Hill Book Co., Inc., New York, N. Y.; 1950.

[3] S. Ramo and J. R. Whinnery, "Fields and Waves in Modern Radio," John Wiley and Sons, Inc., New York, N. Y., 2nd ed.; 1953.

Upon substituting (2) and (4) into (1), the characteristic impedance becomes

$$Z_0 = 60\sqrt{\ln\left(\frac{r_2}{r_0}\right)\left[\ln\left(\frac{r_2}{r_1}\right)+\frac{1}{k}\ln\left(\frac{r_1}{r_0}\right)\right]}\ \text{ohms}. \quad (5)$$

Since the inside diameter of the outer conductor is held constant over the entire length of the line, the basic problem is reduced to the determination of the manner in which the radius of the glass must vary with the axial dimension x, for a specified variation of the center conductor, to maintain the impedance invariant[4] when only TEM waves are presumed to exist.

The investigation is facilitated by observing that (5) can be written

$$\ln\left(\frac{r_2}{r_1}\right) = \frac{k}{k-1}\left[\frac{(Z_0/60)^2}{\ln(r_2/r_0)} - \frac{\ln(r_2/r_0)}{k}\right]. \quad (6)$$

This relation has been employed to obtain the general design curves presented in Fig. 2. Using an assumed characteristic impedance of 50 ohms, the ratio (r_2/r_1) is plotted vs the independent variable (r_2/r_0) over the range of dielectric constant values typically found in the vacuum sealing glasses. Thus, upon selecting a specific value of (r_2/r_0), an associated value of (r_2/r_1) which yields an invariant impedance may be read from the curves. It is therefore possible to select a particular variation of the radius of the center conductor as a function of x and find the required variation of the glass.

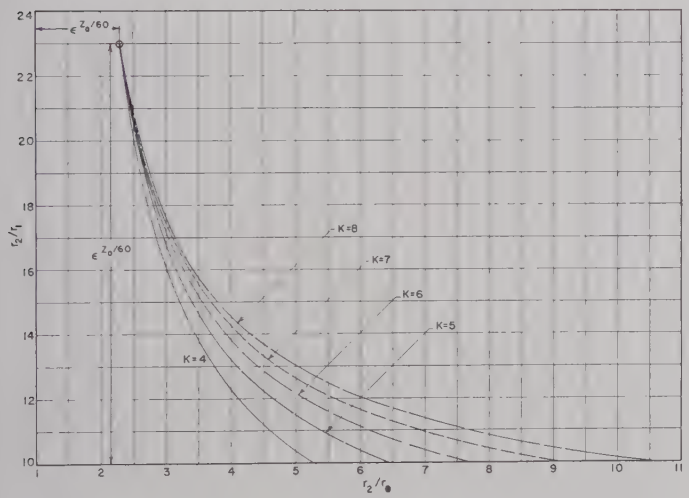

Fig. 2—Universal design curves for a glass-to-metal seal having a prescribed dielectric constant in a transmission line of 50 ohms characteristic impedance.

[4] It is assumed that the change of radii will be sufficiently gradual so as to avoid the generation of longitudinal field components.

Fabrication Procedure

The variation of the radius of the glass as a function of x, which has been experimentally investigated at this laboratory, is the one for which the radius of the center conductor follows a segment of a circle as shown in Fig. 1. If the center of this circle of radius R is chosen at b as indicated, the radial dependence of the center conductor upon the axial coordinate is given by

$$r_0(x) = b \mp \sqrt{R^2 - x^2}\left(|x| \leqq \frac{d}{2}\right), \quad (7)$$

where the upper double sign holds for $y>0$, and the lower sign applies when $y<0$. This relation may be used in conjunction with the design curves of Fig. 2, and the specific numerical data given below, to obtain the desired shape of the glass seal.

Since the inside radius of standard $\frac{1}{8}$-inch Kovar tubing has a fixed value of

$$r_2 = 0.054 \text{ inch},$$

it follows from (5) that the radius r_0 becomes, for a 50-ohm characteristic impedance in air,

$$r_0(x) = 0.02345 \text{ inch}\left(|x| \geqq \frac{d}{2}\right).$$

This radius can be accurately machined by centerless grinding standard 1/16-inch Kovar round stock. Similarly, application of (5) to the region containing only the glass, whose dielectric constant is approximately 5, yields for the 50-ohm impedance condition

$$r_0(x) = 0.00836 \text{ inch} \qquad (x = 0).$$

It may readily be shown from elementary mathematics that the radius R of the "undercut circle" depicted in Fig. 1 is given by

$$R = \frac{h}{2}\left[1 + \left(\frac{d}{2h}\right)^2\right], \quad (8)$$

where d is the length of the undercut measured parallel to the axis of the center conductor, and

$$h = r_0\left(\frac{d}{2}\right) - r_0(0). \quad (9)$$

In (9) the quantity $r_0(d/2)$ designates the radius of the center conductor at $x=d/2$, while $r_0(0)$ designates its radius at $x=0$. Using the previously computed values of $r_0(x)$ in conjunction with (9) it follows that

$$h = 0.01509 \text{ inch}.$$

This quantity is used in conjunction with (8) to obtain a radius R of 2.078 inch, corresponding to a length of undercut d equal to 0.500 inch. The desired radius may easily be obtained to an accuracy of ± 0.001 inch. The

center conductor is then ground to the desired radius of undercut by a surface grinder while the Kovar stock is rotating in a cylindrical grinding attachment.

Having thus established numerical values for the radial dimensions of the coaxial transmission system, as well as one attainable dependency upon x of the center conductor radius, it is now possible to plot the required variation of the glass radius necessary to maintain a constant impedance. Using the graphs of Fig. 2 for the case of a dielectric constant equal to 5, a curve of this type is presented in Fig. 3 for a center conductor containing a 0.500-inch length d of undercut. Near $x=0$ the curve is very nearly flat and exhibits slight rounding as the steep portion is approached. At large values of x the asymptotic behavior of the function is evident.

The mechanical preparation of the outer Kovar tubing is completed by enlarging its inside diameter slightly over a distance of approximately $\frac{1}{8}$ inch from each end. This operation simplifies the insertion of the glassed center conductor and also improves the impedance match in the connector-to-air dielectric region by avoiding abrupt discontinuities.

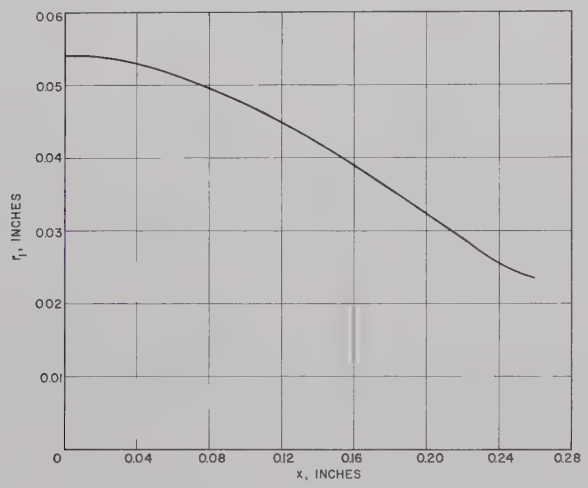

Fig. 3—Variation of glass seal necessary to maintain constant impedance for: $k=5$, $d=0.500$ inch, $r_2=0.054$ inch, $r_0(0)=0.00836$ inch, $r_0(d/2)=0.02345$ inch.

In order to insure the maintenance of vacuum by the 7052 Kovar sealing glass, and to minimize the possibility of reflection of the RF wave, it is essential to avoid the formation of bubbles in the glass. This detrimental condition can be circumvented by observing the customary hydrogen or vacuum firing procedure, and the preheating cycle[5] immediately prior to sealing, which serves to outgas the Kovar tubing. Moreover, the oxide coating necessary to achieve a proper glass-to-metal bond is simultaneously obtained by this process.

The configuration of the glass contour in the glass-air transition region of the dielectric is formed to the general shape of the curve shown in Fig. 3. It is essential to exercise care to insure that excess glass is present on all surfaces. The glass bead is then ground to the desired contour using a $\frac{3}{4}$-inch-diameter grinding wheel, while the entire seal and center conductor is rotating in a glass lathe. The diameter of the center portion of the glass bead is ground until a slip fit is obtained in the Kovar tubing.

The positioning of the center conductor and seal within the Kovar tubing is accomplished by appropriate jigging. The temperature is brought slowly up to the annealing point of the glass with a carbon flame and then quickly elevated to the sealing temperature of the glass for 15 to 20 seconds. The outline of the bead in the vicinity of the tubing will soften and tend to contract to a spherical shape, thereby enlarging the surface of contact with the tubing. In addition to aiding the maintenance of a good vacuum, this configuration has the desired form required to maintain the characteristic impedance constant. In view of the temperature gradient which exists between the center and outer conductors as a result of the short heating time, glass flow along the center conductor is minimized.

Experimental Results

The small size of the coaxial tubing described here was selected to minimize the possibility of exciting higher mode fields in the transmission system. Experimental observations reveal that the seals are capable of maintaining a vacuum well within the range of 10^{-8} to 10^{-7} mm Hg.

Several glass-to-metal seals were constructed and measured over the frequency ranges of 100 to 1000 Mc and 2000 to 11,000 Mc. In the lower of these two ranges, the seal was inserted in a section of coaxial transmission line terminated with a type-N connector at each end. Using the design procedure described above, two such seals were constructed, one with an undercut d equal to 0.500 inch and the other of 0.750 inch. It was found that the average VSWR for both seals was approximately 1.1, with minimum and maximum standing-wave ratios of 1.05 and 1.19, respectively.

Measurements in the frequency range of 2000 to 11,000 Mc are somewhat more difficult to carry out since reflections from the type-N connectors have been found to be undesirably large. The test apparatus involved the construction of a 0.025-inch-wide slot in the coaxial transmission system containing the glass bead. A 9.5-inch-length taper load was inserted in the transmission system immediately following the glass bead. A very gradual taper was achieved by wrapping the center conductor with cotton or nylon thread, and subsequently coating it with several applications of acquadag. Experimental observations made on a transmission system containing the load alone revealed that the standing-wave ratio could be kept to approximately 1.06 over the desired frequency range.

[5] The temperature is raised approximately 200°C above the glass-working temperature with the sealing torch.

The entire bead-and-load coaxial system was attached to a Hewlett-Packard universal probe carriage, with appropriate mechanical supports being constructed to minimize transverse motion of the probe. Since the probe diameter of approximately 0.020 inch was used (thereby allowing a clearance of only 0.002 inch between the probe and slot), precise centering of the probe in the slot was accomplished by observing the standing-wave indicator as the probe was moved along the length of the slot.

Aside from the difficulties associated with variable probe-to-slot coupling,[6] slope effect,[7] radiation from the slot, minimum probe penetration, and proper probe tuning[8] must be carefully considered in order to interpret the data. Upon following the recommended procedures, the results for a glass seal having a one-half-inch length of undercut are plotted in Fig. 4. A second seal of identical design was constructed to determine the degree to which the characteristics could be duplicated. It was found that substantially the same SWR dependence upon frequency was obtained. From these observations it appears that the reflections produced by the glass seal alone lead to a SWR of less than 1.3 over the range of frequencies examined.

[6] E. L. Ginzton, "Microwave Measurements," McGraw-Hill Book Co., Inc., New York, N. Y.; 1957.
[7] C. G. Montgomery, "Technique of Microwave Measurements," M.I.T. Rad. Lab. Ser., McGraw-Hill Book Co., Inc., New York, N. Y., vol. 11; 1947.
[8] J. I. Caicoya, "Tuning a probe in a slotted line," Proc. IRE, vol. 46, pp. 787–788; April, 1958.

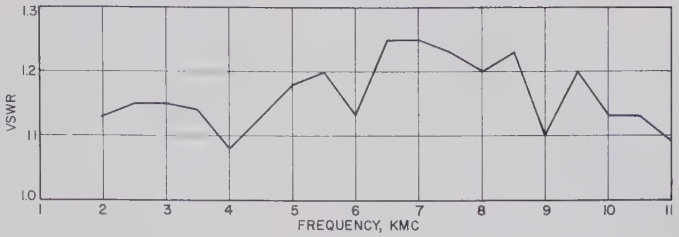

Fig. 4—Experimental results for the glass-to-metal seal.

Conclusions

The design procedure developed in this paper leads to the prediction of the shape of the glass seal required to maintain the characteristic impedance of a TEM wave invariant. The coaxial glass-to-metal seal described here may be employed in the construction of electron beam devices requiring bakeout temperatures as high as 450°C. It should also be possible to replace the Kovar metal with molybdenum and still achieve the same bakeout temperature, while also obtaining a nonmagnetic seal. Moreover, if 1720 or 1723 (aluminum silicate) glass is used in conjunction with molybdenum, a nonmagnetic seal having a bakeout temperature as high as 700°C can be attained.

Acknowledgment

The authors would like to thank D. Williams and K. McCrath for their assistance in assembling the seals and connectors.

Magnetically-Tunable Microwave Filters Using Single-Crystal Yttrium-Iron-Garnet Resonators*

PHILIP S. CARTER, JR.†, MEMBER, IRE

Summary—A new type of magnetically-tunable band-pass microwave filter that makes use of ferrimagnetic resonance in single-crystal yttrium iron garnet is presented. The 3-db bandwidth can be adjusted from about 6 Mc to 100 Mc at *X* band, and the center frequency can be tuned over a wide range of frequencies, by means of a varying dc field. A theoretical analysis of the operation and behavior of this type of filter is presented. Descriptions of single-resonator and two-resonator filters which can be tuned over the *X*-band frequency range are given and experimental data are presented showing their tuning range, insertion loss, and bandwidth.

I. Introduction

With the increased use of continuously tunable microwave receivers, there has been a demand for a nonmechanically tuned, narrow-band filter which is tunable over a broad band of frequencies in the microwave frequency range. Previous attempts to solve this problem have included the use of cavities containtaining ferroelectrics,[1] "Varicaps" or voltage-tuned back-biased diodes,[2,3] and ferrites.[4–6] In general, tuning ranges of a few per cent are possible using these techniques while maintaining a high unloaded resonator $Q(Q_u)$.

The main difficulty with previous tuning techniques is high losses, which are greatly reduced by the use of the ferrimagnetic material, yttrium-iron-garnet (YIG). Single crystals of this material (now available commercially) show extremely low losses when used as the resonant elements in a band-pass (or band-reject) filter. The Q_u of this material considered as a resonator is typically between 2000 and 4000 at *X*-band frequencies and therefore compares favorably with transmission-line and hollow-cavity resonators.

This new approach to the problem of nonmechanical tuning makes use of the equivalence between a resonant circuit, such as an inductively coupled cavity or lumped-element series-resonant circuit, and an inductively coupled magnetic resonator biased with a dc magnetic field.

This equivalent circuit was first worked out analytically by Bloembergen and Pound[7] and was first applied by DeGrasse[8] to the design of an *S*-band limiter, using a single-crystal YIG resonator.

The tunability feature results from the fact that the resonant frequency is nearly a linear function of dc magnetic biasing field. This feature allows a very broad tuning range, limited mainly by the bandwidth of the microwave coupling structure employed.

The first part of this paper consists of a mathematical analysis of the equivalent circuit of a ferrimagnetic resonator coupled to external loads by means of loops, transmission lines, and waveguides. Analytical formulas for the external $Q(Q_e)$ of the ferrimagnetic resonator are given for loops, strip-transmission-lines and TE_{10} mode rectangular waveguide. A formula is given which relates the unloaded $Q(Q_u)$ of the ferrite resonator to the properties of the ferrite (damping time and gyromagnetic ratio).

The second part of this paper consists of descriptions of, and performance data taken on, two types of magnetically tunable filters operating in the *X*-band region and above. These are: 1) a single-resonator filter which has a tuning range from 7.0 kMc to 11.2 kMc, and 2) a two-resonator filter whose tuning range extends from 8.2 to 14.0 kMc.

II. Basic Principle of Operation

The basic idea of the magnetic resonance filter is illustrated in Fig. 1. Two coils have their axes at right angles to each other, and a small ferrite sample is placed at the intersection of the coil axes. When the sample is not magnetized, no power is transferred between the coils because the loop axes are perpendicular to each

* Received by the PGMTT, July 15, 1960; revised manuscript received, March 6, 1961. Sponsored by the U. S. Army Signal Research and Development Lab., Fort Monmouth, N. J., under Contract No. DA 36-039-74862. A shorter version of this paper was presented at the 1960 IRE International Convention (1960 IRE International Convention Record, pt. 3, pp. 130–135).

† Stanford Research Inst., Menlo Park, Calif.

[1] W. J. Gemulla and R. D. Hall, "Ferroelectrics at microwave frequencies," *Microwave J.*, vol. 3, pp. 47–51; February, 1960.

[2] E. M. T. Jones, G. L. Matthaei, S. B. Cohn, and B. M. Schiffman, "Design Criteria for Microwave Filters and Coupling Structures," Stanford Research Inst., Menlo Park, Calif. Tech. Rept. 5, SRI Project 2326, Contract No. DA 36-039 SC-74862; March, 1959.

[3] A. Uhlir, Jr., "The potential of semiconductor diodes in high-frequency communications," Proc. IRE, vol. 46, pp. 1099–1115; June, 1958.

[4] G. R. Jones, J. C. Cacheris, and C. A. Morrison, "Magnetic tuning of resonant cavities and wideband frequency modulation of klystrons," Proc. IRE, vol. 44, pp. 1431–1438; October, 1956.

[5] C. E. Fay, "Ferrite-tuned resonant cavities," Proc. IRE, vol. 44, pp. 1446–1449; October, 1956.

[6] C. E. Nelson, "Ferrite-tunable microwave cavities and the introduction of a new reflectionless tunable microwave filter," Proc. IRE, vol. 44, pp. 1449–1455; October, 1956.

[7] N. Bloembergen and R. V. Pound, "Radiation damping in magnetic resonance experiments," *Phys. Rev.*, vol. 95, pp. 8–12; July 1, 1954.

[8] R. W. DeGrasse, "Low-loss gyromagnetic coupling through single crystal garnets," *J. Appl. Phys.*, Suppl. to vol. 30, pp. 155S–156S; April, 1959.

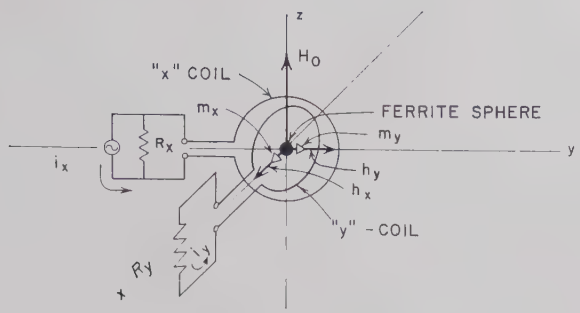

Fig. 1—Magnetic resonance filter.

other and there is no interaction with the ferrite. When a dc field H_0 is applied along the z axis, and an RF driving current $i_x e^{j\omega t}$ is applied to the terminals of the x coil, the magnetic moments of the electrons in the ferrite precess around the x axis, producing an RF magnetic moment along the y axis and inducing a voltage in the y circuit. The precession angle is largest and thus the induced voltage in the y-coil is maximum, at ferromagnetic resonance given by $\omega_0 = \mu_0 \gamma H_0$ for a spherical ferrite,[9] where γ is the gyromagnetic ratio and is very close to 1.759×10^{11} for electrons in most ferrites. The drop-off in response away from resonance is determined by the degree of coupling of the external loads R_x and R_y and the internal losses in the ferrite. It is shown in Section III that the equivalent circuit of this device is a resonant circuit, inductively coupled to the output lines or loads. This circuit is also a gyrator; the phase shift in one direction through the circuit differs from the phase shift in the other direction by 180°.

One requirement on the resonator in a low-insertion-loss, narrow-band-pass filter is that Q_u be high. Although it is necessary to specify the application in more detail in order to specify what exactly is meant by "high-Q_u," it may be stated in general that Q_u's of several hundred or higher are useful for filter design. Q_u's of this order are obtained at microwave frequencies with single-crystal-yttrium-iron-garnet.

The second requirement to obtain low insertion loss in a narrow-band, band-pass filter is that the external Q, Q_e of the resonators be considerably lower than Q_u. It was not apparent from previous work by DeGrasse[8] that sufficiently low Q_e could be obtained over a wide tuning range. It is shown below that sufficient coupling can actually be obtained without the use of the narrow-band impedance matching employed by DeGrasse.[8]

Two other characteristics of single crystal ferrimagnetic resonators must be considered in designing a magnetically tunable filter: 1) magnetocrystalline anisotropy, and 2) the higher-order magnetostatic modes. Their effects on filter characteristics and design are discussed below.

[9] These quantities are defined in Section III.

III. Analysis and Measurement of Coupling Characteristics and Equivalent Circuits of Ferrite Resonators in Lumped-Element Circuits, Transmission Lines, and Waveguides

In the following analysis, the ferrite resonator is assumed to be small enough that the RF field is substantially uniform throughout the volume of the sample and therefore that higher-order modes are not excited. Also magnetocrystalline anisotropy is neglected. In this case, with the dc magnetic field H_0 applied along the z-axis, the RF magnetizations in the x and y directions are given by the following relations:[10]

$$m_x = \chi_{xx}{}^e h_x + \chi_{xy}{}^e h_y, \tag{1a}$$

$$m_y = \chi_{yx}{}^e h_x + \chi_{yy}{}^e h_y, \tag{1b}$$

where

$m_x = x$ component of RF magnetization within ferrite,
$m_y = y$ component of RF magnetization within ferrite,
$h_x = x$ component of applied RF field,
$h_y = y$ component of applied RF field,
$\chi_{xx}{}^e = \chi_{yy}{}^e = x - x(y-y)$ component of effective RF tensor, susceptibility,[11]
$\chi_{xy}{}^e = -\chi_{yx}{}^e = x - y(y-x)$ component of effective RF tensor susceptibility.

Flammer[12] has developed analytical formulas for the effective susceptibility that include the loss in the ferrite. These expressions were derived using the Bloch-Bloembergen[13] formulation of the equations of motion of magnetization, including the effect of the shape-dependent demagnetizing factors N_x, N_y, and N_z for a

[10] MKS units are used here and throughout this paper.

[11] The effective or external susceptibility is the ratio of the RF magnetic moment to the *applied* RF magnetic field (not the RF magnetic field inside the ferrite).

[12] C. Flammer, "Resonance Phenomena in Ferrites," Stanford Research Inst., Menlo Park, Calif. unpublished memorandum; 1956. Stanford plans to publish this memorandum in the near future.

[13] N. Bloembergen, "Magnetic resonance in ferrites," Proc. IRE, vol. 44, pp. 1259–1269; October, 1956. It has been pointed out by Flammer that (5) in this reference contains an error. The term $-M_0/\gamma$ should be deleted.

general ellipsoidal sample.[14] These formulas for the effective tensor susceptibility are

$$\chi_{xx}^{e} = \frac{\omega_m\left[\omega_0 + (N_y - N_z)\omega_m + \dfrac{j\omega/\tau}{\omega_0 - N_z\omega_m}\right] + \dfrac{\omega_m}{(\omega_0 - N_z\omega_m)^2}\left[\omega_0 + (N_y - N_z)\omega_m\right]\cdot\dfrac{1}{\tau^2}}{\left\{\left[\omega_0 + (N_y - N_z)\omega_m + \dfrac{j\omega/\tau}{\omega_0 - N_z\omega_m}\right]\left[\omega_0 + (N_x - N_z)\omega_m + \dfrac{j\omega/\tau}{\omega_0 - N_z\omega_m}\right] - \omega^2 + \dfrac{1}{(\omega_0 - N_z\omega_m)^2\tau^2}\cdot\left[\omega_0 + (N_x - N_z)\omega_m\right]\left[\omega_0 + (N_y - N_z)\omega_m\right]\right\}}, \tag{2a}$$

$$\chi_{yy}^{e} = \frac{\omega_m\omega_0 + (N_x - N_z)\omega_m + \dfrac{j\omega/\tau}{(\omega_0 - N_z\omega_m)^2} + \dfrac{\omega_m}{(\omega_0 - N_z\omega_m)^2}\left[\omega_0 + (N_x - N_z)\omega_m\right]\dfrac{1}{\tau^2}}{\left\{\left[\omega_0 + (N_x - N_z)\omega_m + \dfrac{j\omega/\tau}{\omega_0 - N_z\omega_m}\right]\left[\omega_0 + (N_y - N_z)\omega_m + j\dfrac{\omega/\tau}{\omega_0 - N_z\omega_m}\right] - \omega^2 + \dfrac{1}{(\omega_0 - N_z\omega_m)^2\tau^2}\left[\omega_0 + (N_x - N_z)\omega_m\right]\left[\omega_0 + (N_y - N_z)\omega_m\right]\right\}}, \tag{2b}$$

$$\chi_{xy}^{e} = -\chi_{yx}^{e} = \frac{-j\omega_m\omega}{\left\{\left[\omega_0 + (N_x - N_z)\omega_m + \dfrac{j\omega/\tau}{\omega_0 - N_z\omega_m}\right]\left[\omega_0 + (N_y - N_z)\omega_m + \dfrac{j\omega/\tau}{\omega_0 - N_z\omega_m}\right] - \omega^2 + \dfrac{1}{(\omega_0 - N_z\omega_m)^2\tau^2}\left[\omega_0 + (N_x - N_z)\omega_m\right]\left[\omega_0 + (N_y - N_z)\omega_m\right]\right\}}, \tag{2c}$$

in which

$\omega_m = \mu_0\gamma M_0 = \gamma_0 M_0$,
$\omega_0 = \mu_0\gamma H_0$,
γ = gyromagnetic ratio $= g(e/2m)$,
N_x, N_y, N_z = effective demagnetizing factors in x, y, and z directions,
τ = Bloch-Bloembergen phenomenological relaxation time,
g = Landé "g" factor $\cong 2.00$ for electrons in most ferrites,
e/m = ratio of charge e to mass m of electron, $= 1.759\times 10^{+11}$ coulombs/kg,
M_0 = saturation magnetization in amperes per meter,
μ_0 = intrinsic permeability of free space $= 1.256\times 10^{-6}$ henries per meter,
H_0 = applied dc field in amperes per meter.

For a spherical geometry, $N_x = N_y = N_z = \frac{1}{3}$; and (2) becomes after some algebraic reduction and elimination of terms of order $1/\tau^2$ or smaller,

$$\chi_{xx}^{e} = \chi_{yy}^{e} = \frac{\omega_0\omega_m}{\omega_0^2 - \omega^2 + \dfrac{2j\omega}{\tau}\left(1 + \dfrac{\omega_m/3}{\omega_0 - \omega_m/3}\right)} \tag{3a}$$

$$\chi_{xy}^{e} = -\chi_{yx}^{e} = \frac{-j\omega_m\omega}{\omega_0^2 - \omega^2 + \dfrac{2j\omega}{\tau}\left(1 + \dfrac{\omega_m/3}{\omega_0 - \omega_m/3}\right)}. \tag{3b}$$

[14] C. Kittel, "On the theory of ferromagnetic resonance absorption," *Phys. Rev.*, vol. 73, pp. 155–161; January 15, 1948.

The complete detailed equivalent circuit[15] of the ferrimagnetic resonator located at the intersection of the two loops is shown in Fig. 2. It consists of a resonant circuit coupled inductively to the signal source i_x, to the source impedance R_x, and to the load impedance R_y. In addition to the series-resonant circuit, there is a nonreciprocal phase shifter which produces, with the coil arrangement shown in Fig. 1, an additional *negative* 90° phase shift in the output voltage across R_y. With the signal generator connected to the y terminals an additional *positive* 90° phase shift is produced across R_x.

The complete analytical formulation of the circuit representation of the ferrimagnetic resonator has been carried out for the following cases:

1) Ferrimagnetic resonator located at the intersection of the axes of the two orthogonal loops shown in Fig. 1.

2) Resonator located at a position of an equivalent short circuit along a short-circuited two-wire TEM-mode transmission line, shown in Fig. 3(b).

3) Same as case 2 in a strip-center-conductor line.

4) Resonator located at a position of an equivalent short circuit at the center of a short-circuited TE_{10}-mode waveguide.

[15] P. S. Carter, Jr. and G. L. Matthaei, "Design Criteria for Microwave Filters and Coupling Structures," Stanford Research Inst., Menlo Park, Calif. Tech. Rept. 8, SRI Project 2326, Contract No. DA 36-039 SC-74862; September, 1959.

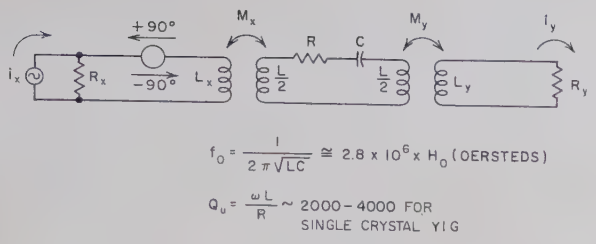

Fig. 2—Equivalent circuit of magnetic resonance filter.

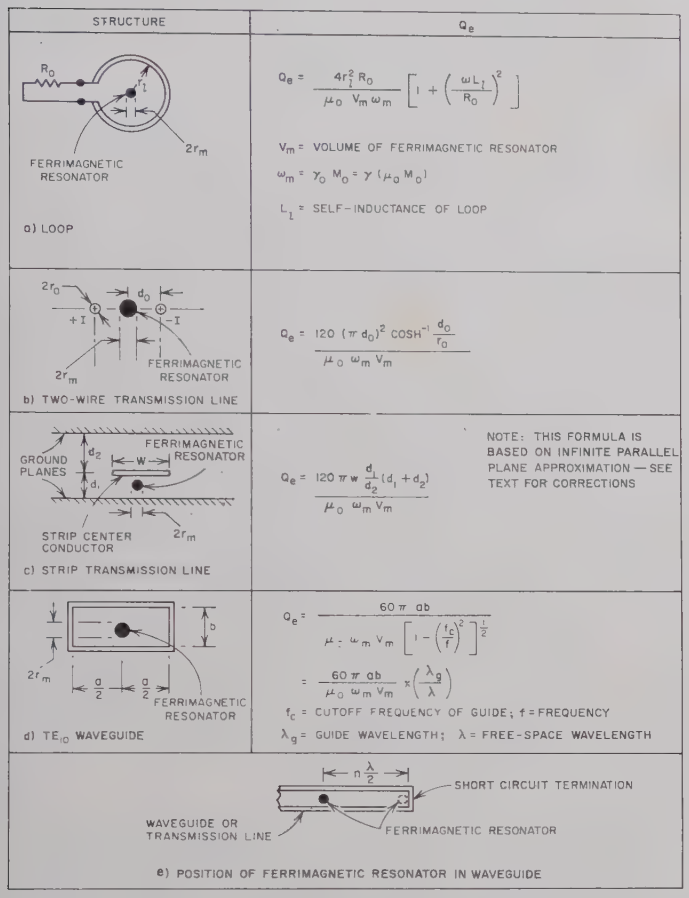

Fig. 3—Q_e of ferrimagnetic resonator in several waveguide structures.

In each case the complete equivalent circuit of the ferrimagnetic resonator coupled to the external circuit is expressed in terms of the unloaded Q_u of the resonator and the coupled or external Q_e.[16]

The unloaded Q_u of the ferrimagnetic resonator is a property of the ferrimagnetic material and is independent of the external circuit.[17] An analytical formula for Q_u derived from the equivalent circuit is given by[15]

$$Q_u = (\omega_0 - N_z\omega_m)\tau/2 = \frac{H_0 - N_z M_0}{\Delta H^i}, \qquad (4)$$

where ΔH^i is the line width given by

$$\Delta H^i = \frac{2}{\gamma_0 \tau}.$$

Eq. (4) predicts low values of unloaded Q_u for low resonant frequencies, and also predicts, in particular, that Q_u will reach zero at value of dc field and RF frequency given by $\omega_0 = N_z\omega_m$. For a spherical YIG resonator, this low cutoff frequency occurs at $f_0 = \omega_m/3 \times 2\pi = 1670$ Mc. Measurements made of Q_u in the frequency range of this cutoff support this theory.[18]

Eq. (4) predicts that Q_u depends on $N_z\omega_m$. In particular, a long-rod geometry with the dc magnetic field along the axis of the rod (so that $N_z \approx 0$) should yield a maximum value of Q_u. This effect of the shape on Q_u has not yet been measured. Finally, (4) shows that, for a constant relaxation time τ, Q_u is higher in the case of a lower saturation magnetization material. For frequencies below around 2000 Mc, a low-M_0, narrow-linewidth material is desirable. This requirement is discussed in Section VII.

The external or coupled Q_e depends upon the volume of the ferrimagnetic resonator V_m, its saturation magnetization M_0, and the type and geometry of the coupling structure. Formulas for Q_e have been derived for the four cases listed. The resulting formulas, tabulated in Fig. 3, may be applied to the calculation of the Q_e of the uniform precessional mode of any ellipsoidally shaped magnetic resonator (rods, disks, etc).

The formulas for Q_e given in Fig. 3 were derived using two different methods: The first, which employs the reciprocity theorem,[15] is valid for lumped-parameter coupling devices such as loops, and for TEM-mode transmission lines. The equation for Q_e of the magnetic resonator in the TE_{10}-mode rectangular waveguide [Fig. 3(d)] was derived using a more general coupling formula discussed by Slater.[19] For the waveguide case, a *linearly-polarized* magnetic moment was assumed. The RF magnetic moment of a magnetic resonator is in general *elliptically* polarized, therefore, both perpendicular components of RF magnetic moment can interact with an elliptically polarized waveguide field. The formula for Q_e given above is thus valid only when the magnetic sample is located in the linearly-polarized field at the center of the guide.[20]

[16] C. G. Montgomery, R. H. Dicke, and E. M. Purcell, "Principles of Microwave Circuits," M.I.T., Rad. Lab. Ser. No. 8, McGraw-Hill Book Co., Inc., New York, N. Y., pp. 228–239; 1948.

[17] This is true for the essentially unperturbed resonator located a sufficient distance from the boundaries of the waveguide. For close wall-to-resonator spacings, resistive losses due to image currents in the waveguide walls and the detuning effects of these images are significant to the resonance characteristics.

[18] P. S. Carter, Jr. and C. Flammer, "Unloaded Q of single crystal garnet resonator as a function of frequency," IRE Trans. on Microwave Theory and Techniques, vol. MTT-8 (Correspondence), pp. 570–571; September, 1960.

[19] J. C. Slater, "Microwave Electronics," D. Van Nostrand Co., Inc., New York, N. Y., ch. 7, p. 150; 1950.

[20] Recently while this paper was being revised, the author was made aware of a more general scattering formula which is applicable in the case where the ellipsoidal sample is at an arbitrary position in the guide. See H. J. Shaw and L. K. Anderson, "Ferrimagnetic resonance in ferrites," in "Interaction of Microwaves with Matter," Microwave Laboratory, Stanford University, Stanford, Calif., Tech. Status Rept. No. 9, Section 1, Contract AF 49(638)-415; May 1–July 31, 1960.

Measurements were made of the Q_e of single-crystal YIG resonators in strip transmission line and TE_{10}-mode rectangular waveguide, and the results of these measurements are shown in Figs. 4 and 5. Fig. 4 shows measurements made on spherical single-crystal YIG resonators of various diameters mounted on a wafer of polyfoam in a section of one-quarter height, standard width, X-band, rectangular waveguide. The waveguide was short-circuited and the YIG sphere was mounted one-half wavelength from the short circuit. The measurements were made in this configuration at 10.0 kMc, using the impedance method described by Ginzton.[21] The solid curve represents the theoretical formula for Q_e. Close agreement between the experimental and theoretical values is evident. When resonator diameters greater than about 0.070 inch were used, measurement accuracy was diminished by the high degree of coupling between the external circuit and the higher-order magnetostatic modes. The effect of the higher-order modes on filter performance is discussed in Section IV.

Fig. 5 shows measurements of Q_e of a strip-transmission-line coupling circuit. The strip-transmission-line configuration (Fig. 5) has a 0.500-inch-wide 0.020-inch-thick center conductor spaced 0.135 inch from the outer conductor on both sides of the center conductor. The inside width of the outer conductor is 1.00 inch. Q_e was measured at a resonant frequency, $f_0 = 3000$ Mc. In these measurements the YIG resonator was mounted close to the short-circuited end of the strip transmission line—the position occupied by the resonator in a magnetically tunable filter where a broad tuning range is desired—since this remains a position of nearly maximum magnetic field as the frequency is varied. The minimum distance between the sphere and the short-circuited end is prescribed by the maximum allowable coupling to higher-order modes. With the resonator touching the short-circuit, appreciable coupling to higher-order modes occurs. In the case shown in Fig. 5 with 0.125-inch spacing between the resonator and the end wall, experiment showed that the coupling to higher-order modes was very loose, *i.e.*, $Q_e > 15{,}000$, for the most strongly coupled higher-order mode. The coupling to the uniform precession resonance at 3000 Mc was not measurably decreased by this 0.125-inch spacing.

The theoretical values for Q_e of the strip transmission line are shown in Fig. 5 as the solid-line curve. This curve was calculated using the formula given in Fig. 3(c), which is very accurate where $w \gg d_1$ and d_2, but not quite so accurate where $w = 0.500$ inch and $d_1 = d_2 = 0.135$ inch (as in Fig. 5). An empirical correction was applied to improve the accuracy of this formula by replacing w in Fig. 3(c) by a slightly larger value, w', which takes into account the fringing of the field at the edge of the

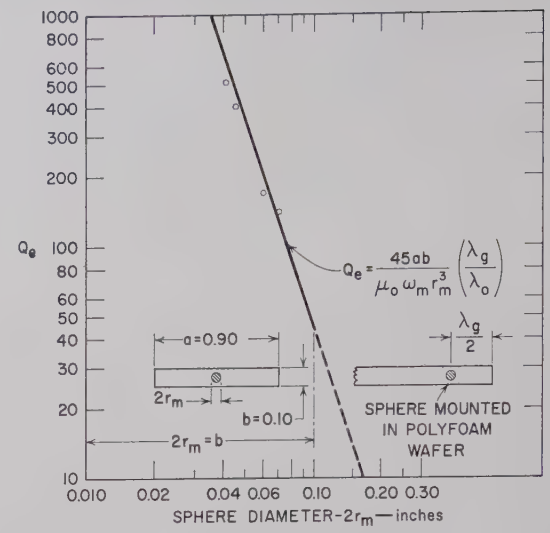

Fig. 4—Theoretical and experimental Q_e of YIG resonators in reduced-height (one-quarter), standard-width X-band waveguide at 10,000 Mc.

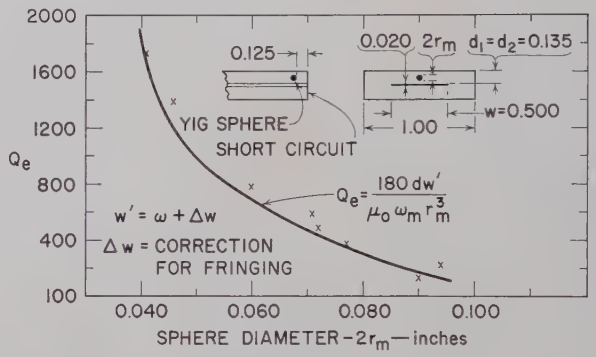

Fig. 5—Theoretical and experimental values of Q_e of YIG resonator using stripline coupling at 3000 Mc.

strip center conductor. This corrected width w' was obtained as follows: the characteristic impedance Z_0' of the actual configuration shown in Fig. 5 was obtained from an accurate formula[22] which includes the effect of the finite thickness of the center conductor and the fringing of the field at the two edges. This value of characteristic impedance Z_0' was then used to compute an effective strip width w', based on the parallel-plane formula, *i.e.*,

$$w' = \frac{\eta_0}{Z_0'} \frac{d_1 d_2}{d_1 + d_2},$$

again using the actual conductor spacings d_1 and d_2, where $\eta_0 = 377$ ohms.

The agreement between the measured and theoretical values of Q_e was quite good (Fig. 5). The measured values of Q_e differ appreciably from the calculated values only for the largest values of YIG sphere diameter

[21] E. L. Ginzton, "Microwave Measurements," McGraw-Hill Book Co., Inc., New York, N. Y., ch. 9, pp. 405–417; 1957.

[22] S. B. Cohn, "Problems in strip transmission lines," IRE TRANS. ON MICROWAVE THEORY AND TECHNIQUES, vol. MTT-3, pp. 119–126; March, 1955.

(around 0.090 inch). For these largest-sphere diameters the measured value of Q_e is also sensitive to the exact location of the sphere with respect to the conducting walls. This shows that the boundary conditions imposed on the motion of the magnetization by the conducting surfaces of the strip transmission line affect the coupling appreciably.

The strip transmission line offers more design flexibility than the waveguide. Examination of the formula in Fig. 3(c) for the Q_e of a strip transmission line shows that it is possible to adjust both the characteristic impedance of the line and Q_e independently, by adjusting the strip outer conductor width w and the ground-plane spacings d_1 and d_2.

IV. Development of a Single-Resonator Tunable Filter

A single-resonator tunable filter using waveguide coupling was constructed which is tunable over the X-band frequency range from 7.00 kMc to 11.00 kMc. The coupling arrangement (Fig. 6) is analogous to the crossed loops in Fig. 1. The single-crystal YIG sphere is mounted on a styrofoam support in the open iris region common to both the input and output waveguides. The depth of this region of interpenetration, as well as the guide height and resonator size, can be varied to control the coupling between the guides and the resonator. The bias field is applied along the common axis of the guides.

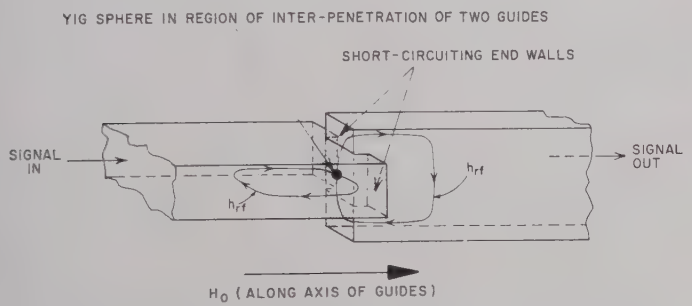

Fig. 6—Coupling principle of single-resonator waveguide filter.

Figs. 7 and 8 show the construction of the experimental single-resonator filter employing a standard-width X-band waveguide. The half-height ($b=0.200$ inch) coupling sections used in this experimental filter are followed by E-plane circular bends (mean radius $=0.300$ inch). These E-plane bends permit the use of a "c" type electromagnet for biasing along the axis of transmission of the guide. Immediately following the E-plane bends are 2.20-inch-long straight tapers joining the half-height sections to the full-height X-band input and output guides. The interpenetration of the two guides was accomplished by milling out 0.035-inch-deep slots in the face of the opposite section, as shown in Figs. 7 and 8.

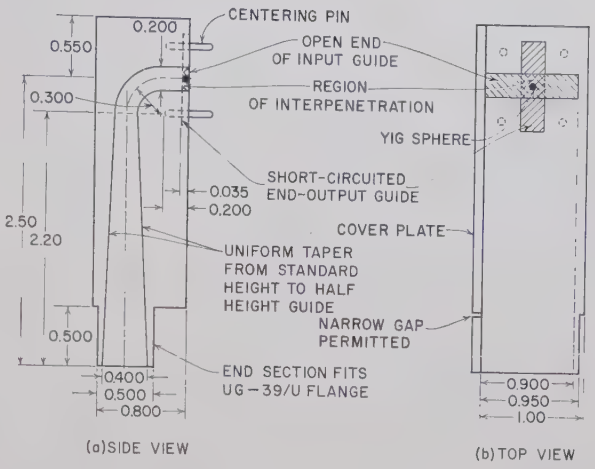

Fig. 7—Construction of half-section of single-resonator waveguide filter.

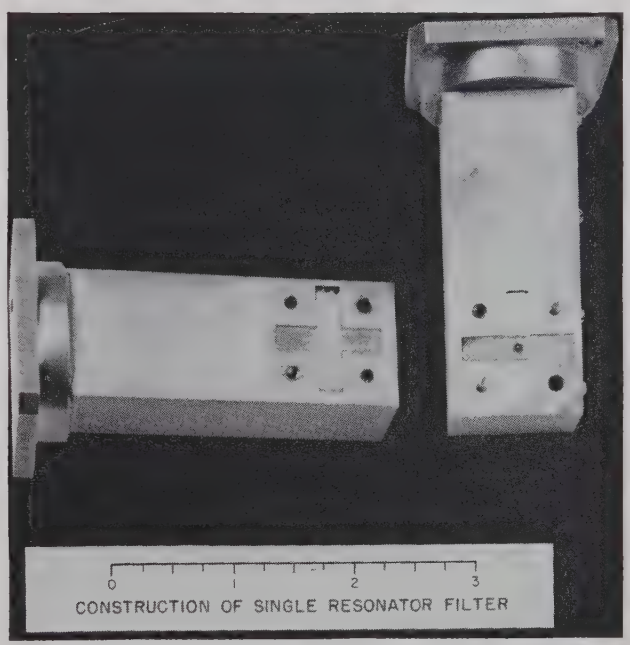

Fig. 8—Experimental single-resonator filter.

The measured responses when this single-resonator filter was tuned to resonate successively at 8.20, 9.00, 10.00, and 11.00 kMc are shown in Fig. 9. Table I shows the measured insertion losses at these frequencies and also at 7.00 kMc, 3-db bandwidths, and the peak response of the strongest subsidiary mode, and the values of Q_u calculated from the insertion loss and bandwidth data (using equations given by Ginzton[23]).

A prominent feature of this single-resonator filter response is the presence of many subsidiary responses which are due to higher-order magnetostatic resonances within the ferrimagnetic sample. These resonances, which were first analyzed by Walker,[24] result from the

[23] Ginzton, *op. cit.*, pp. 403–405.
[24] L. R. Walker, "Magnetostatic modes in ferromagnetic resonance," *Phys. Rev.*, vol. 105; January 15, 1957.

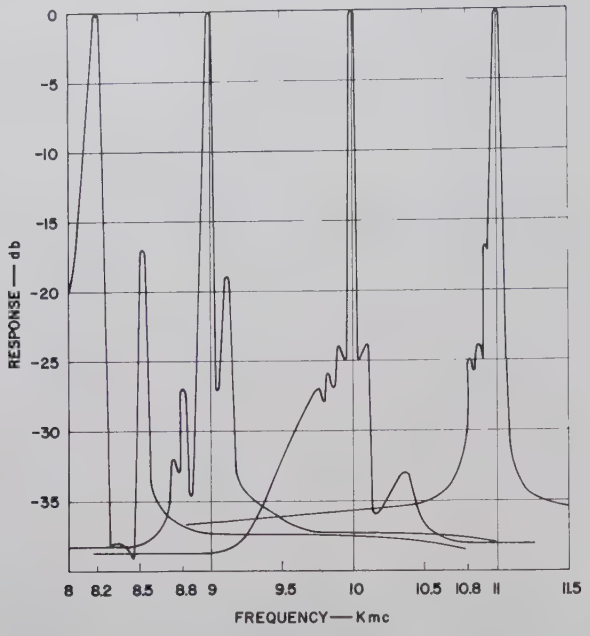

Fig. 9—Single-resonator filter response curves.

TABLE I
PERFORMANCE OF SINGLE-RESONATOR FILTER

f (kMc)	Insertion Loss at Resonance (db)	3-db Bandwidth (Mc)	Q_u	Strongest Magnetostatic Mode Response (db Below Transmission at Main Resonance)
7.00	2.0	not measured	—	—
8.20	1.5	14	3600	−17
9.00	1.2	20	3400	−18
10.00	1.3	25	3200	−23
11.00	1.1	28	3200	−17

nonuniform motion of the magnetization within the ferrimagnetic sample and the resulting dipolar interactions between the magnetic moments. Walker showed that the resonances are characterized by: 1) independence of the size of the sample, *i.e.*, they depend on the shape only, and 2) occurrence only at frequencies given by

$$\omega_0 + \gamma_0 \frac{M_0}{2} \geq \omega \geq \omega_0,$$

where

$$\omega_0 = \gamma_0 H_0.$$

Thus the resonant frequencies of the nonuniform resonances lie somewhere within a spectrum which is $\gamma_0 M_0/2$ cycles wide. For yttrium-iron-garnet in which the saturation magnetization M_0 is approximately 1395×10^2 amperes per meter, the width of this frequency band is 2450 Mc. Coupling to these nonuniform modes occurs when the RF coupling field is nonuniform over the dimensions of the sample. The maximum allowable response to higher-order modes thus dictates the largest-ferrimagnetic resonator that can be used in a specific coupling circuit. In practice, this restriction limits the diameter of the spherical resonator used in the present X-band single-resonator filter to less than 0.100 inch.

The spurious responses due to the higher-order magnetostatic modes are greatly reduced by the use of two or more ferrimagnetic resonators coupled directly together by means of their external RF fields. This is described in detail in Section VI.

A characteristic of this single-resonator filter response using TE_{10}-mode waveguide coupling is the increase of the bandwidth and the decrease of the insertion loss as the center frequency is raised. This increase in bandwidth, and decrease in insertion loss, is due to the decrease of the external Q_e of the waveguide coupling circuit as the frequency increases. Variation of the bandwidth over the tuning range is minimized by the use of a constant characteristic impedance coupling circuit, such as the TEM-mode strip transmission line shown in Fig. 3(c).

Another important aspect of the behavior of a YIG resonator is the saturation occurring at high power levels. This effect is explained in terms of the nonlinear coupling between the uniform mode and the short-wavelength "spin waves," and has been investigated and explained by Suhl.[25,26] This saturation effect was found by experiment to limit the peak power of the X-band single-resonator filter to less than about 15 watts. This effect has been discussed further and experimental results have been presented by Carter and Matthaei.[27] Considerably lower saturation thresholds occur at lower frequencies in the S-band range, both in theory[26] and in experiment.[8]

It has been shown[28] that Q_u is critically dependent on the achievement of a high surface polish on a yttrium-iron-garnet sphere. The spheres used here were ground and polished by a simple tumbling procedure which has been described by Bond.[29] The spheres were ground to shape from the raw crystals by tumbling, using No. 120 grade silicon carbide abrasive paper. They were then ground and polished using this same tumbling technique with successively finer grades of abrasive grinding paper and powder, as follows:

silicon carbide, No. 360, No. 600, No. 900,
emery polishing paper, No. 2/0 and No. 4/0,
Linde fine abrasive, No. B-5125.

[25] H. Suhl, "The non-linear behavior of ferrites at high signal levels," PROC. IRE, vol. 44, pp. 1270–1284; October, 1956.
[26] H. Suhl, "The theory of ferromagnetic resonance at high signal powers," *J. Phys. Chem. Solids*, vol. 1, pp. 209–217; January, 1957.
[27] P. S. Carter, G. L. Matthaei, "Design Criteria for Microwave Filters and Coupling Structures," Stanford Research Inst., Menlo Park, Calif., Final Rept. SRI Project 2326, Contract No. DA 36-039 SC-74862; January, 1961.
[28] R. C. LeCraw, E. G. Spencer, and C. S. Porter, "Ferromagnetic resonance line in yttrium-iron-garnet single crystals," *Phys. Rev.*, vol. 110, pp. 1311–1313; June 15, 1958.
[29] W. L. Bond, "Making small spheres," *Rev. Sci. Instr.*, vol. 22, pp. 344–345; May, 1951.

V. Development of a Two-Resonator Filter

Fig. 10 shows the application of two garnet spheres to form a two-resonator filter. Coupling between the resonators is provided by the long-slot iris in a 0.010-inch-thick conducting wall separating the input and output waveguides.[30] The long vertical coupling slot permits the vertical components of RF magnetic moment to be coupled together through their external RF fields, and prevents the horizontal magnetic fields of the waveguides and horizontal RF magnetic moments from being coupled together appreciably.

The two spheres are synchronously tuned by mounting them in dielectric capsules so that they can turn in any direction. Application of a dc biasing magnetic field results in a torque that causes one of the "easy axes" of magnetization to align itself along the dc magnetic field. Thus, detuning that would be caused by magnetocrystalline anisotropy[31] is easily eliminated.

Fig. 11 shows the disassembled two-resonator filter with the coupling iris, and the garnet spheres in 0.080-inch-diameter dielectric capsules. The capsules mounted on polystyrene rods are adjusted to vary the spacing of the spheres. Two 90° *E*-plane bends make it possible to use a "*c*"-type electromagnet.

In this experimental model, the input and output guides are standard-height *X*-band guides. Here, as for the single-resonator filter, the guide height or the sphere diameter can be varied to obtain the desired filter response. The two YIG spheres used in this model were 0.064 inch and 0.060 inch in diameter.

Fig. 12 shows the measured responses of the two-resonator filter tuned to 8.23 kMc, 9.49 kMc, 10.99 kMc, 12.00 kMc, 13.00 kMc, and 14.25 kMc. The initial adjustment of the filter was made at 9.49 kMc by varying the coupling slot dimensions and the spacing of the resonators to give the slightly overcoupled response with greater than 35-db insertion loss at frequencies far removed from the 9.49-kMc center frequency. This last requirement, *i.e.*, on rejection loss at frequencies far removed from resonance, limits the maximum width of the coupling slot, since the coupling between the guides in the absence of the garnet resonators is proportional to the width of the slot. The isolation obtained in this way can be calculated from the slot dimensions.[32,33] The slot dimensions used in this filter were 0.070 inch by 0.300 inch and were determined experimentally to give greater than 35-db off-channel rejection. The spacing between the centers of the YIG spheres was 0.164 inch. It was found that almost any desired degree of overcoupling could be obtained by closer spacing of the gar-

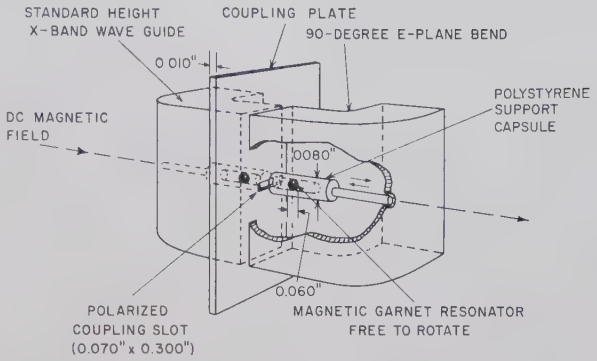

Fig. 10—Internal construction of two-resonator tunable filter.

Fig. 11—Disassembled two-resonator filter.

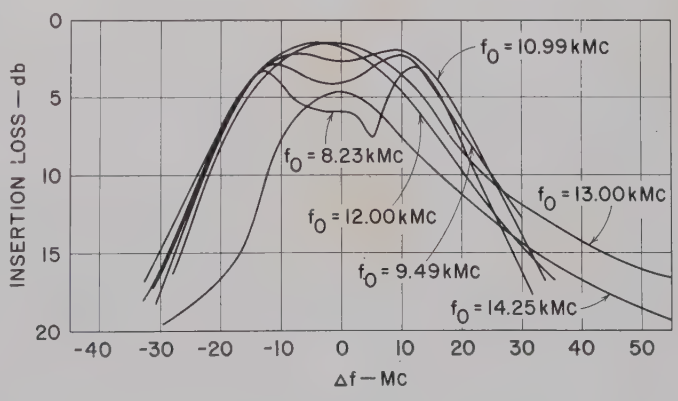

Fig. 12—Measured frequency responses of two-resonator filter.

[30] The use of polarized slot coupling was suggested by E. M. T. Jones of Stanford Research Inst., Menlo Park, Calif.

[31] C. Kittel, "On the theory of ferromagnetic resonance absorption," *Phys. Rev.*, vol. 73, pp. 155–161; January 15, 1948.

[32] H. A. Bethe, "Lumped Constants for Small Irises," M.I.T. Rad. Lab., Cambridge, Mass., Rept. No. 43-22; March 24, 1943.

[33] S. B. Cohn, "Microwave coupling by large apertures," Proc. IRE, vol. 40, pp. 696–699; June, 1952.

net spheres. The 3-db and 10-db bandwidths are nearly constant at about 32 Mc and 56 Mc, respectively, as the center frequency is changed with varying frequency.

The trends observed in Fig. 12 are: 1) a decrease of the degree of over-coupling with increasing frequency, 2) an approximately constant bandwidth throughout the tuning range, and 3) a decrease of insertion loss with increasing frequency. These trends are attributed to the same effect which caused the increase in bandwidth of the single-resonator filter, *i.e.*, the increase, with increasing frequency, of the coupling between the resonators and the waveguides.

The maximum tuning range of this experimental two-resonator filter appears to be limited by the leakage at 15.5 kMc through the coupling slot. This is shown in Fig. 13, which is a plot over a broadband of the response of the filter tuned to 12 kMc. This leakage is due to resonance of the slot at 15.5 kMc; it is then one-half wavelength long, and it couples energy between the two guides since it is not exactly parallel to the electric field of the waveguide. Evidently this slot response might be reduced by more accurate construction—this slot was cut by hand. Also, a shorter, wider slot might give nearly the same response and insertion loss, while moving the half-wave slot resonance to a higher frequency.

Fig. 14 shows the response of the two-resonator filter down to −30 db below the peak response, with the center frequency at 11.0 kMc. No spurious responses are evident here, as they were with the single resonator filter. This greater rejection of the higher-order modes is explained by the fact that the RF fields of the higher-order modes decrease very rapidly with distance away from the spheres, more rapidly than do the RF fields of the uniform mode. The higher-order modes of the two resonators are therefore coupled together very weakly through their external RF fields, making the insertion loss of these modes very high compared to that of the uniform mode. The absence of spurious responses in the two-resonator filter is an important advantage of this type of filter over the single-resonator type.

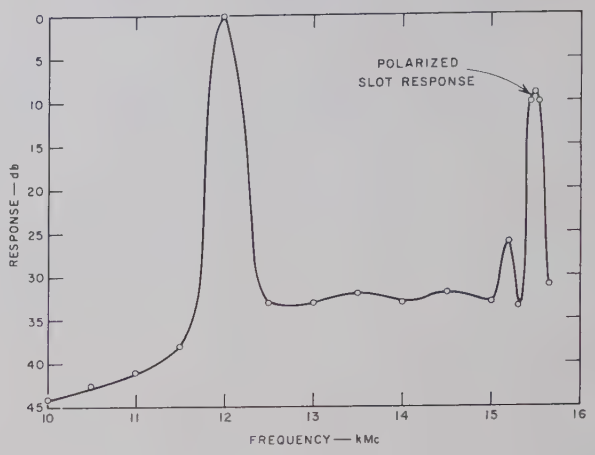

Fig. 13—Response of two-resonator filter tuned to 12 kMc showing polarized slot leakage at 15 kMc.

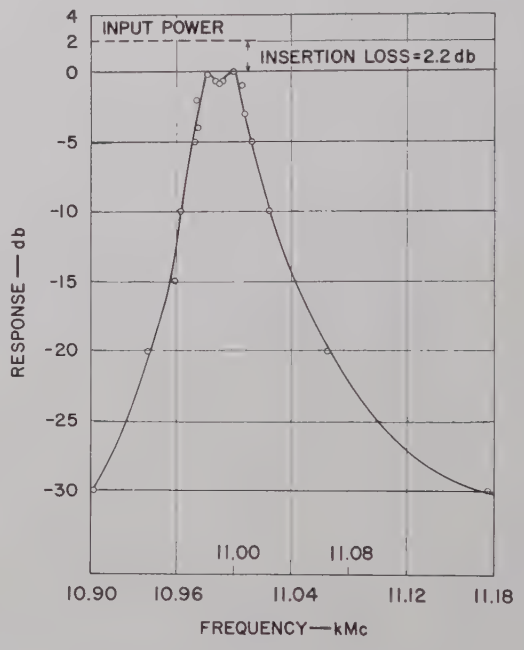

Fig. 14—Response of two-resonator filter tuned to 11 kMc.

VI. Future Developments

A number of useful extensions can be made of this type of tunable filter. It appears that filters can be constructed at frequencies lower and higher than *X*-band frequencies, and employing strip-transmission-line and coaxial-line coupling structures. Filters operating at lower frequencies (below *S*-band) will require a narrow-line-width magnetic material with a lower saturation magnetization than the yttrium-iron-garnet employed here. One material which appears to satisfy these requirements is gallium-substituted yttrium-iron-garnet.[34]

It appears possible to extend the tuning range of these filters beyond that reported here. This can presumably be accomplished by the use of ridged-waveguide, strip-transmission-line, and other inherently-wide-band coupling structures.

VII. Acknowledgment

The author is indebted to a number of his associates at Stanford Research Institute, Menlo Park, Calif., for important contributions. Special acknowledgment is made to Dr. E. M. T. Jones for some of the original ideas presented here. The support and general assistance of Dr. George Matthaei and Dr. Seymour B. Cohn are gratefully acknowledged. The general cooperation and assistance in the over-all supervision of this program by Nathan Lipetz of the U. S. Army Signal Research and Development Laboratory, Fort Monmouth, N. J., is also acknowledged.

[34] E. G. Spencer and R. C. LeGraw, "Line width narrowing in gallium substituted yttrium iron garnet," *Bull. Am. Phys. Soc.*, Ser. 2, vol. 5, pt. 1, p. 58; January 27, 1960.

Correspondence

Linear Tapers in Rectangular Waveguides*

Recently, the special case of a linear double taper in rectangular waveguide propagating the TE_{10} mode in vacuum dielectric was examined.[1] Approximate expressions for the reflection coefficient and voltage standing-wave ratio as functions of the taper dimensions and free space wavelength were derived and experimentally verified. This correspondence generalizes the equations to be applicable for waveguides filled with dielectrics of arbitrary relative permittivity κ. As a matter of convenience, equations are numbered to correspond with similar equations in the referenced paper.

The approximate expression for the reflection coefficient is

$$\Gamma = \frac{1}{4\gamma_0}\left(\frac{d}{dx}\ln Z\right)_0 - \frac{1}{4\gamma_1}\left(\frac{d}{dx}\ln Z\right)_1 \cdot \exp\left[-2\int_0^L \gamma dx\right], \quad (6)$$

where γ is the propagation constant, Z is the characteristic impedance and L is the physical length of the taper. The subscripts 0 and 1 refer to conditions at the initial and terminal ends of the taper, respectively.

Consider a linear taper of length L connecting rectangular waveguides of impedance Z_0 and Z_1. In the taper section, the width and height of the guide are linear functions of the position:

$$a = a(x) = a_0 + \frac{a_1 - a_0}{L}x,$$

$$b = b(x) = b_0 + \frac{b_1 - b_0}{L}x.$$

To interpret (6) in terms of the TE_{10} mode in rectangular waveguide, the integrated characteristic impedance defined on a voltage-current basis is used. Let

$$Z = \frac{\pi\eta_0}{2}\frac{b}{a\sqrt{\kappa - (\lambda/2a)^2}} \quad (7)$$

and

$$\gamma = i\frac{2\pi}{\lambda_g} = i\frac{2\pi}{\lambda}\sqrt{\kappa - (\lambda/2a)^2}, \quad (8)$$

where η_0 is the impedance of free space, κ is the relative permittivity (dielectric constant) of the medium within the waveguide, λ is the free-space wavelength and λ_g is the guide wavelength. The logarithmic derivative in the taper is then found to be

$$\frac{d}{dx}\ln Z = \frac{1}{L}\left[\frac{b_1 - b_0}{b} - \frac{a_1 - a_0}{a}\left(\frac{\kappa}{\kappa - (\lambda/2a)^2}\right)\right]. \quad (9)$$

Substitution of (8) and (9) into (6) yields the following expression for the reflection coefficient:

$$\Gamma = \frac{i}{8\pi L/\lambda}\left[K_1 \exp(-i4\pi l) - K_0\right], \quad (11)$$

where

$$K_0 = \frac{\dfrac{b_1 - b_0}{b_0} - \dfrac{a_1 - a_0}{a_0}\left(\dfrac{\kappa}{\kappa - (\lambda/2a_0)^2}\right)}{[\kappa - (\lambda/2a_0)^2]^{1/2}} \quad (12)$$

$$K_1 = \frac{\dfrac{b_1 - b_0}{b_1} - \dfrac{a_1 - a_0}{a_1}\left(\dfrac{\kappa}{\kappa - (\lambda/2a_1)^2}\right)}{[\kappa - (\lambda/2a_1)^2]^{1/2}}, \quad (13)$$

and

$$l = \int_0^L \frac{dx}{\lambda_g} = \frac{1}{\lambda}\int_0^L \sqrt{\kappa - (\lambda/2a)^2}\,dx. \quad (14)$$

Eq. (14) may be integrated with the result that

$$l = \frac{L}{2(a_1 - a_0)}\left[\frac{2a_1}{\lambda_{g_1}} - \frac{2a_0}{\lambda_{g_0}} + \tan^{-1}\frac{2a_0}{\lambda_{g_0}} - \tan^{-1}\frac{2a_1}{\lambda_{g_1}}\right], \quad (15)$$

where

$$\lambda_{g_0} = \lambda/\sqrt{\kappa - (\lambda/2a_0)^2}$$

and

$$\lambda_{g_1} = \lambda/\sqrt{\kappa - (\lambda/2a_1)^2}.$$

The absolute magnitude of the reflection coefficient is

$$|\Gamma| = \frac{1}{L/\lambda}\left[\frac{K_0^2 + K_1^2}{64\pi^2} - \frac{K_0K_1}{32\pi^2}\cos(4\pi l)\right]^{1/2}. \quad (16)$$

Using

$$\text{VSWR} = \frac{1 + |\Gamma|}{1 - |\Gamma|}, \quad (17)$$

the dominant mode voltage standing-wave ratio (VSWR) can be calculated as a function of frequency and taper length for a linear taper connecting two specified rectangular waveguides. The above equations reduce to those of the referenced paper if κ is replaced by unity.

R. C. Johnson
D. J. Bryant
Engrg. Experiment Station
Georgia Inst. Tech.
Atlanta, Ga.

* Received by the PGMTT, January 6, 1961.

[1] R. C. Johnson, "Design of linear double tapers in rectangular waveguide," IRE Transactions on Microwave Theory and Techniques, Vol. MTT-7, pp. 374–378; July, 1959. (Corrections: Vol. MTT-8, p. 458; July, 1960.)

The Unloaded Q of a YIG Resonator from X-Band to 4 Millimeters*

Carter and Flammer[1] have reported measurements at lower microwave frequencies of Q_u, the unloaded Q of a single crystal YIG sphere treated as a resonator. In their paper a comparison of the measured and theoretical Q_u, the latter computed on the basis of a constant relaxation time, yielded good agreement only in the 2–5 kMc range.

In this paper we report results of the variation of Q_u with frequencies from 9.5 to 67.8 kMc. Our measurements indicate that in this range Q_u is approximately constant.

Q_u may be found theoretically by solving the equation of motion of the freely processing magnetization in a saturated ferrimagnet. This equation, with Landau-Lifshitz damping, is

$$\boldsymbol{M} = \gamma(\boldsymbol{M}\times\boldsymbol{H}) + \frac{\gamma_\alpha}{M_s}\boldsymbol{M}\times(\boldsymbol{M}\times\boldsymbol{H}). \quad (1)$$

We consider the general ellipsoid with principal axes parallel to the x-y-z directions, and with the applied field H_0 in the z direction. Using the MKS rationalized system of units with $\boldsymbol{B} = \mu_0\boldsymbol{H} + \boldsymbol{M}$, the differential equation for m_x is

$$\ddot{m}_x + \alpha|\gamma|\left[2H_0 + [N_x + N_y - 2N_z]\frac{M_s}{\mu_0}\right]\dot{m}_x + \omega_0^2 m_x = 0 \quad (2)$$

where

$$\omega_0 = |\gamma|\left[\left(H_0 + (N_x - N_z)\frac{M_s}{\mu_0}\right)\cdot\left(H_0 + (N_y - N_z)\frac{M_s}{\mu_0}\right)\right]^{1/2}.$$

Q_u is therefore given by[2]

$$Q_u = \frac{\omega_0/|\gamma|}{\alpha\left[\dfrac{4\omega_0^2}{\gamma^2} + \left(\dfrac{M_s}{\mu_0}(N_x - N_y)\right)^2\right]^{1/2}}. \quad (3)$$

For a sphere, where $\omega_0 = \gamma H_0$,

$$Q_u = \frac{1}{2\alpha}. \quad (4)$$

To compute Q_u from the equation of motion with Bloch-Bloembergen damping,[3] we use

$$\dot{M}_{x,y} = \gamma(\boldsymbol{M}\times\boldsymbol{H})_{x,y} - \frac{M_{x,y}}{T_2}. \quad (5)$$

* Received by the PGMTT, January 16, 1961.

[1] P. S. Carter and C. Flammer, "Unloaded Q of single crystal yttrium-iron garnet resonator as a function of frequency," IRE Transactions on Microwave Theory and Techniques, vol. MTT-8, pp. 570–571; September, 1960.

[2] A. R. Von Hippel, "Dielectrics and Waves," J. Wiley and Sons, Inc., New York, N. Y., pp. 101–102; 1954.

[3] N. Bloembergen, "On the ferromagnetic resonance in nickel and supermalloy," *Phys. Rev.*, vol. 78, pp. 572–580; June, 1950.

(At low signal levels, $\dot{M}_z \simeq 0$.) In this case,

$$Q_u = \frac{\omega_0 T_2}{2}. \tag{6}$$

The half-line width ΔH may be expressed as

$$\Delta H = \frac{\alpha\omega_0}{|\gamma|} = \frac{1}{|\gamma| T_2}. \tag{7}$$

If T_2 is a constant, ΔH remains constant and Q_u increases linearly with frequency. On the other hand, if α is constant, then Q_u remains constant, and ΔH increases linearly with frequency.

We performed measurements on a highly polished single crystal YIG sphere (0.020-inch diameter), mounted in a shorted section of waveguide. Using a modification of the method described by Lebowitz,[4] we determined the coupling coefficient β, and the loaded Q, Q_L, at the four frequencies shown in Table I. Q_u is then given by $Q_u = Q_L(1+\beta)$.

Commercial 4-mm wave meters were of insufficient resolution to determine Δf in the measurement of Q_L. Here precise frequency differences were determined by an interferometer technique.

TABLE I

f(kMc)	Q_u	α	H(oe)
9.48	3.3×10^3	1.5×10^{-4}	0.5
17.18	2.9×10^3	1.7×10^{-4}	1.0
35.2	3.1×10^3	1.6×10^{-4}	2.0
67.8	2.3×10^3	2.2×10^{-4}	5.4

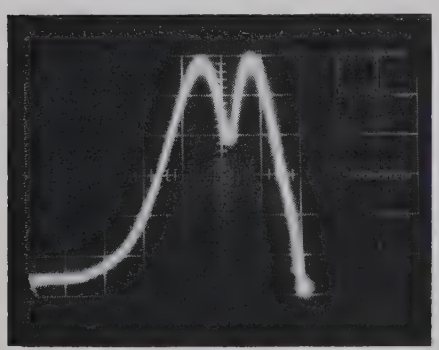

Fig. 1.

The results of Table I show that over this wide range Q_u and α are nearly independent of frequency; the assumption of a constant ΔH and T_2 is, therefore, not borne out by experiment.

It is interesting to note that the material maintains a reasonably high value of Q_u well into the mm wave range. Fig. 1 illustrates the response at the detuned open, while the klystron is swept over a mode in the 4-mm range. Thus, the use of highly polished YIG spheres as resonators in filter circuits[5] may be extended well into the mm wave range.

D. Douthett
I. Kaufman
Space Technology Labs., Inc.
Canoga Park, Calif.

[4] R. A. Lebowitz, "Determination of the parameters of cavities terminating transmission lines," IRE Transactions on Microwave Theory and Techniques, vol. MTT-4, pp. 51–53; January, 1956.

[5] P. S. Carter, Jr., "Magnetically tunable microwave filters employing single crystal garnet resonators," 1960 IRE International Convention Record, pt. 3, pp. 130–135.

Z_0 of Rectangular Coax*

The characteristic impedance Z_0 of rectangular coax has long been the subject of experimental and theoretical investigations. The problem is to obtain an expression for Z_0 which is both simple and precise to facilitate device design. The recent works of Chen[1] and Cohn[2] are summarized in Fig. 1 and compared with simple and precise calculations already known.[3,4]

The curve for $b/g \geq 1$ comes from Chen's equation (3) plus equation (4). The curve $b/g=0$ comes from Cohn's[5] equation (15). The intermediate curves for $g/h \leq 1$ come from scaling Cohn's[2] Fig. 4 to connect $b/g=0$ and $b/g \geq 1$. The intermediate curves for $g/h>1$ are based on Chen's approximation.[6]

Cohn's Fig. 4 is most accurate below $g/h=0.25$. An accurate plot for intermediate values of b/g is known for $g/h=1$[7] and is shown as curve C in Fig. 2(a). In Fig. 2,

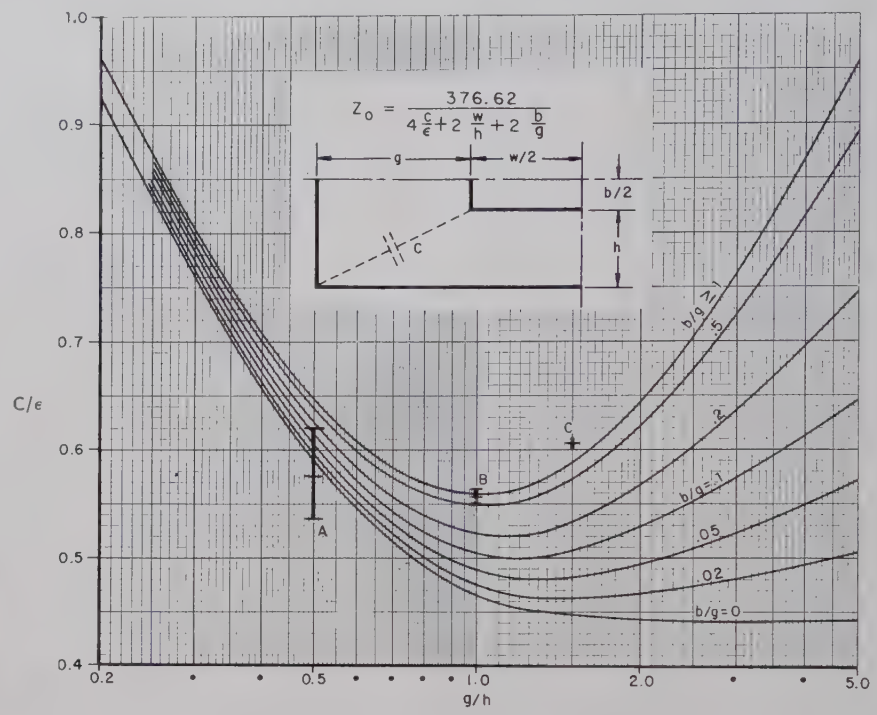

Fig. 1—Capacitance of one corner of rectangular coax.

The principal factor determining the Z_0 of TEM transmission line is its capacitance per unit length. Since the capacitance between parallel plates is readily calculated, the problem of calculating Z_0 of rectangular coax reduces to that of determining its "corner" capacitance. Assuming $w/h \geq 1$, Fig. 1 gives the corner capacitance. The characteristic impedance of air-filled rectangular coax line may then be obtained from

$$Z_0 = \frac{376.62}{4\frac{C}{\epsilon}+2\frac{w}{h}+2\frac{b}{g}}.$$

For $b/g>1$, this equation and Fig. 1 may also be used for eccentric lines; however, each capacitive term will appear separately in the denominator.

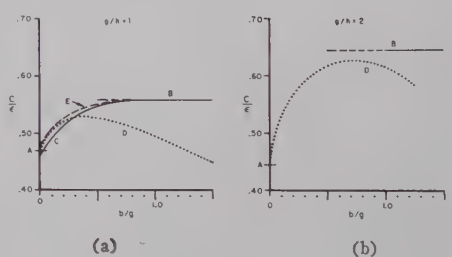

Fig. 2—Corner capacitance or intermediate values of b/g.

points A are from the theoretically derived curve for $b/g=0$; lines B are from the theoretically derived curve for $b/g \geq 1$. The validity of the assumption that Cohn's Fig. 4 can be stretched and made to apply is demonstrated in Fig. 2(a). Curve E is based on this assumption, and it is seen that if curve C were compressed to intersect point A and line B, the difference between the curves would be negligible.

Curves D are based on Chen's approximation. The validity of Chen's approximation is demonstrated by the closeness of

* Received by the PGMTT, January 16, 1961.

[1] T. S. Chen, "Determination of the capacitance, inductance, and characteristic impedance of rectangular lines," IRE Transactions on Microwave Theory and Techniques, vol. MTT-8, pp. 510–519; September, 1960.

[2] S. B. Cohn, "Thickness corrections for capacitive obstacles and strip conductors," IRE Transactions on Microwave Theory and Techniques, vol. MTT-8, pp. 638–644; November, 1960.

[3] Y. A. Omar and C. F. Miller, "Characteristic impedance of rectangular coaxial transmission lines," *Trans. AIEE*, vol. 71, pp. 81–89; January, 1952.

[4] J. J. Skiles and T. J. Higgins, "Determination of the characteristic impedance of UHF coaxial rectangular transmission lines," *Proc. Natl. Electronics Conf.*, Chicago, Ill., October 4–6, 1954, vol. 10, pp. 97–108; 1954.

[5] S. B. Cohn, "Shielded coupled-strip transmission line," IRE Transactions on Microwave Theory and Techniques, vol. MTT-3, pp. 29–38; October, 1955.

[6] Chen, *op. cit.*, equation (26).

[7] *Ibid.*, Fig. 8.

curve D to curve C in Fig. 2(a) for small values of b/g and by its close approach to line B for higher values of g/h and b/g as demonstrated in Fig. 2(b).

Precise calculations of Z_0 in rectangular coax have been made by Skiles and Higgins.[4] Interpretation of the corner capacitance from the three impedance configurations they calculated gives the points A (for $b/g=0$), B (for $b/g=1$), and C (for $b/g>1$) with their average and maximum and minimum limits. It is seen that Skiles's and Higgins's ranges are in close agreement with the curves. Because comparison of points on Fig. 1 is a more severe test than comparing characteristic impedances, it is concluded that the approximations can give fairly accurate characteristic impedances.

A simple empirical formula for Z_0 was developed by Omar and Miller.[3] However when points from their formula are plotted as in Fig. 1, large unsystematic deviations occur. A section of line was built for a Z_0 of 50 ohms according to the Omar and Miller formula. The characteristic impedance was observed to be low at 1–4 Gc, and in fact is predicted to be 31 ohms using Fig. 1.

It is hoped that a computer programming of the Skiles's and Higgins's solution will allow a precise plot of Fig. 1 to solve the problem once and for all. A logical extension of the work is to make calculations for $w/h<1$, and to investigate eccentric lines.

Robert V. Garver
Microwave Branch
Diamond Ordnance Fuze Labs.
Washington, D. C.

An Easy Method of Matching Microstrip Loads and Attenuators*

This note describes a novel method of matching microstrip loads which gives good performance without critical adjustment and is particularly useful when the lossy material has to be chosen for mechanical reasons rather than optimum characteristic impedance. In the present instance, the method was applied to the design of clip-on sliding loads for measurement purposes and to highly stable calibrated attenuators in which a block of iron-dust loaded resin was used as the lossy element.

Microstrip loads normally are made by laying lossy material on the surface of the supporting dielectric, as illustrated in Fig. 1, and obtaining absorption by interaction with the fringe field. Match can be controlled by the surface resistance of the lossy material and also by its shape, but the region of maximum absorption lies in a narrow area close to the strip, so that the latter adjustment is rather sensitive. It has been found that a match is achieved much more easily by raising the leading edge of the lossy material to give a small spacing from the strip. A sliding clip-on load using this arrangement with carbon-coated card is illustrated in Fig. 1, and a plot of its performance over a 40 per cent frequency band, given in Fig. 2, shows that an excellent match is obtained. In particular, this match is not dependent on accurate alignment of the load.

The mode of operation can be understood from the diagram of electric field distribution given in Fig. 3. This shows the way the transverse electric field diminishes with height above the strip, enabling the lossy material to be introduced initially in a region of low field with little discontinuity.

Fig. 4(a) and (b) show curves of measurements made using an iron-dust loaded resin as the lossy material (particularly suitable in giving stable contact to the strip for calibrated attenuators). The leading edge of the block is bevelled where it makes contact with the strip. The small diagram in Fig. 4 shows a cross section of the block perpendicular to the plane of the microstrip and parallel to the strip conductor. The block is considerably wider than the strip conductor but, unlike the load of Fig. 1, is not tapered in the transverse direction. The curves illustrate the effect on VSWR of varying the bevel angle θ and the bevel length L. There is an optimum value for both angle and length, the latter corresponding approximately to a quarter wavelength.

G. H. B. Thompson
Standard Telecommunication Labs., Ltd.
Harlow, Essex, England

* Received by the PGMTT, December 19, 1960. Revised manuscript received, January 20, 1961.

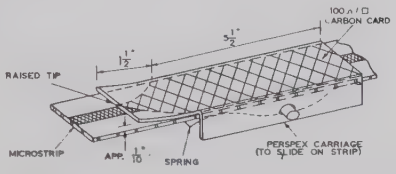

Fig. 1—Microstrip load with raised tip.

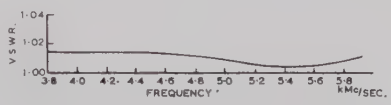

Fig. 2—Plot of VSWR of microstrip load against frequency.

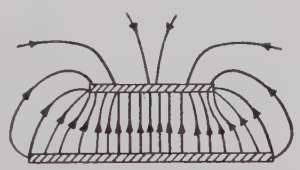

Fig. 3—Electric field distribution for microstrip (without dielectric).

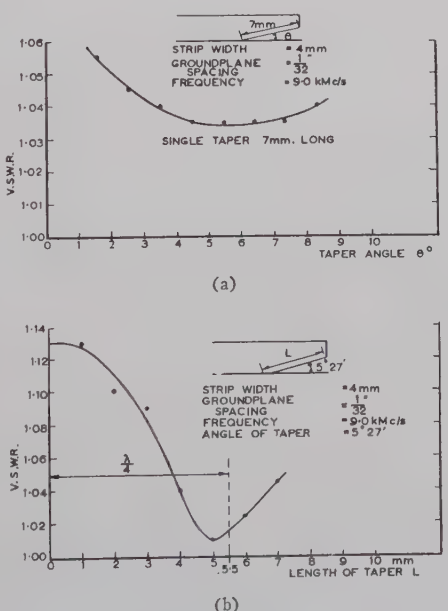

Fig. 4—Effect of angle and length on match of taper in lossy material. (a) Plot of VSWR vs taper angle. (b) Plot of VSWR vs length of taper.

An Empirical Design Method for Multisection Ridge-Guide Transducers of Large-Impedance Transformation*

The available analytical design procedures are inadequate for the design of broad-band ridge-guide transducers of large transformation ratio. Various authors[1–3] have discussed the problem of obtaining maximum bandwidth with multisection quarter-wave transformers, and recently Young[4] has extended the treatment to include inhomogeneous transformers where frequency dispersion varies from section to section. There is, however, no exact theory for dealing with the discontinuity susceptances which appear in practice at the junctions between sections and become important when large transformations are being attempted. Further uncertainties arise when ridge guide is used, because there does not yet seem to be agreement on a means of calculating the characteristic impedance which is applicable over the whole range of ridge sizes.

Here we describe an empirical design approach suitable for correcting errors in the initial design of a multisection transducer, and also present a simple dimensional relationship which may enable the effect of discontinuity susceptance of ridge-guide steps to be minimized in the design stage.

The ridge-guide transducer which was developed by this method is illustrated in Fig. 1. It provides a 12.5 to 1 impedance

* Received by the PGMTT, December 19, 1960. Revised manuscript received, January 20, 1961.

[1] R. E. Collin, "Theory and design of wide-band multisection quarter wave transformers," Proc. IRE, vol. 43, pp. 179–185; February, 1955.
[2] S. B. Cohn, "Optimum design of stepped transmission line transformers," IRE Trans. on Microwave Theory and Techniques, vol. MTT-3, pp. 16–21; April, 1955.
[3] M. J. Riblet, "General synthesis of quarter wave impedance transformers," IRE Trans. on Microwave Theory and Techniques, vol. MTT-5, pp. 36–43; January, 1957.
[4] L. Young, "Inhomogeneous quarter-wave-transformers of two sections," IRE Trans. on Microwave Theory and Techniques, vol. MTT-8, pp. 645–649; November, 1960.

transformation from standard X-band guide to microstrip and employs three quarter-wave sections. The measured performance is given in Fig. 2, which shows a Smith Chart plot of the over-all reflection coefficient, including the ridge-guide microstrip junction. The VSWR is better than 1.2 over a 30 per cent frequency band. The method by which the reflection plot was compacted and centered on the chart can be understood by reference to Fig. 3. This illustrates the effect of various departures from optimum dimensions. Below are listed the means of dealing with them.

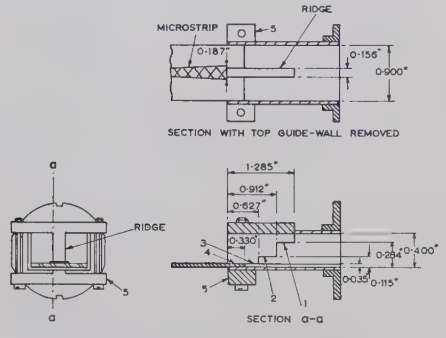

Fig. 1—Binomial step waveguide to microstrip taper.

Resistive Mismatch

It can be shown that the input admittance of the transducer is approximately proportional to the square of the characteristic admittance of all the even-numbered steps and to the reciprocal of this quantity for all the odd-numbered steps. Thus, if the input admittance is too low, as shown in curve 1, Fig. 3(a), the height of the ridge in in the first or the third sections should be increased, or the height in the second section should be reduced. The ratio of change in admittance should be equal to the square root of the required change at the input.

Reactive Mismatch

Reactive mismatch is caused by errors in the length of the quarter-wave sections. An increase in length of the odd-numbered sections produces a capacitative component of admittance at the input, and an increase in length of the even-numbered sections produces an inductive component. In a three-section transducer, errors in the center

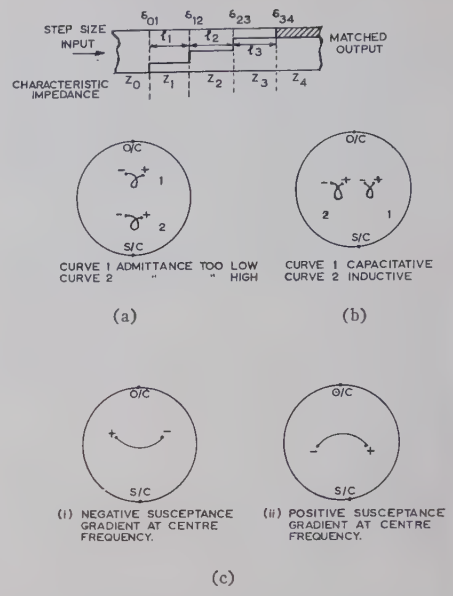

Fig. 3—Admittance curves for imperfect transducers. (a) Resistive mismatch. (b) Reactive mismatch. (c) Excessive frequency spread. (All plots are of admittance. The high and low frequency ends of the curves are indicated by + and − respectively.)

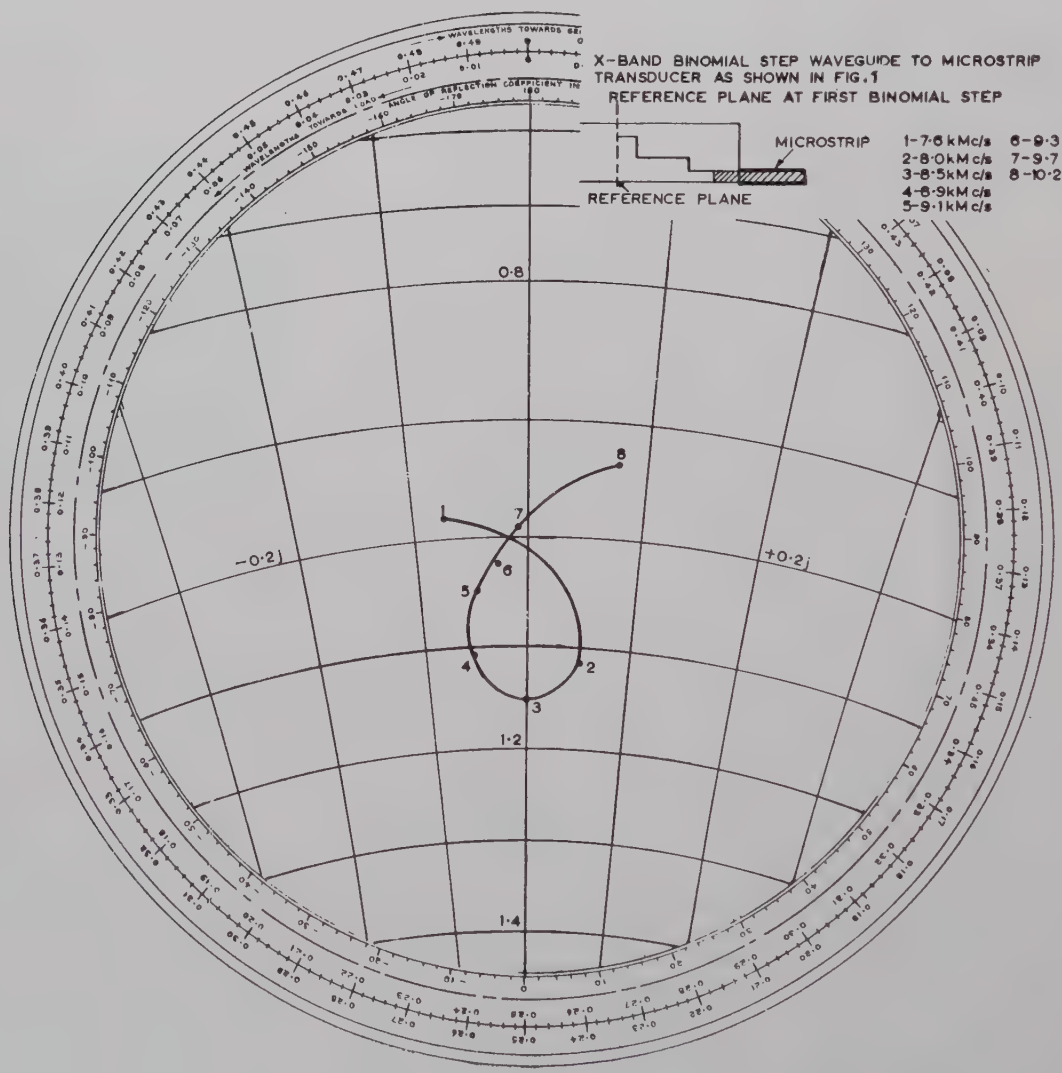

Fig. 2—Smith Chart plot of admittance of X-band binomial step waveguide to microstrip transducer.

section have approximately twice the effect of errors in the end sections. If n is the over-all impedance transformation ($n>1$), $\delta l/l$ is the proportional excess in step length, and B is the normalized input susceptance, then for errors in the end steps of a three-section transducer it can be shown that:

$$B \simeq \pi(n^{1/8} - 1)\delta l/l, \quad (1)$$

and for the center step,

$$B \simeq 2\pi(n^{1/8} - 1)\delta l/l. \quad (2)$$

Curve 1 in Fig. 3(b) shows a response that has an over-all capacitative bias. This can be corrected by reducing the length of section 1 or 3, or by increasing the length, to a smaller extent, of section 2.

Broad-Band Performance

The corrections just described can be carried out by making adjustments to any of the sections. This is satisfactory if only a small correction has to be made, but if a large correction is made to one section only, a considerable departure may result from the optimum broad-band design. When the original response is compact but off-center, a suitable procedure is to distribute the corrections between the different sections. However, some information can be gathered on the relative effect of the three sections from the shape of the Smith Chart pattern over the frequency range. Thus, a response of the form shown by curve 1 in Fig. 3(c), with an excessive decrease of susceptance with frequency, indicates that one or both of the end steps δ_{01} and δ_{34} are too small. Similarly, curve 2, which shows an excessive increase of susceptance with frequency, indicates that the end steps are too large. The intermediate state consists of some form of loop. These effects are much less predictable than those connected with the centering procedure, no doubt due to the dispersion of characteristic impedance with frequency, and it is doubtful if they can be applied usefully to transformers of more than three sections.

After this procedure had been used to obtain a satisfactory performance from the transducer, it was found that the length of all the intermediate sections was considerably less than a quarter of a wavelength. This was attributed to the effect of the susceptance of the steps themselves. Since the relative effect of the three steps could be estimated, it was only necessary to introduce one arbitrary constant to make the over-all impedance transformation, illustrated in Fig. 4, agree reasonably with the measured figures. Here it can be seen that the step capacitances, c_1, c_2 and c_3, produce an effect similar to a lengthening of the following lower-impedance section. In the present instance, this effect can be reduced

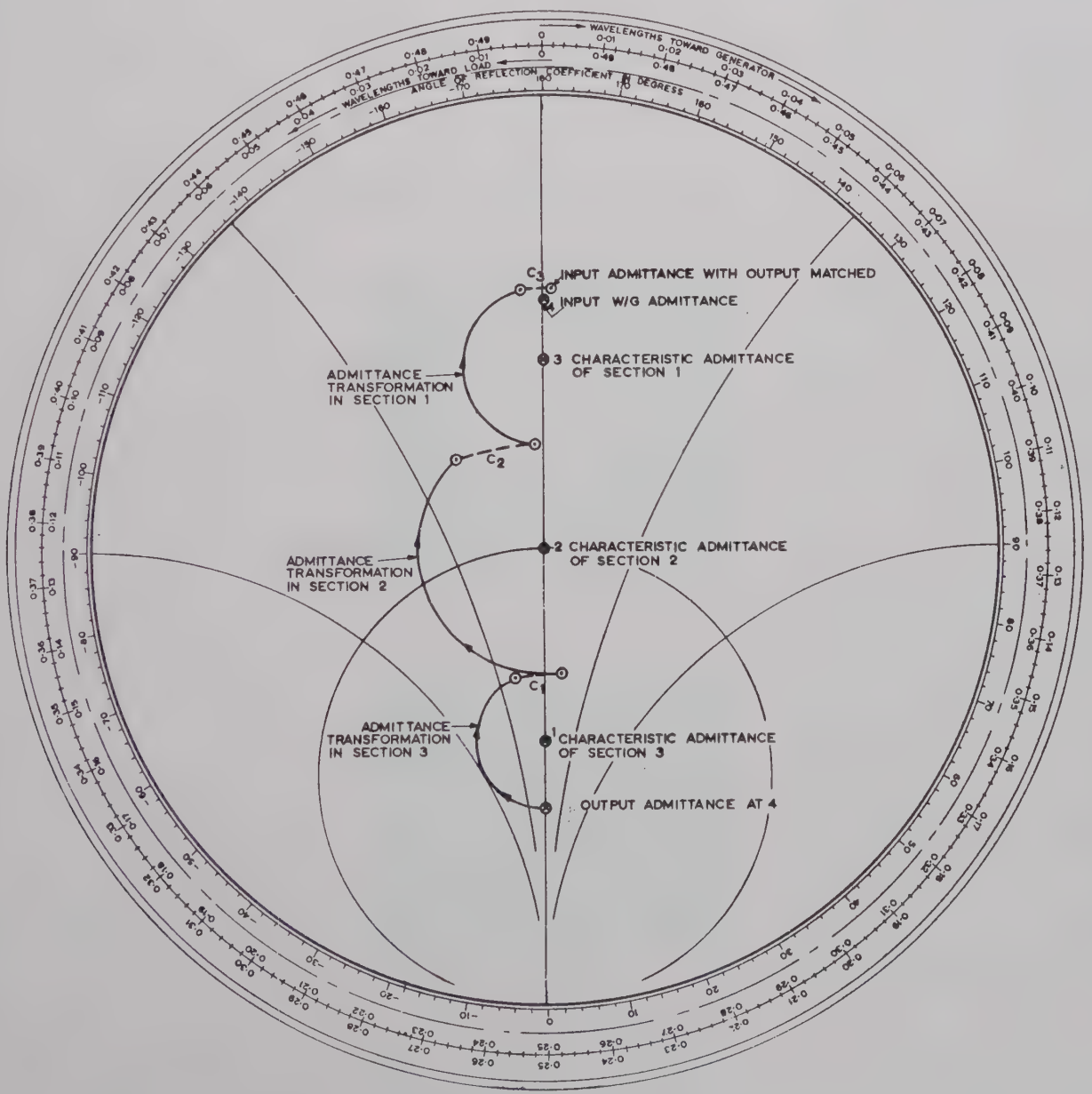

Fig. 4—Calculated admittance transformation in X-band ridge-waveguide transducer.

to quantitative terms. Table I shows a remarkable agreement between the true quarter wavelength in each ridge-guide section and the sum of the length of that section and half the height of the previous step.

TABLE I

Section No.	1	2	3
λ_g	5.15 cm	7.9	12.6
$\lambda/4$ at 9 kMc	1.091 cm	0.915	0.863
Actual length +half step height	1.092 cm	0.938	0.863

The agreement seems too good to be fortuitous and it would be interesting to find out for what range of ridge width and height it holds.

G. H. B. Thompson
Standard Telecommunications Labs., Ltd.
Harlow, Essex, England

Pulse-Operated Circulator Switch*

One of the major disadvantages of employing a ferrite circulator as a microwave switch is the holding current required to maintain the circulator in the switched position. One solution to this problem, reported by Levey and Silber,[1] is the utilization of ferrite tubes as the differential phase shift element in a circulator. Switching is accomplished with a single pulse of current which reverses the magnetization in the closed ferrite tubes, and by virtue of the closed magnetic path, remains permanently magnetized in this new state. Using this technique, microsecond switching speeds have been obtained. This approach requires a ferrite that has both the requisite microwave and dc magnetic characteristics which all too often are unattainable in a commercially available material and necessitates the development of a special material.

For many applications in which microsecond switching speeds are of no consequence, but it is mandatory that the holding current be eliminated, another approach may be followed; the best microwave material for the frequency and application of interest is used in the microwave circuit and a switchable magnetic material, external to the microwave circuit, is used to supply the bias field requirements. This arrangement provides greater flexibility in the realization of pulse actuated ferrite switches. The coercive force of the switchable magnetic material must be such that the remanent magnetization may be reversed with a current pulse of reasonable magnitude and yet retain the proper amount of magnetization at the conclusion of the current pulse. The coercive force required depends on the magnetic circuit, a greater coercive force being required when air gaps are introduced.

Using this technique, a stripline symmetrical junction circulator was converted to a pulse-operated switch. The low bias field requirement of 200 gauss[2] was obtained from a commercial steel (SAE 4130) whose composition is similar to that of a chromium permanent magnet steel. This material was used as the core of an electromagnet consisting of 30 turns of wire, located in each ground plane over the ferrite loaded junction; a soft iron, U-shaped bracket completed the magnetic circuit. Fig. 1 is a photograph of the switch.

Fig. 2 is a photograph of an oscilloscope trace showing the pulse actuated switching action. The top trace shows the train of dc current pulses of opposite polarity that causes reversal of the magnetic bias; the bottom trace is the rectified output of one port showing the switching action. The output drops from 0.5-db insertion loss to 20 db down at an operating frequency of 2050 Mc. In this configuration, 5-ampere current pulses are required to reverse the magnetization and place the "open circuit" magnetic field at 200 gauss. Pulse widths of 140 msec were used because they were readily available in the laboratory, but since the switching time is approximately 5 msec, pulse widths of 10 msec should suffice to produce the switching action for this unit.

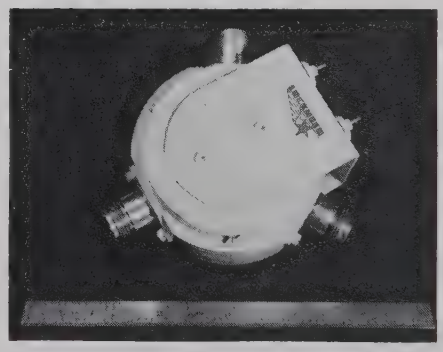

Fig. 1—Model of pulse-actuated ferrite switch.

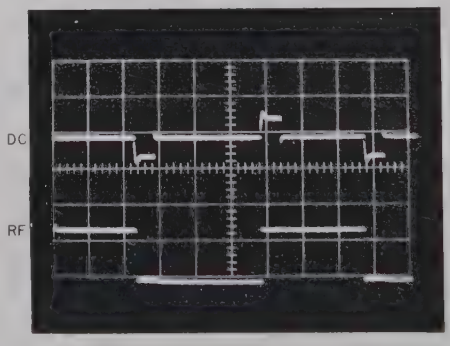

Fig. 2—Oscillograph showing pulse-actuated switching action, 200 msec/cm.

Faster switching times could be obtained by reducing the number of turns in the electromagnet. Fig. 3 shows the characteristics of the circulator-switch biased only by the remanent magnetization of the steel; after 24 hours at room temperature in this state, no changes in these characteristics were noted.

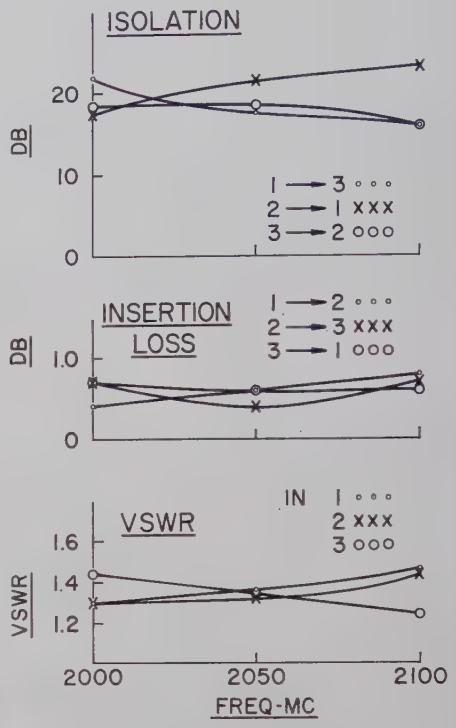

Fig. 3—Characteristics of ferrite circulator-switch.

The author wishes to acknowledge the valuable assistance of J. R. Poulson in taking the photographs and making the laboratory measurements.

L. Freiberg
Missile Systems Div.
Lockheed Aircraft Corp.
Sunnyvale, Calif.

Polishing Technique for Garnet Spheres*

A new technique using a motor-driven polishing head intended primarily for the final stages of polishing yttrium-iron-garnet spheres has been developed. This method has produced several fractional oersted linewidth crystals including a matched pair of 0.060-inch diameter spheres ground simultaneously.

The polishing device shown in Fig. 1 uses a 200-rpm motor with a $\frac{5}{8}$-inch-diameter

* Received by the PGMTT, February 21, 1961.

[1] L. Levey and L. M. Silber, "A fast-switching X-band circulator utilizing ferrite toroids," 1960 IRE WESCON Convention Record, pt. 1, pp. 11–20.

[2] L. Freiberg, "Lightweight Y-junction strip-line circulator," IRE Trans. on Microwave Theory and Techniques, vol. MTT-8, (Correspondence), p. 672; November, 1960.

* Received by the PGMTT, March 1, 1961.

circular pad of metallurgical polishing cloth attached to the end of the shaft. The shallow mortar dish, also lined with metallurgical polishing cloth, contains the sphere. The polishing cloths are impregnated with the appropriate polishing compound. The rotating pad is simply lowered into the dish far enough to make contact with the sphere. A horseshoe-type magnet placed directly under the bowl pulls the steel shaft (which has a short axial travel) firmly against the garnet sphere. It is thought the inhomogeneity of the magnets field causes the sphere to constantly change direction searching for an easy crystal axis of alignment. This action, together with the circular motion of the shaft, produces an unstable orbit and a uniform surface finish. With the arrangement properly adjusted, the sphere leaves a track near the outside edge of the pad.

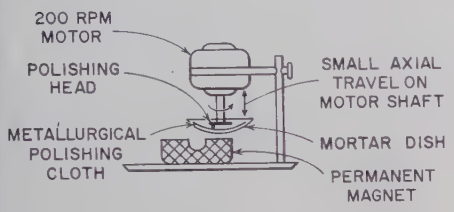

Fig. 1

Samples to be polished should be good spheres with a surface finish comparable to that obtained with no. 0 emery polishing paper. The first stage uses 25-micron diamond paste followed by an 8-micron grit. Time required in each stage depends primarily on the pressure applied to the sphere. If pressure is too great, the sphere does not rotate properly and flat spots occasionally develop. The final polishing procedure is done using ¼-micron diamond paste. Microscopic examination is desirable to check on cutting progress in all stages. Generally speaking, 4 to 6 hours in each stage produces a high surface polish.

The unloaded Q's of the finished spheres were measured at a frequency of 4 kMc using the impedance method described by Ginzton.[1] The spheres were mounted loosely in a thin sheet of polyfoam causing the spheres to be aligned along an easy axis of magnetization when placed in the dc magnetic field. The sphere is placed one-half guide wavelength away from the end of a short-circuited section of G-band waveguide. The results of the measurements on the garnet spheres were as follows:

TABLE I

SUMMARY OF MEASUREMENTS OF Q_u AT 4000 MC

Sphere Diameter-Inches	Unloaded Q, Q_u at 4000 Mc	Linewidth, $\Delta H = \frac{4000}{Q_u \times 2.8}$ -Oersteds
0.056	2700	0.53
0.060	2670	0.54
0.060	2850	0.50
0.095	2760	0.52

[1] E. L. Ginzton, "Microwave Measurements," McGraw-Hill Book Co., Inc., New York, N. Y., ch. 9, pp. 405–417; 1957.

This method of polishing the garnet spheres using a motor driven polishing head has the advantage, over the commonly employed tumbling technique,[2] that no spheres are now damaged due to chipping, which occurred when the spheres bounced off the wall of the tumbling dish.

ARVIA L. PIERCE
Electromagnetics Lab.
Stanford Res. Inst.
Menlo Park, Calif.

[2] W. L. Bond, "Making small spheres," *Rev. Sci. Instr.*, vol. 22, p. 344; May, 1951.

Miniaturized, Temperature Stable, Coaxial Y-Junction Circulators*

INTRODUCTION

The problem of designing a circulator that is extremely small, durable, and lightweight immediately suggests the Y- or T-junction approach. For use with coaxial connectors, the strip transmission line Y-junction suggested by Auld[1] and subsequently demonstrated by Milano, Davis and Saunders,[2] has obvious advantages. A systematic approach to developing such a device calls for the symmetrical alteration of at least two physical characteristics of the junction.[1] The obvious choice for one of these characteristics is the magnitude of the biasing magnetic field. The choice for the complementary characteristics can include any symmetrical change in the geometry of the junction (the adjustable ground plane of Fig. 1 is an example) and the symmetrical placing of isotropic and anisotropic material in the junction. The choice of this complementary characteristic most frequently mentioned in the literature is the diameter of the ferrite post. An alteration of the ferrite post height will also provide adjustment. The use of a metal pin along the axis of symmetry has also been suggested for this purpose.[3] Thaxter and Heller have also reported on the use of a copper sleeve around the ferrite post for operation at 70 and 140 kMc.[4]

The method to be described here involves the magnitude of the biasing field and the use of a dielectric-loading technique that is well suited to the design of very small and rugged devices.

In addition, the problem of temperature stability, high-power behavior, and the crucial role of low field losses in these devices will be treated. In C band, in particular, the use of high-gadolinium content YIG will be shown to offer an attractive solution to temperature problems and high-power problems associated with temperature changes.

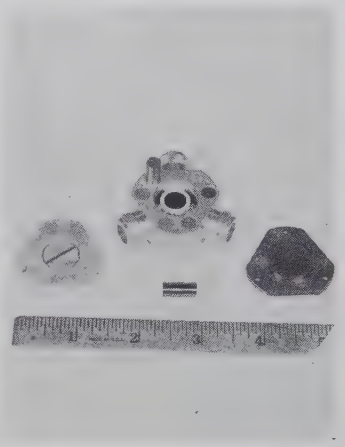

Fig. 1—The C-band circulator.

THE C-BAND CIRCULATOR

Physical Description

The structure of the C-band circulator is shown in Fig. 1. The housing is made of a nonmagnetic material, and the cover plates, which complete the magnetic path through the solid state material, are made of magnetic steel. Exclusive of connectors the device is 1.5 inches in diameter and 0.75 inches in height. The weight is approximately 3.75 ounces. This structure has a slight sensitivity to the proximity of magnetic material. This effect has been shown to be negligible except at the center of band frequencies where isolation between arms may exceed 35 db.

An alternate design can be used to overcome even this slight sensitivity. The exterior of this alternate design is composed entirely of magnetic steel. When fully temperature compensated, this shielded circulator constitutes an exceptionally durable and dependable solid-state device.

Electrical Characteristics

The characteristics of the C-band circulator adjusted for use in the 5.4- to 5.9-kMc range are shown in Fig. 2. These results are typical; slight asymmetries in the structure will generally cause variation in the characteristics from arm to arm. The synthesis procedure provides for design at a single frequency only; the bandwidth is consequently a characteristic of each individul circulator that must be adjusted experimentally.

The Design Technique

The synthesis procedure calls for the alteration of two physical characteristics in order to make the junction a circulator at a

* Received by the PGMTT, January 3, 1961; revised manuscript received, March 2, 1961. The research for this paper was supported in part by Contract No. DA-36-039-78909 of the U. S. Army Signal Corps., Fort Monmouth, N. J.

[1] B. A. Auld, "The synthesis of symmetrical waveguide circulators," IRE TRANS. ON MICROWAVE THEORY AND TECHNIQUE, vol. MTT-7, pp. 238–246; April, 1959.

[2] L. Davis, Jr., V. Milano, and J. Saunders, "A strip-line L-band compact circulator," PROC. IRE (Correspondence), vol. 48, pp. 115–116; January, 1960.

[3] C. Montgomery, R. H. Dicke, and E. M. Purcell, "Principles of Microwave Circuits," McGraw-Hill Book Co., Inc., New York, N. Y., ch. 12; 1948.

[4] J. B. Thaxter and G. S. Heller, "Circulators at 70 and 140 kmc," PROC. IRE (Correspondence), vol. 48, p. 110; January, 1960.

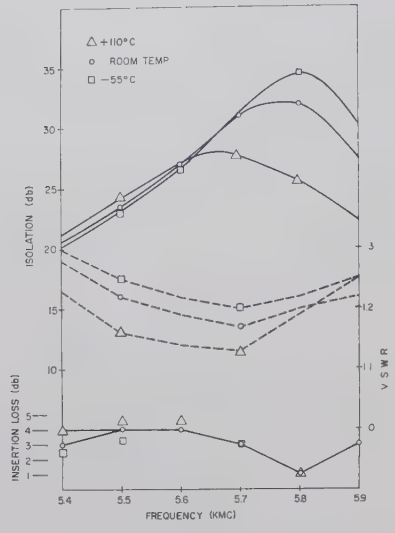

Fig. 2—Typical performance of the *C*-band circulator in the 5.4 kMc to 5.9-kMc range.

given frequency. This assumes that the range of adjustment afforded by this technique includes the desired frequency. It is thus advantageous to employ a technique that will yield a broad range of adjustment.

The technique employed with the miniaturized circulators discussed here involves the magnitude of the biasing field and the dielectric sleeves. (Fig. 1). It is structurally desirable to hold the outer and inner diameter of the dielectric sleeves constant, since these two physical characteristics serve to center the solid state element, thus eliminating one possible source of asymmetry. This leaves the dielectric constant and the height of the sleeves available for adjustment.

Discrete values of dielectric constant presently available in low loss material can be used for broad range, course adjustment. The sleeve height, however, provides fine adjustment and can be made equally effective over a broad range. With the use of Stycast K-20 sleeves, for example, the *C*-band circulator can be made to operate at any selected frequency in the band from 4.4 kMc to beyond 10 kMc by a simple adjustment in the height of the sleeves and a complementary adjustment in the biasing field.

Temperature Stability

Use of unsaturated Alnico-V magnets as biasing elements can give a constant biasing field over a broad range of temperature. This leaves the effects of temperature change on the solid-state material as the principle source of instability in fixed field *Y*-junction circulators. This instability has been observed in below-resonance operation to be the result of a "drift" in optimum frequency of operation as a function of temperature and/or a drift in optimum required biasing field as a function of temperature.

Temperature compensation in the *C*-band circulator was accomplished simply by the selection of a material which minimized these drifts. Figs. 3, 4(a) and 4(b) are plots

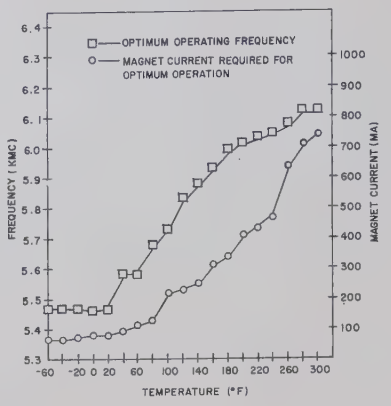

Fig. 3—Optimum operating frequency and required magnet current as a function of temperature for a circulator using an Mg-Mn ferrite.

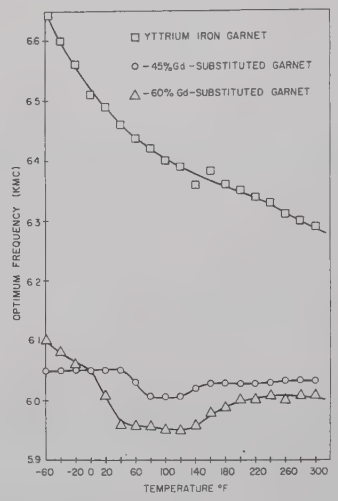

(a)

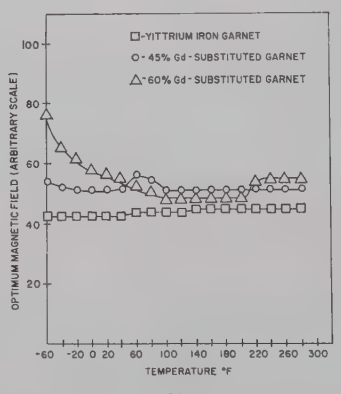

(b)

Fig. 4—Temperature response of three selected garnets in the *C*-band *Y*-junction circulator. (a) Drift in optimum operating frequency with temperature. (b) Drift in optimum magnetic field with temperature.

of optimum operating frequency and required biasing field as functions of temperature for four compositions. The Mg-Mn ferrite[5] is thought to be a good example of a temperature-unstable material for use in junction circulators. At the other extreme the 45 per cent and 60 per cent gadolinium-substituted garnets exhibit a minimum of temperature instability. The yttrium-iron garnet displayed stability in optimum biasing field but the optimum operating frequency is seen to drift over a relatively broad band. The high-gadolinium-content garnets were selected for experimentation on the basis of the observed temperature behavior of these materials in other devices involving resonance and phase shift phenomena.

The characteristics of Fig. 2 were obtained using 60 per cent gadolinium. In another test using 45 per cent gadolinium, the isolation alone was monitored. This isolation remained above 20 db in all three arms of the circulator over the temperature range −60°F to 300°F. In addition, the 60 per cent Gd garnet provides good circulation with low insertion loss in most of the bands under investigation, and should display temperature behavior in these bands that is comparable with that obtained in *C* band.

There are two primary considerations in the operation of these devices at high-power levels; they are high-peak-power breakdown and heating due to absorption of power. Tests revealed that high-power break-down occurs in the *C*-band circulator at approximately 30 kw peak power, 30 watts average, when the unit is fitted with Type N connectors, and operated unpressurized. Now, to determine heating and possibly high-power nonlinear effects, the electrical characteristics of the devices were investigated at low- and high-power levels. At 5.560 kMc, the frequency at which the high-power tests were to be run, the circulator exhibited the following low-power characteristics:

Isolation	35 db
Insertion Loss	0.2 db
Input VSWR	1.05 db.

The most critical parameter, isolation, was monitored during the high-power tests. Successive readings were taken at 5-kw increments with the power maintained for five minutes before each reading. No significant change in isolation was observed throughout the test until arcing occurred. Since isolation remained essentially constant, there is no real basis to expect that other characteristics might vary. The material used in this test was 60 per cent gadolinium garnet.

A similar test was run using the Mg-Mn ferrite. The low-power isolation at 5.650 kMc was 31.5 db. At 25 kw peak power and 25 watts average power, the isolation had dropped to 26 db. At this point the power was removed and the device allowed to cool to room temperature. A reapplication of the 25 kw peak power resulted in an isolation of 31.5 db, which gradually decreased as the power was maintained. The somewhat poor performance of the Mg-Mn ferrite at high power was thus apparently due to temperature instability.

Application to Other Frequency Bands

The techniques developed for *C* and *X* bands were found to be useful in the design of circulators at lower microwave frequencies. Satisfactory circulator performance has been obtained at frequencies as low as 200

[5] Commercial General Ceramics R-5 Ferrite.

Mc in larger structures. Devices that have been designed in S band down to about 2 kMc are quite similar to those in C band and X band. Circulators constructed below approximately 2 kMc differ in one essential feature that warrants further treatment.

Below and Above Resonance Operation

For most frequencies in the microwave spectrum, the ferrimagnetic materials employed in Y-junction circulators can be biased in a low-loss region with a field that is either below or above that required for ferrimagnetic resonance. With a specific material and geometry this suggests the possibility that the conditions for circulation can be satisfied at two widely-separated values of biasing field. In general we must also expect two different frequencies of circulation to be involved.

These suppositions have, indeed, been found to be true. Experience indicates that circulation occurs in opposite directions for the two fields and that the above-resonance biasing field corresponds to a lower frequency of optimum circulator performance. For example, in the "C-band Circulator" use of 60 per cent gadolinium-content garnet posts 0.400 inches in diameter results in good performance at 4.9 kMc with an above resonance field of approximately 1550 gauss. At this field, isolation exceeds 40 db and insertion loss is less than 0.2 db. Another point of good performance is found at 6.3 kMc with a below-resonance field of approximately 100 gauss. Isolation in this case is greater than 40 db and insertion loss less than 0.6 db. Circulation at the two frequencies is in opposite directions.

From the standpoint of miniaturization, below-resonance operation is obviously desirable because of the very appreciable difference in the size of the required biasing magnets. This assumes, of course, that operation below resonance is practical, which is not necessarily the case.

The Role of Low Field Losses

Unfortunately, presently-known material technology results in a low frequency limit to the utility of below-resonance operation. This limit is the frequency at which low field losses become intolerable. Since the below-resonance biasing fields are quite small, this situation can be roughly approximated by an unmagnetized medium, in which case the limiting frequency is given by[6]

$$f_{mc} = \gamma(H_a + 4\pi M_s),$$

where

$4\pi M_s$ = saturation magnetization
H_a = anisotropy field
γ = gyromagnetic ratio.

For the 60 per cent gadolinium-content garnet, $H_a \approx 80$ oersteds,[7] $4\pi M_s = 700$ and $\gamma = 2.8$ Mc/oersted. Thus, $f_{mc} \approx 2200$.

[6] D. Polder and J. Smit, "Resonance phenomena in ferrites," *Revs. Mod. Phys.*, vol. 25, p. 89; 1953.
[7] G. P. Rodrigue, Thesis, Harvard University, Cambridge, Mass.; 1958.

In actual tests with this garnet the authors have been able to achieve below-resonance circulation with insertion loss in the neighborhood of 1 db down to about 2100 Mc. Below this frequency, using the above material, satisfactory results have thus far been achieved only with above-resonance operation.

Conclusion

For use in coaxial circulators, a perturbation technique which employs the magnitude of the biasing field and symmetrical dielectric loading is considered to be of exceptional utility.

The problem of temperature instability in junction-type circulators is thought to be solved by the use of "temperature favorable" materials such as medium- to high-percentage gadolinium substituted yttrium-iron garnets. Yttrium-iron garnet is somewhat less temperature favorable, but will suffice for many applications.

The limit to below ferrimagnetic resonance operation of junction type circulators is thought to be the frequency at which low field losses become intolerable. The lowest practical below-resonance operation using presently available materials appears to be around 2000 Mc. Circulators constructed at lower frequencies and requiring high-level performance, have required above-resonance biasing fields.

Acknowledgment

The authors wish to thank B. J. Duncan and W. C. Heithaus of Sperry Microwave Electronics Company for many valuable suggestions and D. E. Tribby for invaluable technical assistance.

J. Clark
J. Brown
Appl. Phys. Section
Sperry Microwave Electronics Co.
Clearwater, Fla.

K-Band Reciprocal Ferrite Phase Modulator*

Introduction

A rectangular waveguide reciprocal phase modulator, making use of a longitudinal magnetic control field, was reported by Reggia and Spencer[1] in 1957. This X-band phase modulator consisted of a longitudinally magnetized ferrite rod centrally located inside a rectangular waveguide excited in its fundamental TE_{01} mode. The outstanding advantages of this type modulator are the large phase shifts per unit length obtainable, simple geometric configuration, the high figure of merit[2] possible, and the small magnetic control fields required. These modulators have since been designed for use at frequencies ranging from 3000 Mc to 70,000 Mc.

A simplified theoretical analysis of the above phase modulator was made by Weiss.[3] Another theoretical analysis by Tompkins[4] resulted in exact solutions for the field configuration and energy distribution of longitudinally magnetized ferrite rods in circular waveguide as a function of rod diameters. This analysis also included a comparison between the theoretical solutions and the results obtained with the rectangular waveguide phase modulator.

It is the purpose of this paper to present the design data of a K-band phase modulator and the experimental results obtained at 23,640 Mc to 25,000 Mc.

Design Procedure

Beginning with the design data[1] available at X-band and choosing a standard rectangular waveguide (0.170×0.420 inch) for 23 to 25 kMc, it was first necessary to select a suitable ferrite material. A small dielectric and magnetic loss tangent at the operating frequency was required in order to obtain a phase modulator with low insertion loss. Also, since the amount of phase shift obtained is proportional to the magnitude of the saturation magnetization ($4\pi M_s$), a Ni-Zn ferrite[5] having a line width of 40 oersteds and $4\pi M_s$ of 5000 gauss was selected.[6] This material has made possible a phase modulator with a figure of merit in excess of 3000.

The next problem was to determine the minimum rod diameter (d_{min}) required to obtain sufficient concentration of the microwave energy in the ferrite,[4] a necessary condition for obtaining large phase shifts, and the maximum rod diameter (d_{max}) such that the generation of spurious modes in the ferrite-loaded waveguide would not be permitted. Both the maximum and minimum rod diameters are critically dependent on the narrow dimension (0.170 inch) of the rectangular waveguide. With the particular Ni-Zn ferrite chosen, it was found that d_{min} was 0.080 inch and d_{max} was 0.100 inch.

Impedance matching was accomplished by tapering both ends of the ferrite rod and dielectric polyfoam support. An input VSWR of less than 1.20 for the phase modulator for all values of applied magnetic field was considered satisfactory.

* Received by the PGMTT, November 21, 1960; revised manuscript received January 30, 1961. The work reported here was sponsored by the U. S. Army Signal Corps.

[1] F. Reggia and E. G. Spencer, "A new technique in ferrite phase shifting for beam scanning of microwave antennas," Proc. IRE, vol. 45, pp. 1510–1517; November, 1957.

[2] Figure of merit
$$= \frac{\text{maximum phase shift in degrees}}{\text{maximum insertion loss in decibels}}.$$

[3] J. A. Weiss, "A phenomenological theory of the Reggia-Spencer phase shifter," Proc. IRE, vol. 47, pp. 1130–1137; June, 1959.

[4] J. E. Tompkins, "Energy Distribution and Field Configuration in Ferrites," Solid State Physics in Electronics and Telecommunications, Academic Press, Ltd., London, England, pp. 169–180; 1960.

[5] BTL XN5000 (1244, 5131-6). The formula for this Ni-Zn ferite, obtained from L. G. Van Uitert of Bell Telephone Labs., Inc., is
$$Ni_{0.5}Cu_{0.1}Zn_{0.4}O.Fe_{1.9}Mn_{0.1}O_3.$$

[6] L. G. Van Uitert, "Resonance line widths of sintered nickel ferrites having low porosities," *J. Appl. Phys.*, Suppl. to vol. 31, p. 2265; April, 1960.

Reciprocal Ferrite Phase Modulator

A cross-sectional view of the reciprocal phase modulator for 23 to 25 kMc is illustrated in Fig. 1. The ferrite rod used as the phase-shifting element consists of a low-loss Ni-Zn ferrite, having a useful range of diameters from 0.080 to 0.100 inch. It is tapered at both ends for impedance matching and centrally located inside the rectangular waveguide section by a polyfoam dielectric support. The demagnetizing factor of this 3 inch-long ferrite rod, for a longitudinal magnetizing field, is very small.

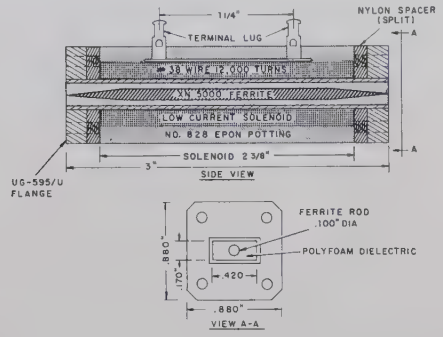

Fig. 1.

The low-current solenoid supplying the magnetic control field consists of 12,000 turns of No. 38 wire wound around the $\frac{1}{4}\times\frac{1}{2}$-inch rectangular waveguide section. The total length of the solenoid is $2\frac{3}{8}$ inches, and its normal operating currents are from 0 to 50 ma, corresponding to a magnetic field strength from 0 to 120 oersteds. A control power of approximately 1 watt was required to obtain a field strength of 60 oersteds. An Epon resin is used to pot the modulator winding.

The phase-shifting characteristics at 23,640 Mc as a function of the applied magnetic field and diameter of the Ni-Zn ferrite rods are shown in Fig. 2. These rods were all 3.00 inches long, including the 9/16 inch impedance matching tapers at both ends, and were taken from the same piece of ferrite material. As seen in the figure, only small phase changes are obtained for rod diameters less than 0.080 inch. When the rod diameter is increased above this value, large phase changes are seen to occur, particularly for fields less than 50 oersteds. It is also seen that the phase shift does not increase linearly with an increase in the rod diameter. This is due to the increased effectiveness of the high dielectric constant ($\epsilon\approx 14$) of the ferrite in concentrating the microwave energy as the rod diameter is increased.[4] For rod diameters greater than 0.100 inch, little increase in phase shift is obtained and large amplitude modulations begin to occur. The phase-shift characteristics of a 0.090-inch MgMn ferrite rod ($4\pi M_s = 1760$ gauss) is also shown in the figure (dashed curve) for comparison. The zero-field insertion loss for each of the three rods indicated in the figure was less than 0.5 db, and less than 0.2-db amplitude modulation was observed at the output. The figure of merit for the phase modulator using a 0.100-inch-diameter NiZn ferrite rod was greater than 3000.

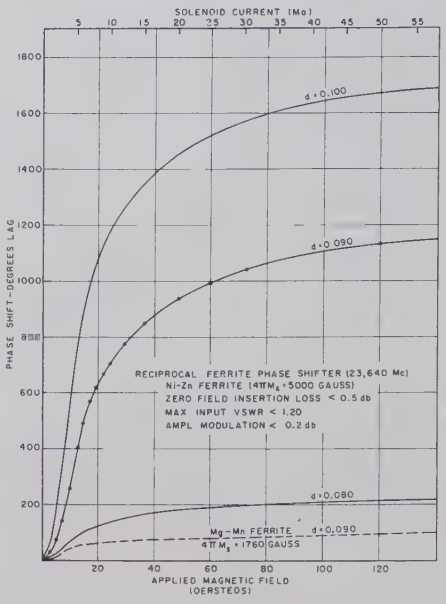

Fig. 2.

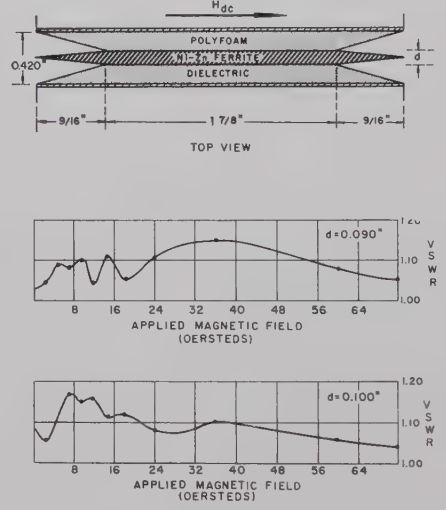

Fig. 3.

A simplified drawing of the rectangular waveguide phase modulator is shown in Fig. 3(a). Linear tapers were used at both ends of the ferrite rod and polyfoam dielectric support for impedance matching. The input VSWR of this phase modulator at 23,640 Mc, using a 0.090-inch- and 0.100-inch-diameter ferrite rod as a function of the applied magnetic field, is shown in Fig. 3(b) and 3(c).

The peak power handling capability and average power rating of the phase modulator are estimated to be approximately 5 kw and 25 w respectively. The maximum average power rating, which depends upon the RF losses in the ferrite, can be increased as better microwave ferrites become available.

The bandwidth characteristics of the reciprocal phase modulator using a 0.090-inch-diameter rod [Fig. 3(a)], are shown in Fig. 4. Phase shifts vs applied magnetic field are given for several frequencies over a bandwidth of greater than 1300 Mc. As seen in the figure, the phase shift obtained increases appreciably with frequency. Above 25,000 Mc, higher-order modes[4] begin to occur, which cause large amplitude variations. The zero-field insertion loss for this rod was approximately 0.4 db, and the variation in transmitted power as a function of applied field was less than 0.3 db. An input VSWR over the bandwidth shown was no greater than 1.2.

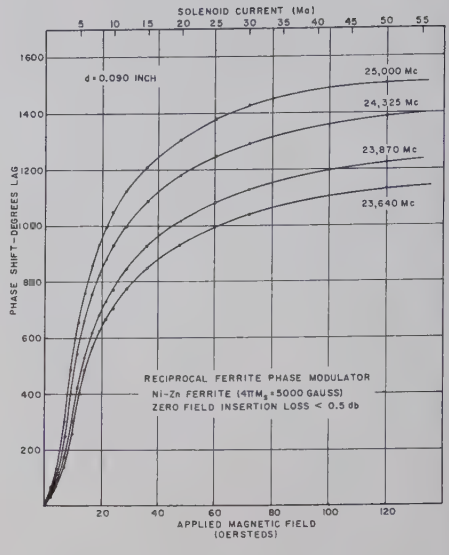

Fig. 4.

A photograph of the reciprocal-phase modulator used for the measurements is shown in Fig. 5. The tapered ferrite rod (0.100-inch-diameter) and polyfoam dielectric insert are shown in the foreground. Standard UG-595/U K-band flanges were used at both ends of the phase modulator. The phase modulator and the ferrite rod were 3 inches long, and the total weight was 5 ounces.

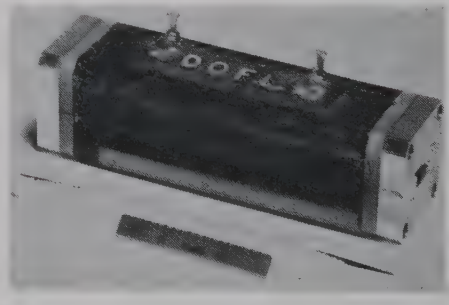

Fig. 5.

The author wishes to extend his thanks to W. H. von Aulock, Bell Telephone Labs., Whippany, N. J., for his helpful discussions and suggestions.

Frank Reggia
Microwave Branch
Diamond Ordnance Fuze Labs.
Washington, D. C.

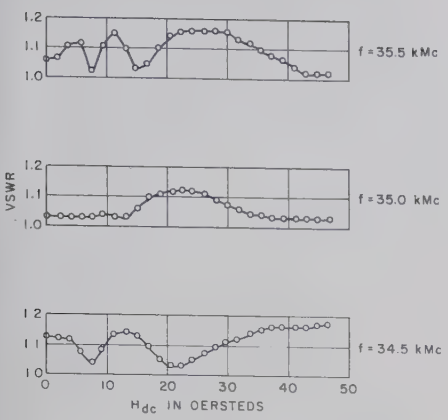

Fig. 1—VSWR characteristics of the prototype ferrite phase shifter.

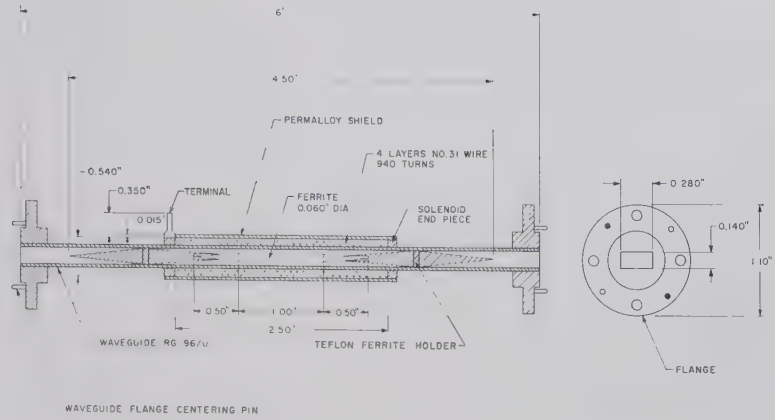

Fig. 2—Assembly drawing of the K_a-band phase shifter.

K_a-Band Ferrite Phase Shifter*

In 1957, Reggia and Spencer[1] utilized a new technique to develop a phase shifter at 9.1 kMc. This letter reports an extension of their technique to K_a-band frequencies. A maximum figure of merit of 1100 degrees of phase shift per db of loss has been achieved at 35 kMc $\pm$ 500 Mc.

Selection of the Ferrite

For a Reggia-Spencer phase shifter the variation in μ' from zero applied field to saturation determines the amount of phase shift for a given geometry.[2] This difference in μ' generally increases as the saturation magnetization ($4\pi M_s$) increases; hence $4\pi M_s$ should be relatively high. However, materials with a high $4\pi M_s$ have been found to increase the loss of the device at very low applied fields. A practical value is $4\pi\gamma M_s/\omega < 0.5$ or $4\pi M_s < 6250$ oersteds at 35 kMc. In addition, the ferrite should have a small dielectric loss tangent and a narrow resonance linewidth for minimum insertion loss.

A nickel ferrite with a linewidth of 100 oersteds and a $4\pi M_s$ of 5000 gauss was selected because of its availability and superior performance. Other materials with $4\pi M_s$ as low as 3300 gauss were tested and found to yield less phase shift and a lower figure of merit.

Phase-Shifter Design

Two dimensions are critical for a Reggia-Spencer phase shifter. These are: 1) the narrow dimension of the waveguide and 2) the diameter of the ferrite rod. The rectangular waveguide has the function of coupling a TE_{10} mode into and out of the ferrite rod; hence, its narrow dimension must be small enough to prevent Faraday rotation in the ferrite-loaded region. A maximum rod diameter exists beyond which the rod will become a "self-sufficient" dielectric waveguide and Faraday rotation will occur.[2,3]

The investigation of the effects of rod diameter on phase-shifter performance revealed that the figure of merit increases with diameter provided there is no Faraday rotation. However, this advantage is tempered by the impedance-matching problem. The most practical diameter was found to be 0.060 inch for the standard K_a-band waveguide with inside dimensions of 0.280 and 0.140 inch. Faraday rotation occurred for a diameter of 0.065 inch.

Conventional matching techniques, consisting of tapering the ferrite rod and employing tapered dielectric supports, were used to obtain a smooth impedance transformation. The teflon insert ($\epsilon = 2.1$) was designed for the dual purpose of supporting the ferrite rod and providing an intermediate characteristic impedance between the ferrite-loaded section and the empty waveguide. The maximum VSWR of this combination (Fig. 1) varied from 1.12 to 1.17 over the band.

The ferrite and its teflon holders are contained in a 6-inch section of RG-(96)/U waveguide (Fig. 2). The complete assembly weighs approximately 4 ounces and has a maximum cross-sectional dimension of 1.1 inches (Fig. 3).

The coil produces a magnetic field of 187 oersteds per ampere. The value of field strength necessary to produce 360° of phase shift at 34.5 kMc is 35 oersteds.

Phase shift and insertion loss of the device are shown in Fig. 4. These data were taken for a range of field strengths from zero to 47 oersteds at 35 kMc and at 34.5 and 35.5 kMc.

Insertion loss is practically independent of frequency in the range of operation. The loss varies from a low of 0.20 db $\pm$ 0.05 db at zero field to a maximum of 0.45 db. The frequency sensitivity of phase shift of the device is approximately 0.18° per megacycle.

At the center frequency of 35 kMc the maximum figure of merit is 1100° per db at a phase shift of 490°.

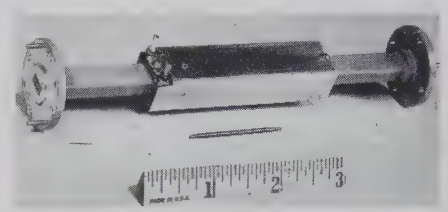

Fig. 3—Photograph of the K_a-band ferrite phase shifter.

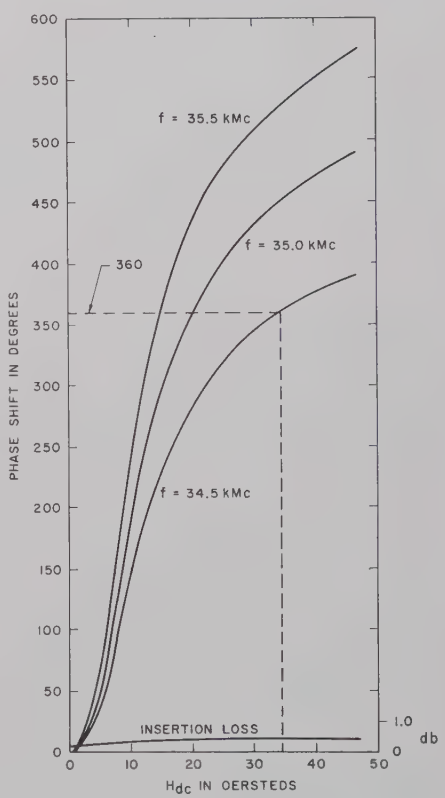

Fig. 4—Phase shift and loss characteristics of the K_a-band ferrite phase shifter.

R. S. McCarter
E. F. Landry
Bell Telephone Labs., Inc.
Whippany, N. J.

* Received by the PGMTT, January 30, 1961. This work was supported by Wright Air Dev. Div. Aerial Reconnaissance Lab., Contract AF33(616)-5499.

[1] F. Reggia and E. G. Spencer, "A new technique in ferrite phase shifting for beam scanning of microwave antennas," Proc. IRE, vol. 45, pp. 1510–1517; November, 1957.

[2] J. A. Weiss, "A phenomenological theory of the Reggia-Spencer phase shifter," Proc. IRE, vol. 47, pp. 1130–1137; June, 1959.

[3] S. A. Schelkunoff, "Electromagnetic Waves," D. van Nostrand Co., Inc., New York, N. Y., Sec. 10.20; 1943.

Low-Temperature Microwave Power Limiter*

A passive microwave power limiter, using the nonlinear properties of ferromagnetic resonance in yttrium-iron-garnet (YIG) has been evaluated at 4.2° K, 77° K, and 297° K. The limiter, of the DeGrasse type,[1] consists of two decoupled, half-wavelength coaxial cavities as shown schematically in Fig. 1. Input and output coupling is made through the use of quarter-wavelength matching transformers. An optically polished sphere of single crystal YIG is placed in the position of maximum RF magnetic fields common to both cavities.

The limiting processes involved in the YIG sphere can be explained by the use of Suhl's theory.[2] For sufficiently high RF fields and for particular dc bias fields a subsidiary ferromagnetic resonance occurs[3] caused by the generation of spin waves at one-half the applied microwave frequency. In general, the field for the subsidiary resonance is different from the field for uniform precession ferromagnetic resonance. In a particular frequency range, the dc magnetic field for uniform precession resonance is *coincident* with the dc field required for the subsidiary resonance. The coincidence frequency region is an octave wide and for a sphere is given by

$$\frac{4\pi M}{3} \leq \frac{\omega}{\gamma} \leq \frac{8\pi M}{3}, \tag{1}$$

where M is the saturation magnetization, ω is the microwave frequency, γ is the gyromagnetic ratio and the factor $\frac{1}{3}$ is the demagnetizing factor for a sphere. The RF field, in the YIG sphere, necessary for the onset of subsidiary resonance is particularly low[4,5] in the coincidence region and is given by

$$h_{\text{crit}} \approx \frac{\Delta H \Delta H_k}{4\pi M}, \tag{2}$$

where ΔH is the measured ferromagnetic resonance line width and ΔH_k is the line width of the spin wave generated, having a wavelength $\lambda = 2\pi/k$. The values of ΔH and ΔH_k as functiions of temperature have been measured on the particular sample used in these experiments[6,7] and are given in Table I.

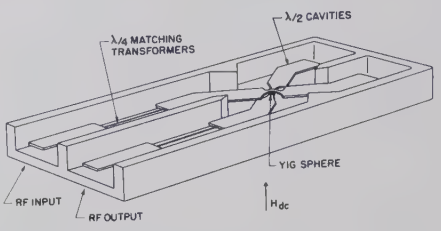

Fig. 1—Cut away view of the limiter structure made of rectangular cross-section coaxial line. The cover plate is not shown.

In the sphere, then, at sufficiently low RF power, the magnet moment M is in uniform precession. The angle of precession increases with increasing RF power until it reaches the value θ_{crit}, where it is said to *stick*. This indicates that the subsidiary resonance is now being generated. As the RF power is further increased, the excess RF energy goes into the generation of the $\omega/2$ spin waves of the subsidiary resonance. The wavelength of these spin waves is so short that they do not radiate or couple to the microwave-measuring circuit. The spin-wave energy is eventually transformed into heat energy in the sphere.

TABLE I*

T°K	$4\pi M$ (gauss)	ΔH (Millioersteds)	ΔH_k	Insertion Loss (db)	P_{crit} (μwatt)	Dynamic Range (db)
297	1750	360	150	0.5	67	28
77	2430	300	100	0.3	7	>25
4.2	2480	150	17	0.2	0.32	>38

* Intrinsic constants of YIG, and limiter characteristics for a 0.042-inch YIG sphere at 3000 Mc. ΔH and ΔH_k were measured at 9340 mc. $4\pi M$ values were obtained from the work of M. A. Gilleo and S. Geller.[9]

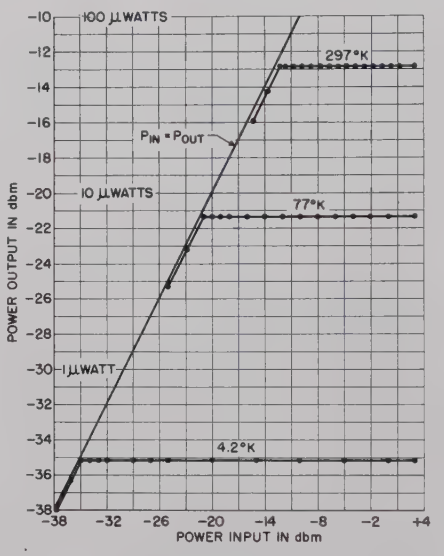

Fig. 2—Measured characteristics of the 3000-Mc limiter using 0.042-inch diameter sphere of single crystal YIG.

In the limiter structure, at low RF powers, the input and output cavities are coupled by the uniform precession resonance, the maximum transfer of energy occurring when $\theta = \theta_{\text{crit}}$. As the RF power is further increased, the coupling remains constant with the excess energy going into the subsidiary resonance of the spin waves, and power limiting occurs.

The saturation magnetization of YIG is 1750 gauss at 297°K and 2480 gauss at 4.2°K giving coincidence frequency octaves of 1635–3270 and 2320–4640 respectively. The frequency of operation, 3000 Mc was chosen so as to be in the center of the coincidence octave at 4.2°K to optimize the results at that temperature. Further, the results shown in Fig. 2 and Table I were for the highest purity YIG sphere. This establishes a criterion of the best results we are able to obtain at this time. The limiting power was measured on an oscilloscope under pulsed conditions, and with a super heterodyne receiver under CW conditions. The perfect flatness as seen in the figure was obtained for both cases. The insertion loss depends on an optimum coupling of the sphere to the structure. The coupling was adjusted for the lowest value of insertion loss, 0.2 db, at 4.2°K. Other room temperature limiters have limited at as low as 10μ watts.

The use of limiters of this type at other frequencies in devices such as masers would require that either a material of a different $4\pi M$ or samples of other shapes be used to shift the coincident frequency octave. Work along these lines is in progress. As an example, for a single crystal YIG sphere[8] in which gallium ions are substituted for iron ions, there is an almost complete preference of the gallium ions for the tetrahedrally

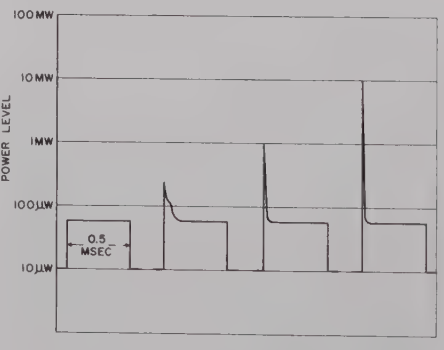

Fig. 3—Response of the limiter to pulsed RF signals. The power shown on the ordinate represents the peak spike power which is equal to the input power and also represents the plateau which is the output power.

* Received by the PGMTT, February 2, 1961. This paper is based on work performed under a contract with the U. S. Army Ordnance Corps.

[1] R. W. DeGrasse, "Low-loss gyromagnetic coupling through single crystal garnets," *J. Appl. Phys.*, vol. 30, pp. 155–156S; April, 1959.

[2] H. Suhl, "Ferromagnetic resonance at high signal powers," *Jour. Phys. and Chem. of Solids*, vol. 1, pp. 209–227; April, 1957.

[3] The observation of the subsidiary resonance was first reported by R. W. Damon, *Rev. Mod. Phys.*, vol. 25, pp. 239–245; January, 1953, and N. Bloembergen and S. Wang, *Phys. Rev.*, vol. 93, pp. 72–85; January, 1954.

[4] E. G. Spencer, R. C. LeCraw, and C. S. Porter, "Ferromagnetic resonance in yttrium iron garnet at low frequencies," *J. Appl. Phys.*, vol. 29, pp. 429–430; March, 1958.

[5] F. C. Rossol, "Subsidiary resonance in the coincidence region in yttrium iron garnet," *J. Appl. Phys.*, vol. 31, pp. 2273–2275; December, 1960.

[6] E. G. Spencer, R. C. LeCraw, and A. M. Clogston, "Low temperature line width maximum in yttrium iron garnet," *Phys. Rev. (Lttrs.)*, vol. 3, p. 32; July, 1959.

[7] E. G. Spencer and R. C. LeCraw, "Spin lattice relaxation of low k-number spin waves in yttrium iron garnet: II temperature dependence," *Bull. Am. Phys. Soc.*, vol. 4, p. 297; April, 1960.

[8] E. G. Spencer and R. C. LeCraw, "Line-width narrowing in gallium substituted yttrium iron garnet," *Bull. Am. Phys. Soc.*, vol. 4, p. 57; January, 1960.

coordinated sites,[9,10] thus reducing $4\pi M$. Using a single-crystal YIG-Ga sphere with a $4\pi M$ of 1000 gauss the measured frequency octave is from 935 to 1870 Mc at room temperature. A limiter has been constructed to operate at 1300 Mc which has an insertion loss of 0.7 db, a limiting power of 10μ watts, and a curve similar in all respects to that of Fig. 2. The 0.7-db insertion loss could be reduced by using a larger sphere.

The response of the limiter to pulses of RF energy always shows a spike on the leading edge. The reason for this is that the subsidiary resonance does not build up instantaneously. The time of build up is associated with the relaxation time of the RF magnetization. When a pulsed RF signal is applied, ferromagnetic resonance occurs and the angle of precession of magnetization increases, opening up to a value $>\theta_{crit}$. Eventually subsidiary resonance occurs and θ decays to its final value of θ_{crit}.

Fig. 3 shows the spike for a sequence of pulses of RF energy. The build-up time of subsidiary resonance becomes shorter as the power is increased [see Suhl's (24)]. For RF power levels moderately in excess of the limiting power, we were able to integrate the area under the spike and show that it remains constant. At higher power levels it was not possible, however, to show definitely that the spike energy remains constant.

We should like to thank R. C. LeCraw for helpful discussions on these experiments, J. J. Kostelnick for suggestions on the structure, S. Geller for many discussions of his work on substituted garnets, and J. W. Nielsen and R. C. Linares for the growth of all the crystals used in these experiments.

F. J. Sansalone
E. G. Spencer
Bell Telephone Labs., Inc.
Murray Hill, N. J.

[9] M. A. Gilleo and S. Geller, "Magnetic and crystallographic properties of substituted yttrium iron garnet, $3Y_2O_3 \cdot XM_2O_3 \cdot (5-X)Fe_2O_3$," *Phys. Res.*, vol. 110, pp. 73–78; April, 1958.
[10] S. Geller, "Magnetic interactions and distribution of ions in the garnets," *J. Appl. Phys.*, vol. 31, pp. 30–37S; May, 1960.

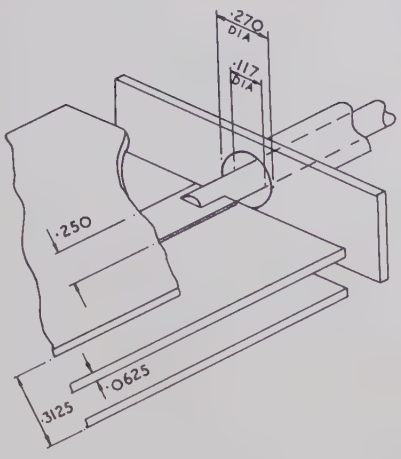

Fig. 1—Standard stripline-to-coaxial line 50-ohm transition.

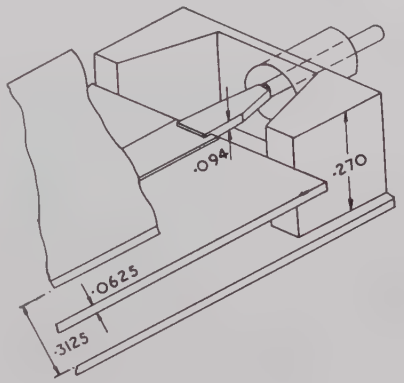

(a)

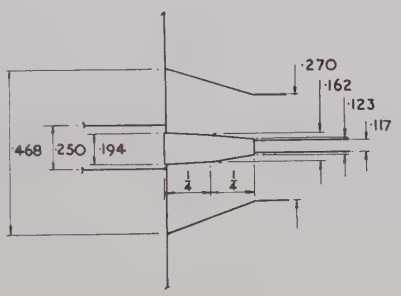

(b)

Fig. 2—Stripline-to-coaxial line tapered transitions using rectangular line.

New Coaxial-to-Stripline Transformers Using Rectangular Lines*

The most common form of coaxial-to-stripline transition consists of a simple in-line butt joint, as described by Barrett.[1] A typical transition between a 50-ohm high-Q triplate and a standard N-type connector is shown in Fig. 1. This gives a VSWR <1.15 at frequencies up to 7000 Mc deteriorating to 1.25 at higher frequencies up to 11,000 Mc. While these results are acceptable for many types of stripline components and assemblies, it was felt that the design of a better transition would be necessary in order both to test and to maintain the performance of high grade components (*e.g.*, hybrids, directional couplers, and filters) and to avoid the manufacture of a special stripline standing-wave detector.

The conventional transition (Fig. 1) is not perfectly matched because the fringing field of the stripline is intercepted by the outer conductor of the coaxial line, in addition to the disparity of dimensions between the inner conductors of the two lines.

A diagram of a well-matched transition is shown in Fig. 2. In this, the side walls at the start of the transition from the stripline end are positioned sufficiently far away from the stripline to avoid discontinuities, a constant 50-ohm impedance is maintained through the transition to the coaxial line, and there are no large dimensional discontinuities. The VSWR of this transition, as deduced from measurements of two such transitions back-to-back cascaded with terminating N-type connectors and a matched load, is probably better than 1.02 at all frequencies up to the highest measured frequency of 11,000 Mc; and, in fact, it is probable that the transition does not deteriorate the VSWR of the N-type connector.

A cross section through the transition in a plane perpendicular to its axis is shown in Fig. 3, and takes the form of a rectangular line. It was necessary to derive a formula for the characteristic impedance of the rectangular line, and this was obtained in the form

$$Z(w/b,\ t/b,\ s/b) = \frac{94.15}{\sqrt{\epsilon}\left[\dfrac{w/b}{1-t/b} + C_{f0}'(t/b,\ s/b)\right]}, \quad (1)$$

where

$$C_{f0}'(t/b,\ s/b) = C_{f0}'(0,\ s/b) + \epsilon t/s. \quad (2)$$

Here ϵ is the *relative* dielectric constant of the dielectric medium of the line, and $C_{f0}'(0,\ s/b)$ is the fringing capacitance of the rectangular line as given by Cohn[2] in the form

$$C_{f0}'(0,\ s/b) = \frac{2\epsilon}{\pi} \log\left[1 + \coth\left(\pi s/2b\right)\right]. \quad (3)$$

A graph of $C_{f0}'(0,\ s/b)$ as a function of s/b is plotted in Fig. 7 of Cohn's paper.

Eq. (1) gives a good approximation to the impedance of the line, valid for $s/t \leq 5$, a condition which is always true in the case of the transition shown in Fig. 2.

More general formulas for the characteristic impedance of rectangular lines have now been derived by Chen[3] with the inde-

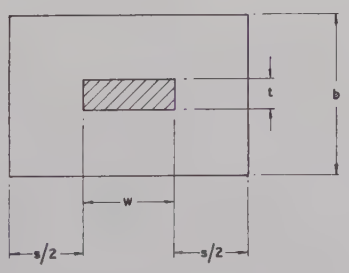

Fig. 3—The rectangular line.

* Received by the PGMTT, February 3, 1961.
[1] R. M. Barrett, "Etched sheets serve as microwave components," *Electronics*, vol. 25, pp. 114–118; June, 1952.
[2] S. B. Cohn, "Shielded coupled-strip transmission line," IRE Trans. on Microwave Theory and Techniques, vol. MTT-3, pp. 29–38; October, 1955.
[3] T. S. Chen, "Determination of the capacitance, inductance and characteristic impedance of rectangular lines," IRE Trans. on Microwave Theory and Techniques, vol. MTT-8, pp. 510–519; September, 1960.

pendent suggestion that such lines might be used as a transition between coaxial and strip-transmission lines.

It is worth noting that an exact formula has been derived for the characteristic impedance of the rectangular line with an inner conductor of zero thickness ($t=0$ in Fig. 3). This is given approximately by Chen in his equation (23), which may be written in the following revised form to conform with the notation of Fig. 3:

$$Z(w/b,\ 0,\ s/b) = \frac{94.15}{\sqrt{\epsilon}\left[w/b + 2/\pi \cdot \log\left(1 + \coth \pi s/2b\right)\right]}. \quad (4)$$

Eq. (4) is in fact identical to (1) with $t=0$.

The conformal transformation of one-half of the rectangular line is shown in Fig. 4. The transformation from the z plane to the t plane is standard, and is given by

$$t = \mathrm{sn}\,(Bz,\ k_1) \quad (5)$$

which upon use of the boundary conditions gives

$$t = \mathrm{sn}\left[\frac{2K(k_1)\cdot z}{w+s},\ k_1\right] \quad (6)$$

and

$$b/(w+s) = K'(k_1)/K(k_1), \quad (7)$$

where $K(k_1)$ is the complete elliptic integral to modulus k_1, and $K_1'(k_1)$ is the complementary integral. The transformation of the t plane to the χ plane, where the field pattern is regular, is also standard and is given by

$$t = k\ \mathrm{sn}\,(\chi,\ k). \quad (8)$$

The impedance of the half line is thus given by $Z=376.6\ K'(k)/2K(k)$, resulting in the formula for the impedance of the complete rectangular line,

$$Z = 94.15\,\frac{K'(k)}{K(k)}. \quad (9)$$

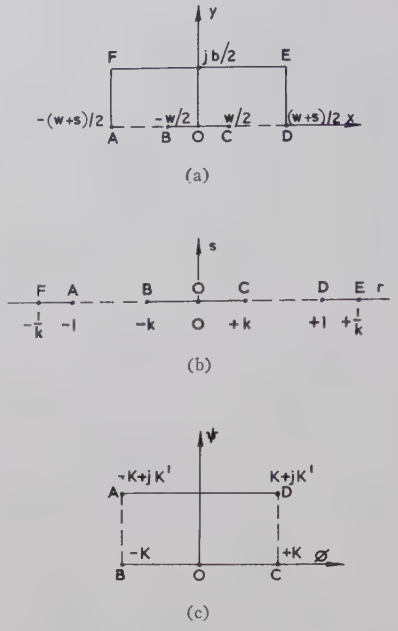

Fig. 4—Conformal transformation of the rectangular line with zero thickness inner conductor. (a) Z plane (b) t plane (c) X plane.

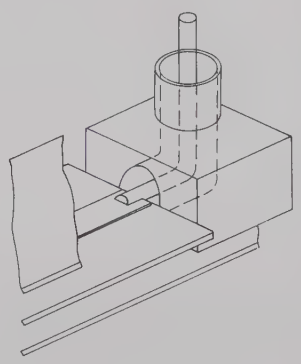

Fig. 5—Right-angled stripline-to-coaxial line transition.

The relationship between k and k_1 is obtained from (6) by using the condition that $t=k$ when $z=w/2$, giving

$$k = \mathrm{sn}\left[\frac{w}{w+s}K(k_1),\ k_1\right],$$

i.e.,

$$\frac{w}{w+s}K(k_1) = F(k,\ k_1) = F(\theta,\ \phi), \quad (10)$$

where $F(k,\ k_1)$ is the incomplete elliptic integral of the first kind of argument k and modulus k_1. It is usual to put $k=\sin\phi$ and $k_1=\sin\theta$ since $F(\theta,\ \phi)$ is usually tabulated.

The procedure for determining the impedance of the line exactly from its parameters w, s, and b is thus to find the modulus k_1 from (7) and to substitute this into (10) to find ϕ and hence k, which is used in the impedance formula (9). In practice, it is found that this procedure is almost as simple as the calculation of (4), since the elliptic integrals have been well tabulated; and therefore, the exact procedure might always be adopted. It is seen that the approximate formula (4) breaks down badly as $s/b\to\infty$, since then the expression for the capacitance in the denominator reduces to that of a simple parallel-plate capacitor, there being no allowance for the fringing capacitance.

It is possible also to construct the stripline-to-coaxial line transition in a right-angled form as shown in Fig. 5, which depicts a simple butt joint followed immediately by a right-angled coaxial bend. The match of this transition is as good as that of the in-line version shown in Fig. 1. This form of transition, where the coaxial line output is normal to the ground plane is particularly useful in integrated assemblies. It is proposed to combine this form of transition with the tapered section to form a well-matched right-angled transition possibly equal in performance to the in-line transition as described above.

R. Levy
Mullard Res. Labs.
Surrey, England

Contributors

Frank R. Arams (S'44–A'49–SM'55), for a photograph and biography, please see page 105 of the January, 1961, issue of these TRANSACTIONS.

❖

Richard O. Bell was born in Havre, Mont., on February 16, 1933. He received the B.S. degree in engineering physics in 1955 from Montana State College, Bozeman. After studying at the University of Freiburg, Germany, and at the University of California at Los Angeles, he received the M.S. degree in physics from the latter institution in 1958. He received the M.A. degree in applied physics from Harvard University, Cambridge, Mass., in 1960.

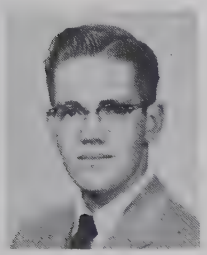

R. O. BELL

From 1955 to 1958, he was a member of the technical staff of Hughes Aircraft Company, Culver City, Calif. During the summer of 1959, he worked as a physicist at Air Force Cambridge Research Center. In February, 1960, he joined the Raytheon Research Division as an associate research staff member. He has been measuring dielectric properties of ferroelectric materials in the microwave region.

Mr. Bell is a member of Tau Beta Pi and Phi Kappa Phi.

❖

Philip S. Carter, Jr., (S'48–A'50–M'56) was born in Marion, Mass., on May 23, 1926. He received the B.E.E. degree from Cornell University, Ithaca, N. Y., in 1948, and the M.S. and Ph.D. degrees in electrical engineering from Stanford University, Stanford, Calif., in 1952 and 1954, respectively.

P. S. CARTER, JR.

From 1948 to 1949 he was employed by Airborne Instruments Laboratories, Inc., Mineola, N. Y., where he was engaged in the research and development of flush-mounted aircraft antennas. From 1949 to 1950 he was a Laboratory Instructor in electronics at Stanford. In 1950 he joined the staff of the Stanford Research Institute where his work has included research in the development of airborne direction-finding antenna systems, studies of radio-frequency properties of rocket exhaust gases, and investigations of mutual impedance properties of electronically-scanned antenna arrays. From 1958 to 1959 he was employed by Lockheed Missile and Space Division, Sunnyvale, Calif., where he was engaged in research in solid-state microwave applications. In June, 1959, he returned to Stanford Research Institute, where he is continuing this research.

Dr. Carter is a member of the Scientific Research Society of America and the American Physical Society.

❖

Edward S. Cassedy, Jr., (A'52–M'57) was born in Washington, D. C., on August 19, 1927. He received the B.S. degree in electrical engineering from Union College, Schenectady, N. Y., in 1949. In 1950 he received the M.S. degree from Harvard University, Cambridge, Mass., and in 1959 the Doctor of Engineering degree from The Johns Hopkins University, Baltimore, Md.

E. S. CASSEDY, JR.

In 1951 he joined the staff at the U. S. Naval Ordnance Laboratory, White Oak, Md., and worked there on telemetering problems, and UHF circuit and antenna design. In 1954 he transferred to the Radiation Laboratory of The Johns Hopkins University, where he was engaged in research on electromagnetic scattering and microwave techniques. In 1960 he joined the academic research staff at the Microwave Research Institute of the Polytechnic Institute of Brooklyn, N. Y. He is presently engaged in research on guided wave structures and parametric phenomena.

Dr. Cassedy is a member of Sigma Xi, the American Physical Society, and the American Association for the Advancement of Science.

❖

Marvin Cohn (S'49–A'51–M'57) was born in Chicago, Ill. on September 25, 1928. He received the B.S. degree in 1950 and the M.S. degree in electrical engineering in 1953, both from the Illinois Institute of Technology, Chicago. In 1960 he received the Doctor of Engineering degree from The Johns Hopkins University, Baltimore, Md.

From 1951 to 1952 he was employed by the Glenn L. Martin Company, Baltimore; he was with the Radiation Laboratory of Johns Hopkins from 1952 until he entered the U. S. Army Signal Corps in 1953. He was stationed at White Sands Proving Grounds where he worked on the analysis of missile tracking systems.

In 1955 he returned to the Radiation Laboratory where he has done research and development work on broad-band and superheterodyne receivers and surface-wave transmission lines. He was Head of the Millimeter Wave Techniques Group of the Radiation Laboratory.

M. COHN

Since July of 1960, Dr. Cohn has been a Research Scientist with the Research Division of Electronic Communications, Inc., Timonium, Md. He is currently engaged in work on millimeter wave systems and ferroelectric materials and devices.

Dr. Cohn is a member of Eta Kappa Nu, Tau Beta Pi, and Sigma Xi.

❖

Robert V. Garver (M'57) was born in Minneapolis, Minn., on June 2, 1932. He attended the University of Maryland, College Park, where he was awarded the B.S. degree in physics in 1956.

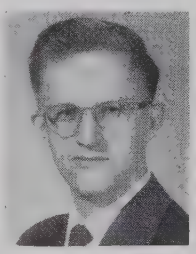

R. V. GARVER

In 1956, he became affiliated with the Microwave Development Section of Diamond Ordnance Fuze Laboratories, Washington, D. C., where he has been working on microwave semiconductors.

Mr. Garver is a member of the American Physical Society.

❖

Bernard Kaplan was born in Brooklyn, N. Y., on December 19, 1936. He received the B.S. degree in physics from Brooklyn College in 1957.

B. KAPLAN

Upon graduation, he joined Sylvania Electric, Woburn, Mass., as a Test Engineer in the Microwave Tube Division. In 1958, he joined Airtron, Inc., Cambridge Division, where he worked on ferrite isolators, circulators, and switches. In 1959,

he joined Airborne Instruments Laboratory, Melville, L. I., N. Y., where he was concerned with the development of wide-band circulators. In 1960, he returned to Airtron, now located in Morris Plains, N. J., where he is presently engaged in work on parametric amplifiers. He is currently taking graduate physics courses at New York University, N. Y.

❖

Walter M. Nunn, Jr. (M'54–SM'55) was born in New Orleans, La., on September 16, 1925. He received the B.S.E.E. degree from Tulane University of Louisiana, New Orleans, in 1950 and the M.S.E.E. degree from Oklahoma State University of Agriculture and Applied Science, Stillwater, in 1952.

W. M. Nunn, Jr.

He taught electrical engineering at Oklahoma State from 1950 to 1952, and at Rensselaer Polytechnic Institute, Troy, N.Y., from 1952 to 1954. From 1954 to 1956 he served as a Research Engineer in the Ground Radar Department of the Hughes Aircraft Company, Culver City, Calif. Since 1956, he has been associated with the Electron Physics Laboratory of the University of Michigan, Ann Arbor, where he has recently completed the requirements for the Ph.D. degree in electrical engineering. He has been engaged in precision microwave measurements and in the study of electrostatically-focused microwave electron beam devices.

Mr. Nunn is a member of the American Physical Society.

❖

Akira Okaya was born in Kobe, Japan on October 10, 1920. He was educated at the Department of Aeronautical Science, Nagoya University, where he received the Kō-Gakushi degree (corresponding to a degree between the Bachelor's and Master's in the U. S.).

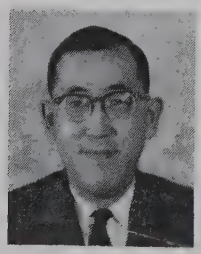

A. Okaya

During World War II, he was engaged in the design of aircraft at the Japan Naval Aeronautical Research Laboratory in Yokosuka. He started his career in physics in 1946 at the Physics Department of Kyoto University, Japan. An instructor there from 1948 to 1957, he began work on microwave spectroscopy in 1950, a study which continues to absorb much of his attention. He was a member of the Japanese Government Committee on Radio Technique and engaged in atomic clock experiments in Japan prior to receiving the Rigaku-Hakase degree (similar to the Ph.D. degree) from Kyoto University in 1956. His thesis for this degree was on the subject of millimeter microwave spectroscopy. In 1955, he became a Research Associate in the Chemistry Department, Columbia University, New York, N. Y., on a Fulbright travel grant, where he worked with nuclear magnetic resonance of liquids and gases. In 1957, he became a staff member of the Columbia Radiation Laboratory, connected with the Physics Department, where, for the past three years, he has been engaged in work on gas maser spectroscopy, the solid-state maser, electron paramagnetic resonance, and microwave electronics.

Dr. Okaya is a member of the American Physical Society and the Physical Society of Japan.

❖

Bernard Peyton (M'60) was born in New York, N. Y., on April 11, 1937. He received the B.S.E.E. degree from the College of the City of New York, N. Y., in 1959 and is presently working toward the M.S.E.E. degree at the Polytechnic Institute of Brooklyn, N. Y.

B. Peyton

He joined Airborne Instruments Laboratory, Melville, L. I., N. Y., in 1959, as an Engineer in the Department of Applied Electronics, where he was concerned with the study of ferrite materials and the development of low-frequency nonreciprocal ferrite devices. Since 1960, he has been active in the design and development of traveling-wave masers.

❖

Lynn E. Paul (M'59) was born in Huntington, Ind., on October 9, 1926. He received the B.S. degree in physics from Purdue University, Lafayette, Ind., in 1951, and the M.S. degree in physics from the University of Michigan, Ann Arbor, in 1957.

L. E. Paul

He has been employed by the University of Michigan Research Institute since 1951 and has been associated with the Electron Physics Laboratory of the Electrical Engineering Department since 1953, where he is concerned with research on electron devices and techniques.

Mr. Paul is a member of both the American and International Vacuum Societies.

Georg Rupprecht was born in Nürnberg, Germany, on May 13, 1922. He received the Diploma in physics in 1950 and the Ph.D. degree in 1953, both from the University of Erlangen, Germany.

G. Rupprecht

From 1953 to 1954, he was a teaching assistant at the Institut für Angewandte Physik, University of Erlangen. During 1955 he served as a scientific co-worker at the AEG Research Laboratory, Belecke/Möhne, Germany. He came to the U. S. in October, 1955, and spent the next two years as a Research Associate at the University of Illinois, Urbana.

In 1958, Dr. Rupprecht joined the Raytheon Research Division, where he is now a senior research staff member of the Solid-State Physics Group working on surface and bulk properties of semiconductors and microwave properties of ferroelectric materials.

❖

Ronald F. Soohoo (SM'60) was born in Canton, China, on September 1, 1928. He received the B.S. degree from the Massachusetts Institute of Technology, Cambridge, Mass., in 1948, and the M.S. and Ph.D. degrees in 1952 and 1957, respectively, from Stanford University, Stanford, Calif. His studies were in electrical engineering and physics.

R. F. Soohoo

From 1948 to 1951 he was engaged in the design and analysis of power systems while an assistant engineer for the Pacific Gas and Electric Company, San Francisco, Calif. He then became a research assistant at the Microwave Laboratory, W. W. Hansen Laboratories of Physics, Stanford, Calif., where he was involved with microwave tube research from 1951 to 1953. He was an electronics research assistant at the Stanford Electronics Laboratories, Stanford, Calif., in 1954 and 1956. From 1954 to 1955, he was a research engineer with the Cascade Research Corporation, Los Gatos, Calif., engaged in the design of ferrite devices. In 1957 he became Director of Research Analysis at the Cascade Research Corporation. His duties there included research in microwave ferrites, microwave tubes, and solid state physics. At present, he is a physicist on the research staff of Lincoln Laboratory, MIT, Lexington, Mass., where he is engaged in theoretical and experimental physics research with particular emphasis on magnetism and resonance.

Dr. Soohoo is a member of the American Physical Society.

INSTITUTIONAL LISTINGS

MICROWAVE ASSOCIATES, INC.
South Avenue, Burlington, Mass.

Waveguide Devices, Microwave Diodes, Magnetrons, Duplexers, TWT's, Ferrite & Solid-State Devices

SCIENTIFIC-ATLANTA, INC.
2162 Piedmont Rd., N.E., Atlanta 19, Ga.

Complete Antenna Pattern Range Instrumentation, Special RF and Antenna Systems Development

THE MICROWAVE JOURNAL
1330 Beacon St., Brookline 46, Mass.

A Magazine Devoted to the Interests of Engineers Working at Microwave Frequencies

STANFORD RESEARCH INSTITUTE
Electromagnetics, Lab., Menlo Park, Calif.

Res., Dev.; Microwave Components and Solid-State Devices; Filters, Couplers, Par. Amps., and Antennas

PHELPS DODGE COPPER PRODUCTS CORP.
300 Park Ave., New York 22, N.Y.

Styroflex, Foamflex Air Dielectric Aluminum Sheathed Coaxial Cables, Connectors and Waveguides

SYLVANIA MICROWAVE DEVICE OPERATIONS
Sylvania Electric Products Inc.
500 Evelyn Ave., Mountain View, Calif.

Magnetrons, Klystron, TWT's, BWO's, Ferrite Devices, Waveguide Windows, Microwave Diodes

PRD ELECTRONICS, INC.
202 Tillary St., Brooklyn 1, N.Y.

Complete Line of Microwave and Electronic Test Equipment Waveguide and Coaxial Components

TECHNICRAFT DIVISION, Electronic Specialty Co.
Thomaston, Conn.

Designers, Developers and Producers of Microwave Components, Transmission Lines, and Assemblies

SAGE LABORATORIES, INC.
3 Huron Dr., Natick, Mass.

Microwave Attenuators, Couplers, Crystal Holders, Filters, Hybrids, Mixers, Rotary Joints

WATKINS-JOHNSON COMPANY
3333 Hillview Ave., Palo Alto, Calif.

Res., Dev., Microwave Electron Devices, TWT's, BWO's, Parametric Amplifiers, Microwave Systems

WHEELER LABORATORIES, INC.
Great Neck, N.Y.
Antenna Lab., Smithtown, N.Y.

Consulting Services, Research & Development, Microwave Antennas & Waveguide Components

(See outside back cover for additional listings.)

INSTITUTIONAL LISTINGS

The IRE Professional Group on Microwave Theory and Techniques is grateful for the assistance given by the firms listed below, and invites application for Institutional Listing from other firms interested in the Microwave field.

AIRTRON, INC.
A Division of Litton Industries
200 East Hanover Ave., Morris Plains, N.J.

Designers and Producers of Complete Line of Microwave Electronic and Aircraft Components

ALFORD MANUFACTURING COMPANY
299 Atlantic Ave., Boston 10, Mass.

RF Instruments, Coaxial Components, Antennas and Air Navigation Aids

CASCADE RESEARCH
Div. of Lewis & Kaufman Electronics Corp.
5245 San Fernando Rd., Los Angeles, Calif.

Research, Development, Production: Microwave Ferrite Devices, Microwave Components & Subsystems

EIMAC TUBES, EITEL-McCULLOUGH, INC.
301 Industrial Way, San Carlos, Calif.

Microwave Tubes, TWT-VTM-Reflex Klystrons, Power Grid Tubes, Amplifier Klystrons

ELECTRONIC SPECIALTY CO.
5121 San Fernando Rd., Los Angeles 39, Calif.

Airborne and Ground Antennas, Towers, Waveguides, Microwave Components, Complete Radiating Systems

FXR, INC.
25-26 50th Street, Woodside 77, N.Y.

Precision Microwave Test Equipment, High Power Microwave Electronics, Microwave Components & Instrumentation

HUGHES AIRCRAFT CO.
Florence and Teale Sts., Culver City, Calif.

Res., Dev., Mfg.: Radar Systems and Components, Microwave Devices and Components, Antennas, Tubes

ITT FEDERAL LABORATORIES
500 Washington Ave., Nutley 10, N.J.

Line-of-Sight and Over-the-Horizon Microwave Systems; Test Equipment and Components

MELABS
3300 Hillview Ave., Palo Alto, Calif.

Microwave Components and Systems for Communications, Countermeasures, Reconnaissance, Radar, Etc.

MICROLAB
570 West Mount Pleasant Ave., Livingston, N J.

Designers and Manufacturers of a Complete Line of Coaxial Microwave Components and Cavity Filters

(See inside back cover for additional listings.)

The charge for an Institutional Listing is $50.00 per issue or $210.00 for six consecutive issues. Applications for Institutional Listings and checks (made out to The Institute of Radio Engineers, Inc.) should be sent to Robert A. Rivers, PGMTT Advertising Editor, Aircom Inc., 354 Main St., Winthrop 52, Mass.